MASTER'S THESIS

Master of Science in Advanced Mathematics and Mathematical Engineering

Title: Shannon wavelets in Computational Finance

Author: Àngel Satorres Almenara

Advisor: Luis Ortiz-Gracia

Department: Universidad Politécnica de Cataluña

Academic year: 2016-2017

UNIVERSITAT POLITÈCNICA DE CATALUNYA
BARCELONATECH
Facultat de Matemàtiques i Estadística

Acknowledgments

First and foremost, I would like to thank my parents for being my inspiration and allowing me to realize my own potential, for their advice, their values, their guidance, their patience, their trust, their encouragement, their caring, but above all, for their endless love. All the support they have provided me with over the years has been the greatest gift anyone has ever given to me. Without them, I certainly would not have ever gotten to where I am today.

I would also like to thank my supervisor Luis Ortiz-Gracia since I am indebted to him for many things. First, for having introduced me to the fascinating subject of Computational Finance and, more specifically, for the choice of the topic of this thesis. Second, for all the time he spent explaining things, his valuable suggestions and comments, his support and guidance along these months. And last, but not least, for his confidence in me.

Finally, I would also like to dedicate a little space in this thesis to Alina and express my gratitude for her small but at the same time great and valuable help.

Abstract

Derivative securities, when used correctly, allow investors to increase their expected profits and minimize their exposure to risk. Options offer leverage and insurance for risk-averse investors while they can be used as ways of speculation for the more risky investors. When an option is issued, we face the problem of determining the price of a product at the same time we must make sure to eliminate arbitrage opportunities.

In this thesis, we introduce a robust, accurate, and highly efficient financial option valuation technique, the so-called SWIFT method (Shannon wavelets inverse Fourier technique), based on Shannon wavelets. SWIFT comes with control over approximation errors made by means of sharp quantitative error bounds.

This method is adapted to the pricing of European options and Discrete Lookback options. Numerical experiments show exponential convergence and confirm the robustness, efficiency and versatility of the method.

Keywords: Option pricing, European options, Lookback options, Shannon wavelets, sinus cardinal function, Fourier transform inversion,

Contents

List of Figures

List of Tables

Chapter 1

Introduction

Financial innovation has been the force driving global finance to greater economic efficiency since the late nineteenth century. Among all the innovations, derivative securities, such as options, have caused some of the most dramatic changes in the financial world.

An option, put in simple terms, is a contract between two parties, giving one of the parties the right but not the obligation to purchase or to sell an underlying asset in the future. For instance, given a share of a company traded at 20 euros today, A and B agree that in one year from now, B will have the option to purchase the share for 24 euros in exchange of a fee. B pays the fee to A today and will exercise his right on expiration date only if the share price is selling at a higher value than 24. This type of option is called a *European call option* and constitutes one of the most actively traded options in the derivative market.

The existence of options traces back thousands of years, in the Phoenicians and Ancient Greek civilizations. The first reputed option buyer was the ancient Greek mathematician and philosopher Thales of Miletus. On a certain occasion, he predicted that the season's olive harvest would be larger than usual, and during the off-season, he rented in advance olive presses at a low price since demand was short during the winter. When spring came and the olive harvest was larger than expected, he rented the presses out at a much higher price, obtaining a profit. Nowadays, options have become extremely popular financial instruments among investors since they are understood as a really attractive and convenient way of investing money. Options are then usually included in portfolios as ways of both hedging and speculation.

The main challenge concerning the options market is how to price them fairly to avoid arbitrage opportunities. Actually, the valuation of options constitutes an extremely active area of research today. Regarding the initial example, several questions naturally arise: what is the optimal tax that A should charge B today for the option he is selling? Would both A and B be in concordance with this value? Which approach should be taken to fix this price?

Unquestionably, the most well-known valuation model in option pricing is the celebrated *Black-Scholes Model* formulated in 1973 by Myron Scholes and Fischer Black in [3]. The model is based on the assumption that the dynamics of the underlying asset price is driven

by a Geometric Brownian motion (an Itô Process) and provides an analytic solution for European options which makes this model highly popular.

It turns out more convenient, however, to introduce more complex and realistic processes such as the *Heston Model* or the *Variance Gamma Process* (see [15] and [6] respectively) which best fit the dynamics of market prices and provides more reliable results. Although most of these relevant models do not allow a closed formula for the option value, they all have a feature in common: the fair price of the option is determined by the distinguished *Feynman-Kac Theorem*. This theorem essentially says that the option value $v(x,t)$ at time t can be found as a discounted expectation of the option at maturity $t = T$ as follows:

$$v\left(x,t\right) \;=\; e^{-r(T-t)}\mathbb{E}^{\mathbb{Q}}\left(v\left(x,T\right)|x\right) \;=\; e^{-r(T-t)}\int_{\mathbb{R}} v\left(y,T\right) f\left(y|x\right) dy.$$

Here, $v\left(y,T\right)$ denotes the so-called pay-off function and depends on the kind of option under consideration. For its part, $f\left(y|x\right)$ is the probability density function governing the stochastic asset price dynamics in the *risk neutral world* and is not available in most cases. Instead, we do have its Fourier transform (or Characteristic function).

A strain of literature exploding the knowledge of the characteristic function and dealing with highly efficient pricing of these contracts already exists. Methods based on quadrature and the fast Fourier transform (FFT) (see [17], [16] and [10]) and methods based on Fourier cosine expansions (see [7] and [28]) are among the most outstanding examples.

In this thesis, we particularly introduce a robust, accurate and highly efficient financial option valuation technique, the *SWIFT method* (Shannon wavelets inverse Fourier technique). This method relies on the extraordinary approximation features of Shannon Wavelets to accurately invert the Fourier transform of the density function and determine an approximation of a European option price with exponential convergence.

New types of options arise as investors try to create their preferred risk return profile for their portfolios. A special case of options called *exotic options* has gain popularity and offers more attractive features than European options. Returning to the above example, assume that the share price rises up to 40 euros in the first half of the year. In the second half of the year, however, the company loses competitiveness and the share price falls bellow 10 euros. The European call option is then worthless at expiration, becoming more convenient for B to take into account the price of the option throughout all its lifetime.

Lookback Options settle this problem by allowing the holder, at expiration, to look back at how the price of the underlying asset has performed and maximize their profits by taking advantage of the biggest price differential between the strike price and the price of the underlying asset. For option traders, this is obviously a major benefit since the chances of a contract expiring worthless are much lower. These advantageous features have made Lookback Options become increasingly popular in the last few years, specially in insurance contracts and structured notes as a way of hedging risk.

The development of the theory of pricing *Discrete Lookback Options* has been slower and relies basically on numerical methods. The efficient pricing of *Discrete Lookback Options*

is therefore one of the greatest challenges in computational finance. Initially, these pricing methods were based around binomial methods (see [2] and [11]), partial differential equations (see [23] and [24]) and numerical integration (see [1] and [31]). However, these methods just focused on the Brownian motion model and were not easily extended to other models of asset returns. The next major breakthrough in the pricing of discrete lookback options was made by [18] who used the Spitzer identity to derive a recursive formula for the valuation of the characteristic function of the *discretely monitored maximum asset price*. This was an important result that [25] and [4] extended to a range of stochastic models. Finally, [9] derived in 2014 an highly efficient method which uses B-spline approximation theory to provide an accurate closed-form approximation to a Fourier transform representation of the discrete lookback option price.

This thesis researches for a robust, accurate, and highly efficient numerical technique for the valuation of Discrete Lookback Options by adapting the SWIFT method derived for European Options to this kind of derivatives. It also aims to develop a versatile strategy adaptable to a wide range of asset processes and able to price the option at any monitoring point during the lifetime of the derivative contract.

1.1 Structure of the thesis

We start out in **Chapter 2** introducing basic definitions and theorems in stochastic calculus and financial mathematics as well as setting some of the mathematical framework and notations. We also give a short overview in the Black-Scholes theory to provide the reader with the required background to fully understand the objectives pursued and the future analysis carried out in this thesis. **Chapter 3** derives a robust, accurate and highly efficient financial option valuation technique for European options, the so-called *SWIFT method* which explores the potential of approximation of Shannon wavelets and benefits from them to provide accurate and efficient results. In **Chapter 4**, we research and propose an efficient and versatile methodology for pricing Discrete Lookback options by adapting the SWIFT method presented in Chapter 3 and we check the accuracy and efficiency of this novel technique by comparing it with the results obtained by [9]. Finally, **Chapter 5** gives a brief summary of the main conclusions drawn from the thesis, the contributions of our research and the future work to be made in order to improve our methodology.

Chapter 2

The Black-Scholes Theory of Derivative Pricing

Based on works previously developed by market researchers and practitioners, such as Louis Bachelier, Sheen Kassouf and Ed Thorp among others, it was in the early 1970s when Fischer Black, Myron Scholes and Robert Merton make a major breakthrough in the pricing of stock options. This involved the development of what has become known as the Black-Scholes model. The model has had a huge influence on the way that traders price and hedge options. It has also been pivotal to the growth and success of financial engineering in the 1980s and 1990s. One can understand the repercussion that this formula cased by recalling that Myron Scholes and Robert Merton were awarded the 1997 Nobel Memorial Prize in Economic Sciences for their work entitled "The Pricing of Options and Corporate Liabilities" (see [3]) published in 1973. Sadly, Fischer Black died in 1995; otherwise he also would undoubtedly have been on of the recipients of this prize.

This chapter aims then to give a short overview in the Black-Scholes theory to provide the reader with the required background to understand the objectives pursued and the future analysis carried out in this thesis. Particularly, we give basic definitions and theorems in stochastic calculus and financial mathematics, and we define some of the mathematical framework and notations that will be used. Also some financial interpretations of these mathematical concepts are given. For a more elaborate insight into these and other concepts the reader is referred to the book of Hull [12].

2.1 Mathematical framework

The purpose of this thesis is to derive an efficient and robust numerical method to construct the value of a financial derivative. To its computation, it becomes essential to know how the *underlying asset* behaves. Let us denote the asset price at time t as S_t and define its *return*

$$\text{Return} = \frac{\text{Stock tomorrow} - \text{Stock today}}{\text{Stock today}} = \frac{S_{t+\triangle t} - S_t}{S_t}.$$

To illustrate a typical stock behaviour, we consider in Figure 2.1 the daily closing prices and returns of the stock of currency exchange Euro Dollar. We note that the asset price looks very unpredictable and the daily returns seem to be driven by a white noise as it becomes more ostensible in its histogram and Normal Q-Q plot. Therefore, we model them as a noise and a probability space consisting on states that occur randomly should be defined.

We then set throughout the thesis the probability space $(\Omega, \mathcal{F}, \mathbb{P})$, where Ω is the sample space containing all possible outcomes ω, $\mathcal{F}$ is the set of events where each event is in turn a set containing one or more outcomes, and $\mathbb{P}$ is the probability measure $\mathbb{P} : \mathcal{F} \longrightarrow [0, 1]$ corresponding to the assignment of probabilities to the events. To fix ideas, suppose $\Omega = \mathcal{C}([0, +\infty), \mathbb{R})$ is the space of continuous trajectories that a stock may take, $\mathcal{F}$ is the σ-algebra containing all sets of the form $\{w \in \Omega : |w(s)| < R,\ s \leq t\}$ and $\mathbb{P}$ is the probability distribution of a zero-mean Gaussian with variance t. On the probability space $(\Omega, \mathcal{F}, \mathbb{P})$, we will model the underlying asset dynamics by a stochastic process. Before, we should introduce several concepts such that the notion of *Brownian motion* and *stochastic process*.

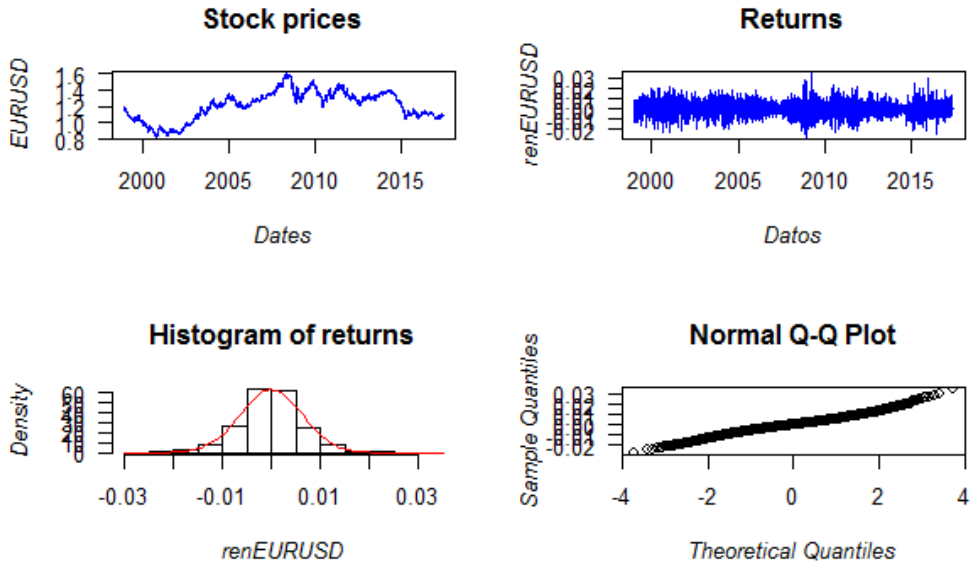

Figure 2.1: Daily closing prices of the stock Euro Dollar from 04/01/1999 until 11/05/2017, 4829 trading days. trading days.

2.1.1 The standard Brownian motion

The standard Brownian motion, also known as standard Wienner Process, plays a central role in the mathematical theory of finance since it constitutes a fundamental component in the construction of stochastic differential equations and represent a crucial engine for modeling the randomness in the financial market. Before introducing it, we define a stochastic process as a collection of random variables $\{X_t\}_{t \geq 0} = \{X_t(\omega) : t \geq 0,\ \omega \in \Omega\}$ given in $(\Omega, \mathcal{F}, \mathbb{P})$.

Definition 2.1 (Brownian motion)**.** *The real-valued stochastic process* $\{W_t\}_{t\geq 0}$ *defined in the probability space* $(\Omega, \mathcal{F}, \mathbb{P})$ *is called a Brownian motion if the following properties hold:*

1. W_t *has continuous trajectories starting at* 0 *(*$W_0 = 0$*).*
2. W_t *has independent increments: for any* $0 < t_1 < \cdots < t_n$ *the random variables* W_{t_1}, $W_{t_2} - W_{t_1}$,..., $W_{t_n} - W_{t_{n-1}}$ *are independent.*
3. *For any* $0 \leq s < t$*, the increment* $W_t - W_s$ *is normally distributed with zero mean and variance* $t - s$*. In particular,* $W_t \sim N(0, t)$*.*

The independence of increments makes the Brownian motion an ideal candidate to define a complete family of independent infinitesimal increments dW_t which will serve as a model of the random fluctuations of the stock price and its volatility. The main drawback is that the trajectories are not of bounded variation. Another important shortcoming is that although a Brownian motion is continuous everywhere, it is differentiable nowhere, that is, the derivative does not exist. Actually, one shows that it has fractal geometry.

2.1.2 Stochastic Differential Equations

We introduced the Brownian motion as a mean of modeling asset prices and volatility paths. However, a standard Brownian Motion has a non-zero probability of being negative. This is clearly not a property shared by real-world assets which cannot be less than zero. Hence, although it is convenient to retain the stochastic nature of a Brownian motion, adjustments need to be done, emerging the concept of Stochastic Differential Equation (SDE). First, one should note that some of the rules of ordinary calculus do not work as expected in the stochastic world. We need to modify them in order to take into account both the random behaviour of Brownian Motion and its non-differentiable nature.

Definition 2.2 (Stochastic integral)**.** *The stochastic integral of a process* $\{f(X_t)\}_{t\geq 0}$ *with respect the Brownian motion* $\{W_t\}_{t\geq 0}$ *is defined as the stochastic process* $\{Y_t\}_{t\geq 0}$ *obtained by taking the limit in the* $L^2(\Omega)$ *mean-square sense of*

$$Y_t := \int_0^t f(X_s) dW_s = \lim_{N\to\infty} \sum_{k=1}^{N} f(X_{t_{k-1}}) \left(W_{t_k} - W_{t_{k-1}}\right) ,$$

where $t_k = \frac{kt}{N}$ *for* $k = 1, \ldots, N$*. In differential form, this equation reads*

$$dY_t = f(X_t) dW_t.$$

Definition 2.3 (Stochastic differential equation)**.** *Let* $\{X_t\}_{t\geq 0}$ *be a stochastic process and* $\{W_t\}_{t\geq 0}$ *a Brownian motion defined in a probability space* $(\Omega, \mathcal{F}, \mathbb{P})$*. A stochastic differential equation (SDE) is an expression of the form*

$$dX_t = \mu(t, X_t)\, dt + \sigma(t, X_t)\, dW_t, \tag{2.1}$$

which should be understood in integral form as

$$X_t = X_0 + \int_0^t \mu(s, X_s)\, ds + \int_0^t \sigma(s, X_s)\, dW_s. \tag{2.2}$$

The function μ is called the drift and corresponds to the deterministic part of the SDE, while the function σ is called the volatility coefficient and constitutes the random component. They should satisfy almost surely

$$P\left[\int_0^t |\mu(s, X_s)|\, ds < \infty, \forall t \geq 0\right] = 1,$$

$$P\left[\int_0^t \sigma(s, X_s)^2\, ds < \infty, \forall t \geq 0\right] = 1.$$

Theorem 2.1 (Existence and uniqueness)**.** *Consider the stochastic differential equation (2.1). Assume that μ and σ satisfy the following growth condition*

$$|\mu(t,x)| + |\sigma(t,x)| \leq C_1(1 + |x|), \qquad t \in [0,T],\ x \in \mathbb{R},$$

for some constant C_1. Then the global existence of solution is guaranteed. Additionally, if the following Lipshitz condition holds

$$|\mu(t,x) - \mu(t,y)| + |\sigma(t,x) - \sigma(t,y)| \leq C_2 |x - y|, \qquad t \in [0,T],\ x, y \in \mathbb{R},$$

for some constant C_2, then the SDE has a unique continuous solution $X(t)$ given by (2.2).

2.1.3 Itô's Formula

Itô's Formula is an essential tool to determine the derivative of a time-dependent function of a stochastic process $g(t, X_t)$ as well as being very useful for solving SDEs. The formula performs the role of the chain rule in a stochastic setting, analogous to the chain rule in ordinary differential calculus.

Theorem 2.2 (Itô's Formula)**.** *Let $\{X_t\}_{t\geq 0}$ be a stochastic process driven by a SDE of the form (2.1) and let $g(x,t) \in C^2(\mathbb{R}^2)$. Then $g(t, X_t)$ is a new stochastic process and its differential is given by the so-called Itô's Formula*

$$\begin{aligned} dg(X_t, t) = &\left(\frac{\partial g}{\partial t}(X_t, t) + \mu(X_t, t)\frac{\partial g}{\partial x}(X_t, t) + \frac{1}{2}\sigma^2(X_t, t)\frac{\partial^2 g}{\partial x^2}(X_t, t)\right) dt \\ &+ \sigma(X_t, t)\frac{\partial g}{\partial x}(X_t, t)\, dW_t, \end{aligned} \tag{2.3}$$

where it has been used that it holds $(dW_t)^2 = dt$ and $dt^2 = dt \cdot dW_t = 0$.

2.2 The Black-Scholes Model

This section gives a brief insight in the foundations of the celebrated Black-Scholes model and how it is applied for the valuation of European call and put options on a non-dividend-paying stock. The model of prices will be first derived and motivated making clear the assumptions and simplifications of the market. Efficient market hypothesis are particularly assumed. It basically says that current price fully reflects past history and responds immediately to any new information. Because of these assumptions, asset price is said to satisfy Markov properties which essential means that the probability distribution of the price at any particular future time is not dependent on the path followed by the price in the past.

Second, we introduce the concept of *financial derivative contract* and focus in European put and call options to derive the distinguished Black-Scholes Formulas that provides a closed-form expression to price these financial derivatives. Additionally, we make use of this model to introduce and illustrate several elemental concepts in derivative pricing such that the *risk-neutral measure*, *hedging and self-financing strategies* and the *connection of mathematical finance with partial differential equations (PDEs)*.

2.2.1 The market and stock price model

The Black-Scholes model assumes a market constituted by two underlying assets. One is a *risk-less asset* (cash, bond) which appreciates at the constant risk-less rate of return r and whose price B_t at time t satisfies the ordinary differential equation,

$$\frac{dB_t}{dt} = rB_t. \tag{2.4}$$

The price S_t of the other asset, the *risky stock* or *underlying asset*, corresponds to a continuous stochastic process. After an infinitesimal amount of time dt, the asset price changes by dS_t, to $S_t + dS_t$. Rather than measure the absolute change dS_t, we evaluate the return on the asset dS_t/S_t which is assumed to be constituted by two components that lead to the following stochastic differential equation (SDE),

$$\frac{dS_t}{S_t} = \mu dt + \sigma dW_t. \tag{2.5}$$

This SDE is known as geometric Brownian motion (GBM) and is the most popular stochastic processfor generating prices. The first component is predictible and deterministic. The parameter μ is called the drift rate and measures the average rate of growth of the stock price. The second term determines centered random fluctuations which are independent of the past up to time t. $\{W_t\}_{t\geq 0}$ is a standard Brownian motion, and $\sigma > 0$ is the volatility of the stock. The model supposes μ and σ to be constants, giving rise to the unique solution of the SDE (2.5) with initial condition S_0,

$$S_t = S_0 \exp\left(\nu W_t + \left(\mu - \frac{\nu^2}{2}\right) t\right), \tag{2.6}$$

where this formula is derived using Itô's Formula (2.3). We then deduce that the stock price S_t is a log-normally distributed random variable with mean $S_0 e^{\mu t}$ and variance $S_0^2 e^{2\mu t}\left(e^{\sigma^2}-1\right)$.

Further assumptions on the market need to be made, including the possibility of buying and selling any fraction of stock as well as borrowing and lending any amount of cash at risk-less rate. The market is also assumed to be efficient (market movements cannot be predicted), arbitrage-free (there is no way to make a risk-less profit) and frictionless (transactions without fees or costs).

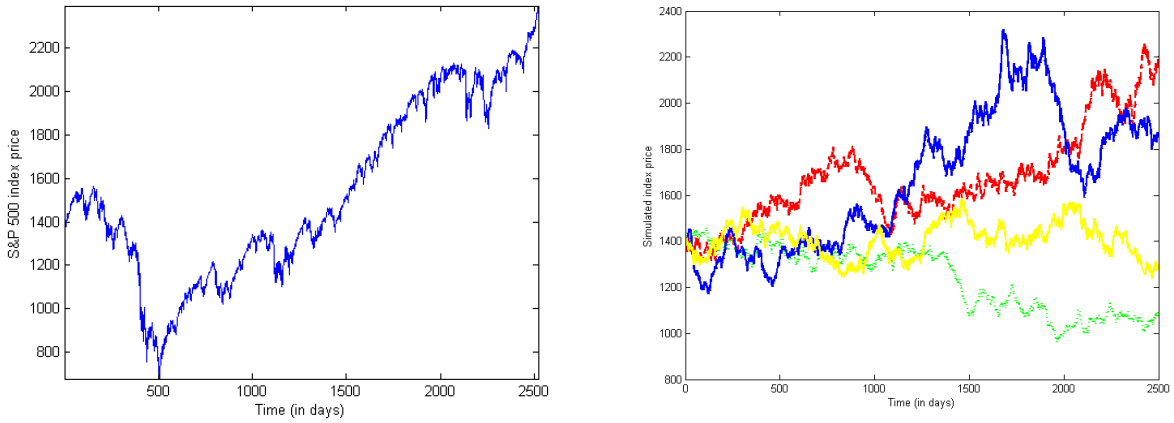

Figure 2.2: S&P index prices from March 03, 2007 to March 03, 2017 (left). Simulation of index prices using GBM dynamics with $\mu = 0.005$ and $\sigma = 0.1$ (right).

2.2.2 Derivative Contracts

We shall consider that there is a derivative security also trading in this market. A *derivative security*, also called *contingent claim*, can be seen as a insurance and hedging contract on the financial market in order to remove and avoid potential downside risk. A derivative derives its value from some underlying asset, hence the name derivative. Today derivatives can be derived by among different number of underlying assets: stocks, indexes, interest rates, commodities, electricity and so on. As one can see derivatives can be applied to almost any type of asset. There is a great variety of derivative contracts treated in the market. Actually, the market for derivatives is much bigger than the market of underlying assets and stocks themselves. We mainly focus here in forward and option contracts.

A Forward Contract is a type of derivative security in which the holder of the contract gives the obligation to buy/sell the underlying asset at some prescribed date T, known as *expiration or maturity date*, and a predetermined price or *strike price* K. The payer's position on a underlying asset S_t has the following value at maturity T, known as *pay-off function*,

$$F\left(S_T, T\right) := S_T - K.$$

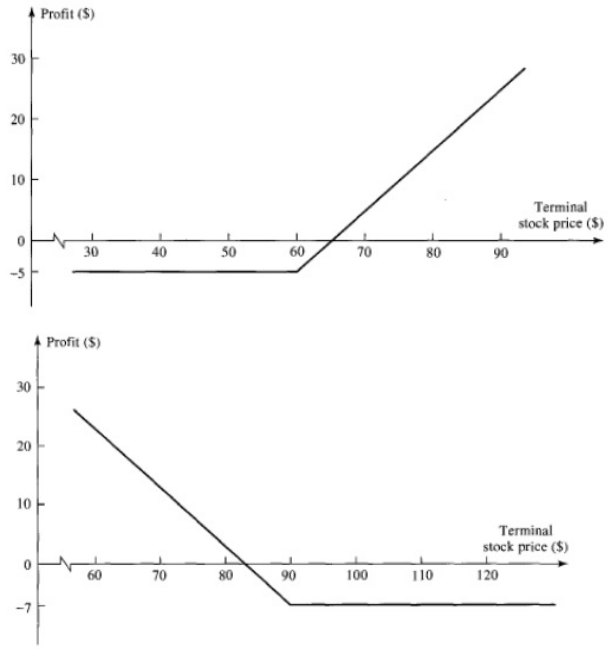

Figure 2.3: Pay-off function of a European call option and a European put option (left). Moneyness of call and put options (right).

An Option Contract is essentially the same as a forward contract, but instead to be forced to buy/sell the underlying asset at a specified date in the future, the option provides the holder with the choice to do it. The holder is thereby not forced to do something, and is only left with a positive outcome. In order to compensate this obvious advantage that the holder acquires, he must pay a premium on the date of writing the contract. The objective of option pricing is precisely to give a fair value to this premium. More generally, we are interested in the valuation of the option at any time t in the lifetime of the option $[0, T]$.

There are many different sorts of rules for how and when the option can be exercised. The simplest kind of option is the **European option** which can only be exercised on one specified expiration date T. In contrast, an **American option** can be exercised in any day during the option lifetime $[0, T]$. The options mentioned above are generally called *vanilla options* to express the fact that they are standardized and less interesting than *exotic options*.

We now focus on European call options and European put options since, as has already been mentioned, closed-form formulas will be derived later under the Black-Scholes model. A **European call option** consists on a contract which provides its holder with the option of purchasing the underlying asset at expiration date T for a predetermined strike price K. A **European put option** is defined in the analogue opposite way, where the holder of the option has the choice of selling the underlying asset with the same conditions. Their pay-off functions are given respectively by,

$$C(S_T, T) \;=\; (S_T - K, 0)_+ \;=\; \max\left(S_T - K, 0\right), \tag{2.7}$$

$$P(S_T, T) \;=\; (K - S_T, 0)_+ \;=\; \max\left(K - S_T, 0\right). \tag{2.8}$$

An important concept concerning option derivatives is that of moneyness. Moneyness of an option at time t is defined as the quotient of the strike and the stock price K/S_t and turns out to be an useful quantity that indicates whether the option is worth exercising or not. Three terms are used to define the moneyness of an option.

Definition 2.4 (ITM, OTM and ATM option)**.** *Let us consider an option at a given time t. We say that the option is in-the-money (ITM) if it would produce a cash inflow for the holder by exercising it at that time. In contrast, an out-of-the money (OTM) option would not produce any benefit if it were exercised at time t. Finally, we say that the option is at-the-money (ATM) is its value equals the strike price at time t.*

The moneyness categories listed in the following table will be used throughout this thesis:

MONEYNESS	**CALL**	**PUT**
<0.94	deep ITM	deep OTM
0.94 - 0.97	ITM	OTM
0.97 - 1.03	ATM	ATM
1.03 - 1.06	OTM	ITM
>1.06	deep OTM	deep ITM

Table 2.1: Moneyness of call and put options.

2.2.3 Connection with partial differential equations

The Black-Scholes analysis of a European-style derivative leads to a replicating strategy in the underlying stock and bond whose terminal payoff equals the payoff of the derivative at maturity. Thus, selling the derivative and holding this dynamically adjusted portfolio covers an investor against all risk of eventual loss. The essential step in this methodology is the construction of a replicating strategy and arguing, based on no arbitrage, that its value at time t is the fair price of the derivative. This argument will also allow us to derive the celebrated Black-Scholes partial differential equation.

Definition 2.5 (Self-financing replicating portfolio)**.** *Consider a market consisting on a risk-less asset with price e^{rt} and K risky assets with share prices S_t^1, S_t^2, …, S_t^K. A portfolio is a vector whose entries are individual stochastic processes*

$$\phi_t \;=\; \left(\phi_t^0, \phi_t^1, \ldots, \phi_t^K\right),$$

where ϕ_t^i denotes the number of shares of asset i held at time t. The value of this portfolio at time t is given by the following linear combination

$$\Pi_t \;=\; \phi_t^0 e^{rt} \;+\; \phi_t^1 S_t^1 \;+\; \ldots \;+\; \phi_t^K S_t^K.$$

We say that the portfolio is self-financing if the variations of its value are only due to the variations of the underlying asset market, that is, it does not require an extra inversion during the trading period except for the initial capital,

$$d\Pi_t = r\phi_t^0 e^{rt}dt + \phi_t^1 dS_t^1 + \ldots + \phi_t^K dS_t^K. \tag{2.9}$$

Additionally, the portfolio is said to replicate a derivative with payoff $V(S_T, T)$ at maturity time T if its value coincides with the payoff of the derivative, that is,

$$V(S_T, T) = \phi_T^0 e^{rT} + \phi_T^1 S_T^1 + \ldots + \phi_T^K S_T^K.$$

Let us denote the pricing function for a European-style contract by $V(S,t)$. Our next goal is to construct a self-financing portfolio that replicates the derivative at maturity T and which consists on ϕ_t units of risk-less bond and $\triangle_t$ shares of stock. The replicating property and the impossibility of arbitrage opportunities yields that the value of the portfolio and the price of the derivative at time t coincide

$$\phi_t e^{rt} + \triangle_t S_t = V(S_t, t) \quad \text{for any } 0 \leq t \leq T. \tag{2.10}$$

Differentiating and using the self-financing condition (2.9) on the left-hand side and Itô's formula (2.3) on the right-hand side, one gets

$$\left(r\phi_t e^{rt} + \mu\triangle_t S_t\right)dt + \sigma\triangle_t S_t dW_t = \left(\mu S\frac{\partial V}{\partial S} + \frac{1}{2}\sigma^2 S^2\frac{\partial^2 V}{\partial S^2} + \frac{\partial V}{\partial t}\right)dt + \sigma S_t\frac{\partial V}{\partial S}dW_t,$$

where all the partial derivatives of V are evaluated at (S_t, t). Equating the coefficients of the dW_t term and using (2.10), we determine the self-financing replicating strategy

$$\triangle_t = \frac{\partial V}{\partial S}(S_t, t), \quad \phi_t = \left(V(S_t, t) - \frac{\partial V}{\partial S}(S_t, t)\, S_t\right)e^{-rt}.$$

Finally, equating the dt term, using the expressions of ϕ_t and $\triangle_t$, and rearranging terms, one gets the so-called Black-Scholes partial differential equation

$$\frac{\partial V}{\partial t} + \frac{1}{2}\sigma^2 S^2\frac{\partial^2 V}{\partial S^2} + rS\frac{\partial V}{\partial S} - rV = 0. \tag{2.11}$$

2.2.4 The Arbitrage Free Price

In this section, we provide another general approach that gives us an expression to price a derivative contract and which will be a key result to derive the SWIFT method in both Chapter 3 and 4. This result is the so-called *Risk Neutral Valuation Formula* or *Feynman-Kac Formula* and states that any asset risky and non-risky will all have the same expected return as the risk-free rate of interest r. This essentially means that in a risk neutral world, where it does not exist arbitrage opportunity, all assets will have the same expected return. Next, we proceed to formulate the mentioned Feynman-Kac Theorem.

Theorem 2.3 (Feymann-Kac Theorem)**.** *Let us consider a derivative contract whose pay-off function is denoted by $V(S_t, t)$. The arbitrage free price $\Pi(t, V)$ at time t of this contingent claim is given by*

$$\Pi(t, V) \;=\; e^{-r(T-t)}\mathbb{E}^{\mathbb{Q}}\left(V\left(S_t, T\right)|\mathcal{F}_t\right) \;=\; e^{-r(T-t)}\int_{\mathbb{R}} V\left(y, T\right) f\left(y|\mathcal{F}_t\right) dy,$$

where $\mathbb{Q}$ denotes the risk-neutral probability measure and $\mathcal{F}_t$ is the filtration which contains all the information about the underlying asset price S_t until time t. We have also introduced the conditional probability density function for the asset prices $f\left(y|\mathcal{F}_t\right)$.

The Feymann-Kac Formula essentially says that the option value at time t can be computed as a discounted expectation of the pay-off function under the risk-neutral probability measure $\mathbb{Q}$. One also deduces from the integral expression of the Feymann-Kac Formula that the value of a derivative contract can be uniquely determined if the pay-off function and the probability density function are available. Precisely, we will explode this last expression in the following chapters to price options by approximating the probability density function of the process. Finally, it is worth noting that the Feymann-Kac Formula solves a PDE similar to (2.11), thus both approaches to price options are closely connected.

2.2.5 The Black-Scholes Formula

The Black-Scholes PDE (2.11) together with terminal and boundary conditions allow to price any derivative security depending on the current stock value S_t and on t. Particularly, it gives a closed formula for plain vanilla options. Let us consider the simplest financial derivative, a European call option. The payoff of the option determines the final condition

$$C(S_T, T) \;=\; \left(S_T - K, 0\right)_+ \;=\; \max\left(S_T - K, 0\right). \tag{2.12}$$

Our asset-price boundary conditions must be applied at $S = 0$ and as $S \to \infty$. We can see from (2.5) that if S is ever zero then dS is also zero and S can never change. Additionally, if $S = 0$ at expiry the payoff is zero. Thus on $S = 0$ the call option is worthless

$$C(0, t) \;=\; 0. \tag{2.13}$$

Increasing the asset price makes the call option more likely to be exercised and the magnitude of the strike becomes less and less important. Actually, it is immediate to deduce that the value of the option becomes that of the asset in the limit, that is,

$$C(S_t, t) \sim S_t \quad \text{as} \quad S_t \to \infty. \tag{2.14}$$

After performing several changes of variables, the Black-Scholes PDE (2.11) and the conditions (2.12), (2.13) and (2.14) become the one-dimensional Heat equation problem on the real line which gives rise to the acclaimed Black-Scholes Formula for the price of a European call option. This expression could also have been derived with the Feymann-Kac Formula.

Theorem 2.4 (The Black-Scholes Formula)**.** *The value of an European call option at time t with strike K and expiration date T given by the Black-Scholes model is*

$$C_{BS}(S_t, t) = S_t N(d_+) - K e^{-r(T-t)} N(d_-), \tag{2.15}$$

where $N(\cdot)$ is the cumulative distribution function of a standardised normal random variable given by

$$N(x) = \frac{1}{\sqrt{2\pi}} \int_{-\infty}^{x} e^{-\frac{1}{2}y^2} dy,$$

and

$$d_\pm = \frac{\log(S_t/K) + \left(r \pm \frac{1}{2}\nu^2\right)(T-t)}{\nu\sqrt{T-t}}.$$

We will denote C_{BS} by $C_{BS}(t, S; K, T; \nu)$ to emphasize the dependence on the parameters K, T and ν. Only the volatility ν, the standard deviation of the returns scaled by the square root of the time increment, needs to be estimated from data.

2.3 Limitations of Black-Scholes Model

Once the Black-Scholes Model has been introduced and analyzed, several natural questions about its validity arise: How well do Black-Scholes option prices fit market prices? Are the probability distributions of asset prices really lognormal? Does the price market volatility remain constant? In this section we answer these questions and we see that this model is not that accurate in capturing the features in the stock markets in reality. There are several major drawbacks of the Black-Scholes model, mainly because the idealized assumptions do rarely hold in the real world. First, the volatility smile is simply a violation of the constant volatility assumption. Secondly, the assumption of a lognormal distribution of stock prices is under critique. Combined factors of extreme events, fat tails, high peak and volatility clustering make the assumption of non-lognormal distribution more appropriate.

2.3.1 Implied volatility and the Smile Curve

One of the attractive features of the Black-Scholes model is that the parameters in the model other than the volatility σ (the expiration time T, the strike K, the risk-free interest rate r and the current stock price S_0) are unequivocally observable in the market and can be considered as inputs of the model. All other things being equal, an option's theoretical value is a monotonic increasing function of implied volatility:

$$\frac{\partial C_{BS}}{\partial \sigma}(t, S) = \frac{S e^{-\frac{d_+^2}{2}} \sqrt{T-t}}{\sqrt{2\pi}} > 0. \tag{2.16}$$

This property allows us to define uniquely the concept of implied volatility which turns out to be a useful quantity to test the model and reveal its limitations in practice.

Definition 2.6 (Implied Volatility)**.** *Given an observed European call option price C_{obs} for a contract with strike K and expiration date T, the implied volatility I_{BS} is defined to be the value of the volatility parameter that must go into Black-Scholes formula (2.15) to match this price:*

$$C_{BS}\left(t, S; K, T; I_{BS}\right) = C_{obs}. \tag{2.17}$$

At first glance, implied volatility seems a convenient tool to tweak the input volatility parameter to make the Black-Scholes formula work. If the Black-Scholes model held, meaning that observed options prices equaled the Black-Scholes prices $C_{BS}\left(t, S; K, T; \sigma\right) = C_{obs}$, then $I_{BS} = \sigma$. That is, the implied volatility for the stock would be the same constant for all strikes K and maturities T. In practice, the volatility surface (the 3D graph of implied volatility against strike and expiration) is not flat as one would expect. In particular, the most quoted phenomenon testifying to the limitations of the model is the so-called smile effect: the implied volatilities are not constant across the range of options prices but vary with strike price. This phenomenon is illustrated in Figure 2.4 for the equity index S&P 500. The Standard & Poor's 500, often abbreviated as the S&P 500, is an American stock market index based on the market capitalizations of 500 large companies having common stock listed on the NYSE or NASDAQ. Figure 2.4 particularly shows a higher implied volatility in out-of-the-money options than at-the-money and in-the-money options.This phenomenon is commonly found in equity markets and risky assets where derivatives such as index options are traded. Actually, implied volatility is closely affected by the supply and demand relationship. A plausible explanation for the volatility smile of Figure 2.4 is that in-the-money options are

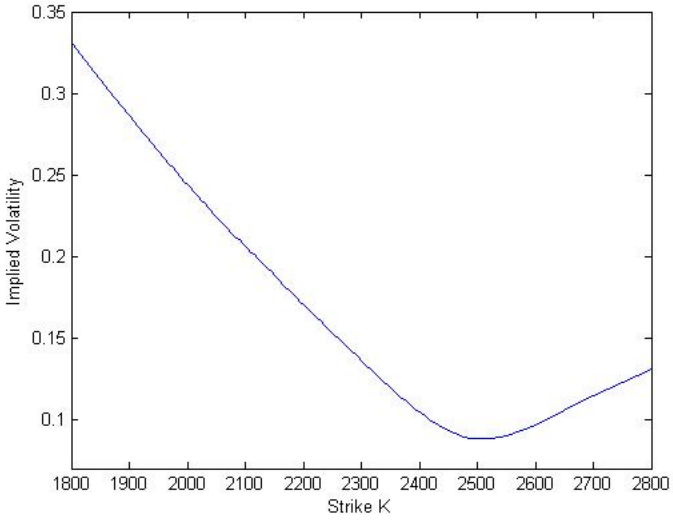

Figure 2.4: S&P 500 implied volatility curve as a function of strike K from SP 500 index options on February 24, 2017. The current index value is $S_0 = 2367.34$ and options have over 50 trading days to maturity.

more desired by investors and consequently lower strikes are heavily traded. Because increased demand bids the prices of such options up and option prices are a monotonic increasing functions of I_{BS}, the implied volatility seems to be higher. Another possible explanation for the smile paradigm is that options with strike prices increasingly farther from the current spot price of the underlying asset account for extreme market moves. Such events are characterized by extreme volatility and increase the price of an option.

2.3.2 Shortcomings of lognormal distribution

We assume in subsection 2.2.1 that underlying asset prices dS_t/S_t are log-normally distributed random variables. In order to test this assumption, it is convenient to consider the daily stock log-returns $\log(S_t/S_{t-1})$. This quantity turns out to be a normal distribution with mean $r - \frac{\sigma^2}{2}$ and variance σ^2. Unfortunately, the properties of the Gaussian distribution fails to capture the probability of extreme events in the real market. A normal distribution states that, given enough observations, all values in the sample will be distributed equally above and below the mean. About 99.7% of all variations falls within three standard deviations of the mean and therefore there is only a 0.3% chance of an extreme event occurring.

However, history would suggest financial markets don't always act this way and rather, they exhibit fatter tails and higher peak than traditionally predicted. This fact is illustrated in Figure 2.5 where one can notice that S&P 500 index log-returns distribution is highly peaked and fat-tailed relative to the normal distribution. Additionally, the Q-Q plot in Figure 2.6 shows just how extreme the tails of the empirical distribution are relative to the normal distribution. This plot would be a straight line if the empirical distribution were normal. Fat tails returns are usually consequence of traumatic "real-world" events including an oil shock, a large corporate bankruptcy or an abrupt change in a political situation. They also have some behavioral origins investor such as excessive optimism or pessimism.

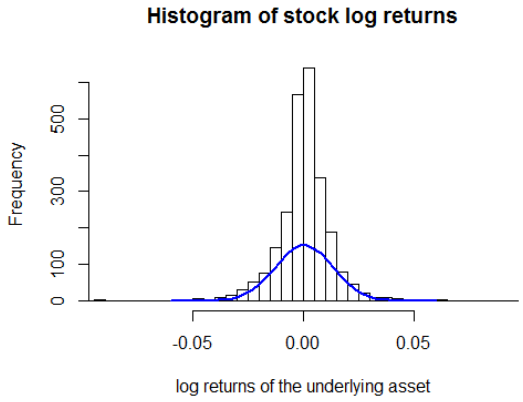

Figure 2.5: S&P 500 log-return histogram compared with the normal distribution.

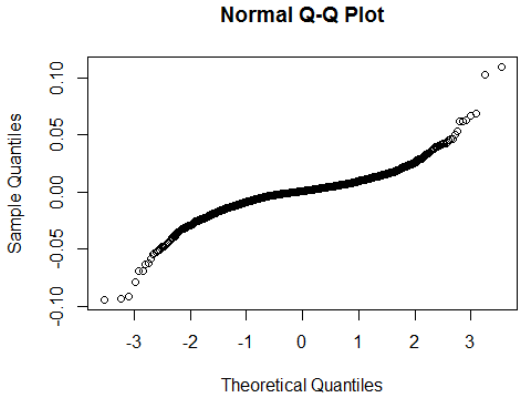

Figure 2.6: Normal Q-Q Plot showing that S&P 500 index has heavy tails.

Chapter 3

The Shannon Wavelet Inverse Fourier Technique for pricing European Options

The pricing of European options in computational finance is governed by the numerical solution of partial differential or partial integro-differential equations. However, option pricing is often done by the discounted expected payoff approach, which is nothing but a Green's function integral formulation for the PDEs mentioned. The connection between the solution of the option pricing PDEs and the discounted expected payoff lies in the Feynman-Kac theorem. It states that the corresponding solution $v(x,t)$ at time t can also be found as a discounted expectation of the option value at final time $t = T$, the acclaimed pay-off function, as follows:

$$v\left(x,t\right) \;=\; e^{-r(T-t)}\mathbb{E}^{\mathbb{Q}}\left(v\left(x,T\right)|x\right) \;=\; e^{-r(T-t)}\int_{\mathbb{R}} v\left(y,T\right) f\left(y|x\right) dy.$$

In many cases in option pricing, we do not have the Green's function $f\left(y|x\right)$ (also known as the conditional probability density function for the asset prices) available, but we do have its Fourier transform, that is, its characteristic function. A strain of literature exploiting this fact to develop highly efficient pricing numerical methods already exists.

In this chapter, we present a robust, accurate and highly efficient financial option valuation technique, the so-called *SWIFT method* (Shannon wavelet inverse Fourier technique). This is a numerical wavelets method based on the usage of the Shannon wavelets to accurately invert the Fourier transform of the density function $f\left(y|x\right)$.

The chapter will be organized as follows. In sections 3.1 and 3.2, we provide a brief summary of multiresolution analysis and Shannon wavelets. This theory will be launched in section 3.3 to develop the SWIFT method: first we consider an expansion of the density function $f\left(y|x\right)$ in terms of the Shannon scaling functions and provide two efficient alternatives to compute the density coefficients, one relying on the Vieta's formula and the other one based on Parseval's identity. Finally, in section 3.4 we apply the method for several Eu-

ropean options and derive the expression of its pay-off coefficients. In section 3.5 numerical examples are given for different asset-price dynamics.

3.1 Multiresolution analysis and wavelets

In the derivation of the *SWIFT method* in section 3.3, we will assume that the density probability function belongs to the Lebesgue space $L^2(\mathbb{R})$ of square integrable functions,

$$L^2(\mathbb{R}) = \left\{ f : \int_{\mathbb{R}} |f(x)|^2 \, dx < \infty \right\}.$$

Our aim is to construct a general structure for wavelets in this space which will allow us to decompose the density function f as the sum of a wavelets orthonormal basis and truncate it to an accurate level of resolution. We shall start with the introduction of the concept of multiresolution analysis.

Definition 3.1 (Multiresolution analysis)**.** *A multiresolution analysis of the space of square integrable functions $L^2(\mathbb{R})$ consists on a family of closed nested subspaces*

$$\{0\} \subset \cdots \subset V_{-n} \subset \cdots \subset V_{-1} \subset V_0 \subset V_1 \subset \cdots \subset V_n \subset \cdots \subset L^2(\mathbb{R}),$$

satisfying the following completeness and self-similarity properties:

1. *Completeness: the union of these nested subspaces fill the whole space and they are not too rebundant, that is, their intersection contains only the zero element,*

$$\overline{\bigcup_{j\in\mathbb{Z}} V_j} = L^2(\mathbb{R}), \quad \bigcap_{j\in\mathbb{Z}} V_j = \{0\}.$$

2. *Self-similarity in time: each subspace V_j is invariant under shifts by multiples of 2^j,*

$$f(x) \in V_j \iff f\left(x - m \cdot 2^j\right) \in V_j, \quad \text{for all } m \in \mathbb{Z}.$$

3. *Self-similarity in scale: all subspaces are time-scaled versions of each other, that is,*

$$f(x) \in V_j \iff f\left(2^{l-j}x\right) \in V_l, \quad \text{for all } l, j \in \mathbb{Z}.$$

The conditions of definition 3.1 ensure the existence of a function $\phi \in V_0$ such that the model space V_0 is generated by its integer shifts. This function ϕ is known as the *scaling function* or *father wavelet* since the family of functions $\{\phi_{j,k}\}_{k\in\mathbb{Z}}$ defined as

$$\phi_{j,k}(x) = 2^{j/2}\phi\left(2^j x - k\right), \tag{3.1}$$

generates an orthonormal basis for each one of the remaining multiresolution subspaces V_j.

With the aim of constructing wavelets given the multiresolution analysis $\{V_j\}_{j\in\mathbb{Z}}$, we introduce a new family of subspaces $\{W_j\}_{j\in\mathbb{Z}}$ defined in such a way that $V_j \oplus W_j = V_{j+1}$. In other words, W_j is the space of functions in V_{j+1} but not in V_j. This family of subspaces gives rise to an orthogonal decomposition of the space of square integrable functions

$$\oplus \sum_{j\in\mathbb{Z}} W_j = L^2(\mathbb{R}).$$

In the same way that happened with the subspaces $\{V_j\}_{j\in\mathbb{Z}}$, one can show that there exists a function $\psi \in W_0$, called the *mother wavelet* such that the family $\{\psi_{j,k}\}_{k\in\mathbb{Z}}$ defined by

$$\psi_{j,k}(x) = 2^{j/2}\psi\left(2^j x - k\right), \tag{3.2}$$

forms an orthonormal basis for each W_j and $\{\psi_{j,k}\}_{j,k\in\mathbb{Z}}$ is a wavelet basis of $L^2(\mathbb{R})$. As a consequence, a projection map on the subspace V_m can be defined.

Proposition 3.1 (Projection map)**.** *Let $P_m : L^2(\mathbb{R}) \longrightarrow V_m$ be the projection map of $L^2(\mathbb{R})$ onto the multiresolution subspace V_m. Then, any $f \in L^2(\mathbb{R})$ can be expanded as*

$$\begin{aligned} P_m f(x) &= \sum_{j=-\infty}^{m-1} \sum_{k=-\infty}^{\infty} d_{j,k}\psi_{j,k}(x) \\ &= \sum_{k=-\infty}^{\infty} c_{m,k}\phi_{m,k}(x), \end{aligned} \tag{3.3}$$

where $d_{j,k} = \int_{\mathbb{R}} f(x)\psi_{j,k}(x)dx$ are the wavelet coefficients *and $c_{m,k} = \int_{\mathbb{R}} f(x)\phi_{m,k}(x)dx$ are the* scaling coefficients.

Note that the first equality in (3.3) is a truncated wavelet series obtained from the projection of f onto $V_m = \oplus\sum_{j=-\infty}^{m-1} W_j$, hence, considering higher values of m, the accuracy of the truncated series improves. The second equality is just an equivalent sum in terms of the basis functions $\{\phi_{m,k}\}_{k\in\mathbb{Z}}$ of V_m.

3.2 Shannon Wavelets

For our future analysis in this thesis, we shall focus in a specific wavelet family, the so-called *Shannon wavelet family*. The starting point for its definition is the *cardinal sine function* or *sinc function* which constitute the Shannon scaling or father function

$$\phi(x) = \operatorname{sinc}(x) = \frac{\sin(\pi x)}{\pi x}.$$

Its dilated and translated instances forms the Shannon scaling functions,

$$\phi_{m,k}(x) = 2^{m/2}\phi\left(2^m x - k\right) = 2^{m/2}\frac{\sin\left(\pi\left(2^m x - k\right)\right)}{\pi\left(2^m x - k\right)}, \quad m,k \in \mathbb{Z}. \tag{3.4}$$

It holds that the functions $\{\phi_{m,k}\}_{k\in\mathbb{Z}}$ forms an orthonormal basis of its spanned subspace V_m. Thus, the sequence $\{V_m\}_{m\in\mathbb{Z}}$ gives a multiresolution analysis and the theory introduced in section 3.1 applies. Particularly, an orthogonal decomposition of the space $L^2(\mathbb{R})$ in subspaces $\{W_m\}_{m\in\mathbb{Z}}$ and a wavelet basis $\{\psi_{m,k}\}_{m,k\in\mathbb{Z}}$ can be defined. The wavelet functions in W_m are given in this case by

$$\psi_{m,k}(x) = 2^{m/2}\frac{\sin(\pi(2^m x-k-1/2))-\sin(2\pi(2^m x-k-1/2))}{\pi(2^m x-k-1/2)},\quad k\in\mathbb{Z}. \tag{3.5}$$

Since only the characteristic function is known in most cases, it turns out convenient to work in the frequency domain. Consequently, the Fourier transform of the scaling and wavelet functions should be considered

$$\hat{\phi}_{m,k}(w) = \frac{e^{-i\frac{k}{2^m}w}}{2^{m/2}}\text{rect}\left(\frac{w}{2^{m+1}\pi}\right), \tag{3.6}$$

$$\hat{\psi}_{m,k}(w) = -\frac{e^{-i\frac{k+1/2}{2^m}w}}{2^{m/2}}\left(\text{rect}\left(\frac{w}{2^m\pi}-\frac{3}{2}\right)+\text{rect}\left(-\frac{w}{2^m\pi}-\frac{3}{2}\right)\right), \tag{3.7}$$

where *rect* denotes the *rectangle* function which is defined as following

$$\text{rect}(x) = \begin{cases} 1 & \text{if } |x|<1/2 \\ 1/2 & \text{if } |x|=1/2 \\ 0 & \text{if } |x|>1/2 \end{cases}.$$

Figure 3.1 shows the Shannon scaling function, the Shannon mother wavelet and their Fourier transforms. Since the expressions (3.4) and (3.6) are simpler, our analysis will be mainly focused on the Shannon scaling functions $\phi_{m,k}$ rather than the wavelet functions $\psi_{m,k}$.

3.3 The SWIFT method

In this section, the *SWIFT method* is presented. As has already been mentioned, this numerical technique relies on the Shannon wavelets introduced in last section to accurately invert the characteristic function of the the asset price.

To this end, we consider an expansion of the density function f in terms of the Shannon scaling fuctions at a fixed approximation level m and recover the coefficients from their Fourier transforms. We provide two different alternatives to compute the coefficients. The first one expands the cardinal sinus function into a combination of cosines by making use of the celebrated *Vieta's formula*. The second one is based on the application of *Parseval's identity* which avoids the truncation of the infinite domain of integration due to the compact support of the Fourier transform of the Shannon basis functions.

Although both approaches are very similar in terms of efficiency, we will select the first one since a bound to estimate the trucantion error can be found.

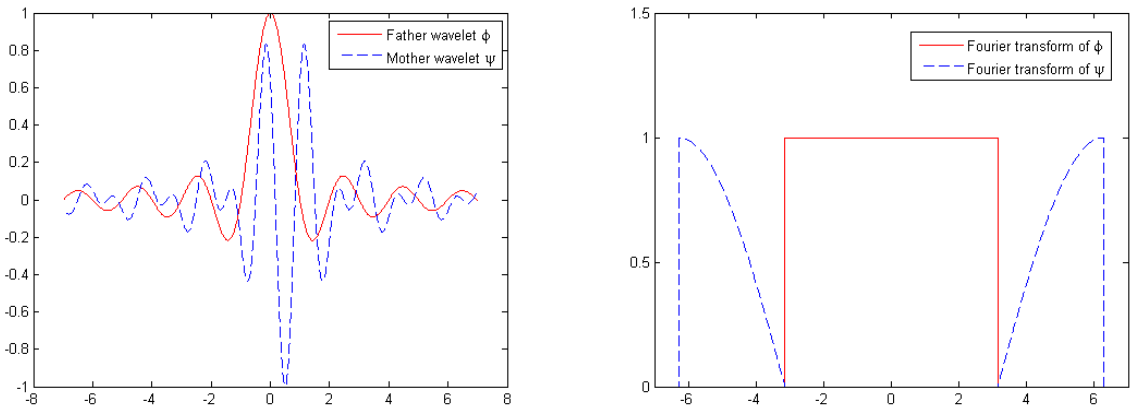

Figure 3.1: The thick red line shows the Shannon father function $\phi(x)$ (left) and its Fourier transform $\hat{\phi}(x)$ (right). The dashed blue line display the Shannon mother function $\psi(x)$ (left) and its Fourier transform $\hat{\psi}(x)$ (right)

.

3.3.1 Approximation of the density function

Let f denote the probability density function of certain continuous random variable X. Our aim in this chapter is to derive an approximation of f by making use of the Shannon scaling functions (3.4) at a fixed approximation level m. Assume f belongs to $L^2(\mathbb{R})$. Following the wavelet theory, f can be represented by

$$f(x) = \sum_{j,k\in\mathbb{Z}} d_{j,k}\psi_{j,k}(x), \tag{3.8}$$

where $\{\psi_{m,k}\}_{m,k\in\mathbb{Z}}$ is assumed to be the Shannon wavelet family (3.5). The first step is to truncate this infinite sum into a finite sum at a level of resolution m. To do this, we consider $P_m f$, being P_m the projection map defined in proposition 3.1. We obtain

$$f(x) \approx P_m f(x) = \sum_{j<m}\sum_{k\in\mathbb{Z}} d_{j,k}\psi_{j,k}(x) = \sum_{k=-\infty}^{\infty} c_{m,k}\phi_{m,k}(x). \tag{3.9}$$

The expression of the error of this approximation can be determined by subtracting the representation of f (3.8) from its truncation $P_m f$ and using the orthonormality of the Shannon wavelet family in $L^2(\mathbb{R})$,

$$\|f - P_m f\|_2^2 = \sum_{j\geq m}\sum_{k\in\mathbb{Z}} |d_{j,k}|^2 . \tag{3.10}$$

Note that taking the limit $m \to \infty$, it follows that $P_m f$ converges to f in $L^2(\mathbb{R})$. Actually, the truncation error (3.10) is closely related with the Fourier transform of f. In effect, recall

that $d_{j,k} = \langle f, \psi_{j,k} \rangle$. By Parseval's identity and expression (3.6),

$$\begin{aligned} \langle f, \psi_{j,k} \rangle &= \frac{1}{2\pi} \left\langle \hat{f}, \hat{\psi}_{j,k} \right\rangle \\ &= -\frac{2^{-j/2}}{2\pi} \left(\int_{2^j\pi}^{2^{j+1}\pi} \hat{f}(w)\, e^{\frac{iw(k+1/2)}{2^j}} dw + \int_{-2^{+1}\pi}^{-2^j\pi} \hat{f}(w)\, e^{\frac{iw(k+1/2)}{2^j}} dw \right). \end{aligned}$$

From this expression we deduce the following bound for the wavelet coefficients $d_{j,k}$

$$|d_{j,k}| \leq 2^{j/2-1} \left(\max_{w\in[2^j\pi, 2^{j+1}\pi]} \left|\hat{f}(w)\right| + \max_{w\in[-2^{j+1}\pi, -2^j\pi]} \left|\hat{f}(w)\right| \right). \tag{3.11}$$

Therefore, the truncation error in (3.10) is highly dependent on the rate of decay of the Fourier transform. The approximation $P_m f$ still involves, however, the sum of infinite terms. It turns out convenient to truncate this infinite sum (3.9). The following lemma will allow us to choose a proper approximation.

Lemma 3.1. *Assume that the density function f decays to zero at plus and minus infinity. Then, $f\left(\frac{h}{2^m}\right) \approx 2^{\frac{m}{2}} c_{m,h}$, $h \in \mathbb{Z}$, and the scaling coefficients $c_{m,k}$ satisfy*

$$\lim_{k\to\pm\infty} c_{m,k} = 0. \tag{3.12}$$

Proof. From the expression of the scaling functions (3.4), one deduces that $\phi_{m,k}\left(\frac{h}{2^m}\right) = 2^{\frac{m}{2}}\delta_{k,h}$, being $\delta_{k,h}$ the Kronecker delta. Thus, if we evaluate the second equality of the approximation of in f (3.9), this gives us

$$f\left(\frac{h}{2^m}\right) \approx P_m f\left(\frac{h}{2^m}\right) = 2^{\frac{m}{2}} \cdot \sum_{k\in\mathbb{Z}} c_{m,k}\delta_{k,h} = 2^{\frac{m}{2}} c_{m.h}. \tag{3.13}$$

Since the density function is assumed to decay to zero at plus and minus infinite, the same will hold for the scaling coefficients $c_{m,k}$. □

Lemma 1 ensures that, for certain accurately chosen values k_1 and k_2, the infinite sum in (3.9) is well-approximated by a finite summation without loss of considerable density mass,

$$f(x) \approx P_m f(x) \approx f_m(x) := \sum_{k=k_1}^{k_2} c_{m,k}\phi_{m,k}(x). \tag{3.14}$$

Proceeding as before, an expression for the error of truncating the infinite series (3.9) can be achieved. In effect, subtracting $P_m f$ and its approximation f_m, and recalling that $\{\phi_{m,k}\}_{k\in\mathbb{Z}}$ constitutes an orthonormal basis of the subspace V_m one gets,

$$\|P_m f - f_m\|_2^2 = \sum_{k<k_1 \text{ or } k>k_2} |c_{m,k}|^2. \tag{3.15}$$

Thus, the error of this second truncation will depend on the size of scaling coefficients $c_{m,k}$, which in turn depend on the decay rate of f as we have seen in Lemma 3.1.

At this stage, it is worth pointing out a remarkable feature of Shannon scaling functions regarding the area underneath the density function f.

Remark 3.1. *An approximation of the area under the curve of the density function f can be computed while the coefficients are being calculated. We just need to apply a trapezoidal rule using as grid points $\left\{\frac{k_1}{2^m}, \frac{k_1+1}{2^m}, \ldots, \frac{k_2-1}{2^m}, \frac{k_2}{2^m}\right\}$. As shown in expression (3.13) in Lemma 3.1, the value of f evaluated at $h/2^m$ is directly obtained from the computation of the coefficient $c_{m,h}$. The resultant approximation of the area will be given by the following expression*

$$\mathcal{A} = \frac{1}{2^{m/2}}\left(\frac{c_{m,k_1}}{2} + \sum_{k_1<k<k_2} c_{m,k} + \frac{c_{m,k_2}}{2}\right) \approx 1. \tag{3.16}$$

The following proposition summarizes the most important results obtained in this section.

Proposition 3.2 (Approximation of the density function and error)**.** *Let f be a probability density function belonging to $L^2(\mathbb{R})$. For certain accurately values m, k_1 and k_2, the density function f is well-approximated by the following linear combination of Shannon scaling functions*

$$f(x) \approx f_m(x) = \sum_{k=k_1}^{k_2} c_{m,k}\phi_{m,k}. \tag{3.17}$$

Additionally, the L^2 error made by this truncation can be splitted in two terms

$$\|f - f_m\|_2^2 = \sum_{j>m}\sum_{k\in\mathbb{Z}} |d_{j,k}|^2 + \sum_{k<k_1 \text{ or } k>k_2} |c_{m,k}|^2. \tag{3.18}$$

The first term depends on the rate of decay of the Fourier transform of f and can be reduced by increasing the value of m. The second term depends on the decay of the function f and can be reduced by enlarging the width of the interval $[k_1, k_2]$.

3.3.2 Coefficients computation

In last section, we showed that the density probability function can be accurately approximated by the finite sum of Shannon scaling functions (3.17). The coefficients of this linear combination involve the computation of the following integrals

$$c_{m,k} = \langle f, \phi_{m.k}\rangle = \int_{\mathbb{R}} f(x)\,\bar{\phi}_{m,k}(x)\,dx = 2^{m/2}\int_{\mathbb{R}} f(x)\,\phi(2^m x - k)\,dx. \tag{3.19}$$

The main problem of this expression is that the density probability function f is unknown in most cases, becoming impossible the direct computation of coefficients $c_{m,k}$. Instead, one disposes of the Fourier transform $\hat{f}$. Thus, our next goal in this section is to present an

alternative to settle this problem. To this end, an approximation of the density coefficients $c_{m,k}$ based on the classical Vieta's formula is derived. The expression obtained will depend on the characteristic function $\hat{f}$ and allow us to provide an estimate for its error.

Vieta's Fomula (see [8]) gives rise to a representation of the cardinal sinus, *sinc(t)*, as the following infinite product of cosine functions

$$\operatorname{sinc}(t) = \prod_{j=1}^{\infty} \cos\left(\frac{\pi t}{2^j}\right). \tag{3.20}$$

If we truncate this expression by taking a finite product with J factors and make use of the cosine product-to-sum identity (see [27]), one gets the following finite approximation for the cardinal sine function,

$$\operatorname{sinc}(t) \approx \operatorname{sinc}^*(t) = \prod_{j=1}^{J} \cos\left(\frac{\pi t}{2^j}\right) = \frac{1}{2^{J-1}} \sum_{j=1}^{2^{J-1}} \cos\left(\frac{2j-1}{2^J}\pi t\right). \tag{3.21}$$

An approximation for the coefficient $c_{m,k}$ is consequently obtained replacing ϕ in (3.19) by its estimated expression (3.21),

$$c_{m,k} \approx c^*_{m,k} := \frac{2^{m/2}}{2^{J-1}} \sum_{j=1}^{2^{J-1}} \int_{\mathbb{R}} f(x) \cos\left(\frac{2j-1}{2^J}\pi\left(2^m x - k\right)\right) dx. \tag{3.22}$$

It turns out convenient, however, to rewrite approximation (3.22) in terms of the characteristic function $\hat{f}$ in order to sort out the problem with the unknown probability density function. This can be done by noticing that the real part of $\hat{f}\left(\frac{(2j-1)\pi 2^m}{2^J}\right) \mathrm{e}^{ik\pi\frac{2j-1}{2^J}}$ coincides with the integral in expression (3.22). We end up with:

$$c_{m,k} \approx c^*_{m,k} = \frac{2^{m/2}}{2^{J-1}} \sum_{j=1}^{2^{J-1}} \Re\left[\hat{f}\left(\frac{(2j-1)\pi 2^m}{2^J}\right) \mathrm{e}^{ik\pi\frac{2j-1}{2^J}}\right]. \tag{3.23}$$

Thus, we will approximate the density coefficients $c_{m,k}$ using expression (3.23). Nevertheless, several questions still arise since we should decide how to determine the truncation factor J to get an accurate estimation. The following lemma gives us an estimate of the error when approximating the sinus cardinal function. As we will observe, the convergence in a fixed interval is exponential.

Lemma 3.2. *Let us define the absolute error of the sinc approximation in (3.21) by* $\mathcal{E}_V(t) := \operatorname{sinc}(t) - \operatorname{sinc}^*(t)$ *and take* $c \in \mathbb{R}^+$. *Then for* $t \in [-c, c]$ *and* $J \geq \log_2(\pi c)$ *holds:*

$$|\mathcal{E}_V(t)| \leq \frac{(\pi c)^2}{2^{2(J+1)} - (\pi c)^2}.$$

Proof. Evaluating expression (3.20) at the point $t/2^J$ gives

$$\operatorname{sinc}\left(\frac{t}{2^J}\right) = \prod_{j=1}^{\infty} \cos\left(\frac{\pi t}{2^{j+J}}\right) = \prod_{j=J+1}^{\infty} \cos\left(\frac{\pi t}{2^j}\right),$$

deducing that $\operatorname{sinc}(t) = \operatorname{sinc}\left(\frac{t}{2^J}\right)\operatorname{sinc}^*(t)$. Therefore, the absolute error can be written as

$$|\mathcal{E}_V(t)| = \left|\operatorname{sinc}\left(\frac{t}{2^J}\right) - 1\right| |\operatorname{sinc}^*(t)| \leq \left|\operatorname{sinc}\left(\frac{t}{2^J}\right) - 1\right|. \tag{3.24}$$

If we take into account the Taylor series of the sinus cardinal function (see, for instance, [8])

$$\operatorname{sinc}\left(\frac{t}{2^J}\right) = \sum_{n\geq 0} (-1)^n \pi^{2n} \frac{1}{(2n+1)! \cdot 2^{2Jn}} |t|^{2n},$$

and using it in (3.24) leads to the following bound for the error

$$|\mathcal{E}_V(t)| \leq \sum_{n\geq 1} \pi^{2n} \frac{1}{(2n+1)! \cdot 2^{2Jn}} |t|^{2n}.$$

Recalling that $|t| \leq c$ and noticing that $\frac{1}{(2n+1)!} \leq \frac{1}{2^{2n}}$ for all $n \geq 1$, we obtain a geometric series which converges when $J \geq \log_2(\pi c)$ and, in this case, we have

$$|\mathcal{E}_V(t)| \leq \sum_{n\geq 1} \left(\frac{\pi c}{2^{J+1}}\right)^{2n} = \frac{(\pi c)^2}{2^{2(J+1)} - (\pi c)^2}.$$

□

Theorem 3.1 (Approximation of the density coefficients and error estimate)**.** *Let $f(x)$ be the probability density function and $F(x)$ the distribution function of a random variable X. Define $H(x) := F(-x) + 1 - F(x)$ and consider a constant $a > 0$ such that $H(a) < \epsilon$ for $\epsilon > 0$. Define $M_{m,k} := \max(|2^m a - k|, |2^m a + k|)$ and take $J \geq \log_2(\pi M_{m,k})$. Then, the density coefficients $c_{m,k}$ are well-approximated by the following expression:*

$$c_{m,k} \approx c^*_{m,k} = \frac{2^{m/2}}{2^{J-1}} \sum_{j=1}^{2^{J-1}} \Re\left[\hat{f}\left(\frac{(2j-1)\pi 2^m}{2^J}\right) e^{ik\pi\frac{2j-1}{2^J}}\right]. \tag{3.25}$$

Additionally, an error estimate for this approximation is given by

$$\left|c_{m,k} - c^*_{m,k}\right| \leq 2^{m/2}\left(2\epsilon + \sqrt{2a}\,\|f\|_2 \frac{(\pi M_{m.k})^2}{2^{2(J+1)} - (\pi M_{m.k})^2}\right). \tag{3.26}$$

Proof. The expression for the approximation of the density coefficients has already been deduced in (3.23). We just need to prove the error estimate (3.26). We begin observing that from (3.19) and (3.22) we find

$$\begin{aligned}\left|c_{m,k}-c_{m,k}^{*}\right| &= 2^{m/2}\left|\int_{\mathbb{R}} f(x)\left(\operatorname{sinc}\left(2^{m}x-k\right)-\operatorname{sinc}^{*}\left(2^{m}x-k\right)\right)dx\right| \\ &\leq 2^{m/2}\left[\int_{\mathbb{R}\setminus[-a,a]} f(x)\left|\operatorname{sinc}\left(2^{m}x-k\right)-\operatorname{sinc}^{*}\left(2^{m}x-k\right)\right|dx\right. \\ &+ \left.\int_{-a}^{a} f(x)\left|\operatorname{sinc}\left(2^{m}x-k\right)-\operatorname{sinc}^{*}\left(2^{m}x-k\right)\right|dx\right].\end{aligned} \tag{3.27}$$

Let us start examining the first integral in (3.27). As $F(x)$ is a the distribution function, for all $\epsilon>0$ should exist a positive constant $a>0$ satisfying $H(a)<\epsilon$. Bearing in mind that $\left|\operatorname{sinc}\left(2^{m}x-k\right)-\operatorname{sinc}^{*}\left(2^{m}x-k\right)\right|\leq 2$ for all $x\in\mathbb{R}$, one concludes that the first integral is bounded by 2ϵ. For the second integral in (3.27), we apply the Cauchy-Schwarz inequality

$$\begin{aligned}&\int_{-a}^{a} f(x)\left|\operatorname{sinc}\left(2^{m}x-k\right)-\operatorname{sinc}^{*}\left(2^{m}x-k\right)\right|dx \\ &\leq \|f\|_{2}\left(\int_{-a}^{a}\left|\operatorname{sinc}\left(2^{m}x-k\right)-\operatorname{sinc}^{*}\left(2^{m}x-k\right)\right|dx\right)^{\frac{1}{2}}.\end{aligned}$$

We observe that if $-a\leq x\leq a$, then $-2^{m}a-k\leq 2^{m}x-k\leq 2^{m}a-k$. Therefore, $2^{m}x-k\in[-M_{m,k},M_{m,k}]$ and Lemma 3.2 applies to deduce (3.26) and conclude the proof. □

Remark 3.2. *The most computationally involved part in (3.25) is the evaluation of $\hat{f}$ at the grid points. Thus, it may seem appropriate at first glance to take the smaller possible value of J for each k, that is, $J=\lceil\log_2(\pi M_{m,k})\rceil$, where $\lceil x\rceil$ denotes the smallest integer value greater or equal than x. It is more convenient, conversely, to fix a constant J for each k, defined here by $\jmath:=\lceil\log_2(\pi M_m)\rceil$, where $M_m:=\max_{k_1<k<k_2}M_{m,k}$. In this way, we can reduce the number of evaluations of $\hat{f}$ to only one at each grid point by using the Fast Fourier Transform (FFT) algorithm. We should rewrite expression (3.25) as follows:*

$$\begin{aligned}c_{m,k}^{*} &= \frac{2^{m/2}}{2^{\jmath-1}}\sum_{j=1}^{2^{\jmath-1}}\Re\left[\hat{f}\left(\frac{(2j-1)\pi 2^{m}}{2^{\jmath}}\right)e^{ik\pi\frac{2j-1}{2^{\jmath}}}\right] \\ &= \frac{2^{m/2}}{2^{\jmath-1}}\Re\left[e^{-\frac{ik\pi}{2^{\jmath}}}\sum_{j=1}^{2^{\jmath-1}}\hat{f}\left(\frac{(2j-1)\pi 2^{m}}{2^{\jmath}}\right)e^{\frac{ik\pi j}{2^{\jmath-1}}}\right] \\ &= \frac{2^{m/2}}{2^{\jmath-1}}\Re\left[e^{-\frac{ik\pi}{2^{\jmath}}}\sum_{j=0}^{2^{\jmath-1}-1}\hat{f}\left(\frac{(2j+1)\pi 2^{m}}{2^{\jmath}}\right)e^{\frac{ik\pi(j+1)}{2^{\jmath-1}}}\right] \\ &= \frac{2^{m/2}}{2^{\jmath-1}}\Re\left[e^{\frac{ik\pi}{2^{\jmath}}}\sum_{j=0}^{2^{\jmath-1}-1}\hat{f}\left(\frac{(2j+1)\pi 2^{m}}{2^{\jmath}}\right)e^{\frac{ik2\pi j}{2^{\jmath}}}\right].\end{aligned} \tag{3.28}$$

The last step is to assume that $\hat{f}\left(\frac{(2j+1)\pi 2^m}{2^J}\right) = 0$ *from* 2^{J-1} *to* $2^J - 1$*, so that the last equality* (3.28) *is equivalent to*

$$c^*_{m,k} = \frac{2^{m/2}}{2^{J-1}} \Re\left[e^{\frac{ik\pi}{2^J}} \sum_{j=0}^{2^J-1} \hat{f}\left(\frac{(2j+1)\pi 2^m}{2^J}\right) e^{\frac{ik2\pi j}{2^J}} \right]. \tag{3.29}$$

This expression (3.29) *allows to apply the FFT algorithm to compute the density coefficients. The computational complexity is reduced from* $\mathcal{O}\left(2^{J-1} \cdot (k_2 - k_1 + 1)\right)$ *when we use* (3.25) *to* $\mathcal{O}\left(\log(2) \cdot J \cdot 2^{J+1}\right)$ *by using the FFT algorithm.*

Remark 3.3. *The compactness of the support of the Fourier transform of the scaling functions* $\hat{\phi}_{m,k}$ *leads to an alternative technique to compute the density coefficients based on Parseval's identity. First of all, note that*

$$\begin{aligned} \left\langle \hat{f}, \hat{\phi}_{m.k} \right\rangle &= \frac{1}{2^{m/2}} \int_{\mathbb{R}} \hat{f}(w)\, e^{\frac{ikw}{2^m}}\, rect\left(\frac{w}{2^{m+1}\pi}\right) dw \\ &= \frac{1}{2^{m/2}} \int_{-2^m\pi}^{2^m\pi} \hat{f}(w)\, e^{\frac{ikw}{2^m}} dw \\ &= 2\pi 2^{m/2} \int_{-\frac{1}{2}}^{\frac{1}{2}} \hat{f}\left(2^{m+1}\pi t\right) e^{i2\pi kt} dt, \end{aligned} \tag{3.30}$$

where the change of variables $t := \frac{w}{2^{m+1}\pi}$ *has been performed in the last equality. Finally, using Parseval's identity together with expression* (3.30) *and recalling that the density coefficients are real-valued, we obtain*

$$c_{m,k} = \langle f, \phi_{m.k} \rangle = \frac{1}{2\pi} \left\langle \hat{f}, \hat{\phi}_{m.k} \right\rangle = 2^{m/2} \int_{-\frac{1}{2}}^{\frac{1}{2}} \Re\left(\hat{f}\left(2^{m+1}\pi t\right) e^{i2\pi kt} \right) dt. \tag{3.31}$$

Therefore, an approximation of the coefficients can be obtained by computing, for instance, a trapezoidal rule in (3.31)*. As before, this computation can be speed up by using the FFT transform.*

3.4 Option pricing problems

In the following subsections we will derive expressions for the computation of the pay-off coefficients for different European options. This will constitute the last step of the SWIFT method and will allow us to give an accurate estimate of the derivative value as we will see with further detail in the section of numerical results.

In order to apply the Wavelet Theory and approximation expressions derived in previous sections, we will employ the celebrated *Feynman-Kac formula*, where the option value at

time t is computed as a discounted expectation of the pay-off function under the risk-neutral probability measure $\mathbb{Q}$:

$$v(x,t) \;=\; e^{-r(T-t)}\mathbb{E}_{\mathbb{Q}}\left(v(y,T)|x\right) \;=\; e^{-r(T-t)}\int_{\mathbb{R}} v\left(y,T\right) f\left(y|x\right) dy, \tag{3.32}$$

where v denotes the option value, T is the maturity or expiration, t is the initial date, $\mathbb{E}_{\mathbb{Q}}$ is the expectation operator under the risk-neutral measure $\mathbb{Q}$, x and y are state variables at time t and T respectively, $f(y|x)$ is the probability density of y given x, and r is the deterministic risk-neutral risk.

In most cases, we only hold the characteristic function of the log-asset price as the Fourier transform of f. It turns out convenient then to represent the option values as functions of the scaled log-asset prices and denote these prices by

$$x \;=\; \ln\left(S_t/K\right) \quad \text{and} \quad y \;=\; \ln\left(S_T/K\right),$$

being S_t the underlying asset price at time t and K the strike price.

The strategy to follow to determine the price of the option is to approximate the density function f in terms of the Shannon scaling functions as stated in Proposition 3.2, that is,

$$f\left(y|x\right) \;\approx\; f_m\left(y|x\right) \;=\; \sum_{k=k_1}^{k_2} c_{m,k}\left(x\right)\phi_{m,k}\left(y\right), \tag{3.33}$$

where $c_{m,k}$ are the density coefficients which will be computed by applying the FFT in (3.29).

3.4.1 Cash-or-nothing options pricing

Cash-or-nothing options belong to the class of *binary options* in which the payoff is either some fixed monetary amount or nothing at all. We particularly consider a cash-or-nothing call option which pays some fixed amount of cash if the option expires in-the-money while it pays nothing otherwise. The pay-off function $v(y,T)$ in scaled log-asset space reads then

$$v\left(y,T\right) \;=\; \begin{cases} 1 & \text{if } y > 0, \\ 0 & \text{otherwise.} \end{cases}$$

If we replace the density f by its approximation f_m (3.33) in the valuation formula (3.32), we obtain an expression for the pay-off coefficients

$$\begin{aligned} v\left(x,t\right) \;&=\; e^{-r(T-t)}\int_0^{\infty} f\left(y|x\right) dy \\ &\approx\; v_1\left(x,t\right) \;=\; e^{-r(T-t)}\int_0^{\infty} f_m\left(y|x\right) dy \;=\; e^{-r(T-t)}\sum_{k=k_1}^{k_2} c_{m,k}\left(x\right) V_{m,k}, \end{aligned}$$

where we have defined the pay-off coefficients as $V_{m,k} = \int_0^\infty \phi_{m,k}(y)\,dy$. Notice, however, that this integral cannot be analytically computed. Next lemma states an alternative expression for these pay-off coefficients which will be the basis to derive an accurate approximation in Proposition 3.3.

Lemma 3.3. *The coefficients $V_{m,k}$ for a cash-or-nothing call option can be computed as*

$$V_{m,k} = \frac{1}{2^{m/2}}\left(sgn(k)\cdot Si(|k|)+\frac{1}{2}\right), \tag{3.34}$$

where sgn is the sign function and Si is the sine integral function defined respectively as

$$sgn(x) := \begin{cases} 1 & if\ x>0 \\ 0 & if\ x=0 \\ -1 & if\ x<0 \end{cases}, \qquad Si(x) := \int_0^x sinc(t)\,dt.$$

Proof. Bearing in mind the definition of the scaling functions $\phi_{m,k}$ and performing the change of variables $t = 2^m x - k$, the coefficient $V_{m,k}$ reads

$$\begin{aligned} V_{m,k} &= \int_0^\infty \operatorname{sinc}(2^m y - k)\,dy = \frac{1}{2^{m/2}}\int_{-k}^\infty \operatorname{sinc}(t)\,dt \\ &= \frac{1}{2^{m/2}}\left(\int_{-k}^0 \operatorname{sinc}(t)\,dt + \int_0^\infty \operatorname{sinc}(t)\,dt\right). \end{aligned}$$

The fact that $\int_0^\infty \operatorname{sinc}(t)\,dt = \frac{1}{2}$ concludes the proof. □

Proposition 3.3 (Approximation of cash-or-nothing pay-off coefficients and error estimate)**.** *Let $V_{m,k}$ be the pay-off coefficients for a cash-or-nothing call option. If we take $J \geq \log_2(\pi|k|)$, this coefficients can be accurately approximated by*

$$V_{m,k} \approx V^*_{m,k} := \frac{1}{2^{m/2}}\left(sgn(k)\cdot Si^*(|k|)+\frac{1}{2}\right), \tag{3.35}$$

where $Si^*(x)$ is an approximation of the sinc integral given by

$$Si^*(x) := \frac{2}{\pi}\sum_{j=1}^{2^{J-1}} \frac{1}{2j-1}\sin\left(\frac{2j-1}{2^J}\pi x\right). \tag{3.36}$$

Additionally, the absolute error made by this approximation can be bounded by

$$\left|V_{m,k} - V^*_{m,k}\right| \leq \frac{1}{2^{m/2}}\cdot\frac{sgn(k)\,\pi^2 k^3}{2^{2(J+1)} - (\pi k)^2}. \tag{3.37}$$

Proof. Let us first derive the sinc integral approximation. We just need to substitute the approximation of the sinc function (3.21) in $\mathrm{Si}(x)$,

$$\begin{aligned}\mathrm{Si}\,(x) \;\approx\; \mathrm{Si}^*\,(x) \;&=\; \sum_{j=1}^{2^{J-1}} \frac{1}{2^{J-1}} \int_0^x \cos\left(\frac{2j-1}{2^J}\pi y\right) dy \\ &=\; \frac{2}{\pi}\sum_{j=1}^{2^{J-1}} \frac{1}{2j-1}\sin\left(\frac{2j-1}{2^J}\pi x\right).\end{aligned}$$

We will approximate the pay-off coefficients by replacing $\mathrm{Si}(x)$ by its approximation $\mathrm{Si}^*\,(x)$ in expression (3.34) obtaining (3.35).

To derive the error estimate, we start noticing that

$$\left|V_{m,k} - V_{m,k}^*\right| \;=\; \frac{1}{2^{m/2}} \cdot |\mathrm{sgn}\,(k)| \cdot \left|\mathrm{Si}\,(|k|) - \mathrm{Si}^*\,(|k|)\right|.$$

If $k = 0$, it holds that $V_{m,k} = V_{m,k}^*$. Otherwise, $|\mathrm{sgn}\,(k)| = 1$ and therefore

$$\left|V_{m,k} - V_{m,k}^*\right| \;=\; \frac{1}{2^{m/2}} \cdot \left|\mathrm{Si}\,(|k|) - \mathrm{Si}^*\,(|k|)\right| \;\leq\; \int_0^{|k|} \left|\mathrm{sinc}\,(t) - \mathrm{sinc}^*\,(t)\right| dt.$$

If we take $J \geq \log_2(\pi\,|k|)$, Lemma 3.2 applies and leads to expression (3.37):

$$\int_0^{|k|} \left|\mathrm{sinc}\,(t) - \mathrm{sinc}^*\,(t)\right| dt \;\leq\; \int_0^{|k|} \frac{(\pi\,|k|)^2}{2^{2(J+1)} - (\pi\,|k|)^2} dt \;=\; \frac{\pi^2\,|k|^3}{2^{2(J+1)} - (\pi k)^2}.$$

□

Remark 3.4. *The evaluation of function $Si^*(x)$ turns out to be the most computationally involved part in equation (3.35). Several approaches may be taken in order to obtain an efficient computation. The first one is based on the observation that any of the values of $Si^*\,(|k|)$ depend on neither the parameters of the option pricing problem nor the scale of approximation m. Thus, we can calculate and store them at a high accuracy level beforehand using expression (3.36) and use them later. The second strategy is analogue to the one used for the density coefficients computation in Remark 3.2. First, we fix a constant J-value, defined here by $\bar{\jmath} := \left\lceil \log_2\left(\pi \bar{M}\right)\right\rceil$, where $\bar{M} := \max\left(|k_1|, |k_2|\right)$. Then, we rewrite expression (3.36) to apply an FFT algorithm to evaluate the sine integral function $Si^*(x)$ at integer values $|k|$,*

$$\begin{aligned}Si^*\,(|k|) \;&=\; \frac{2}{\pi}\sum_{j=1}^{2^{\bar{\jmath}-1}} \frac{1}{2j-1}\sin\left(\frac{2j-1}{2^{\bar{\jmath}}}\pi x\right) \;=\; \frac{2}{\pi}\sum_{j=0}^{2^{\bar{\jmath}-1}-1} \frac{1}{2j+1}\sin\left(\frac{2j+1}{2^{\bar{\jmath}}}\pi x\right) \\ &=\; \frac{2}{\pi}\Im\left[\sum_{j=0}^{2^{\bar{\jmath}-1}-1} \frac{1}{2j+1} e^{i\frac{j+1/2}{2^{\bar{\jmath}-1}}\pi x}\right] \;=\; \frac{2}{\pi}\Im\left[e^{\frac{i\pi x}{2^{\bar{\jmath}}}} \sum_{j=0}^{2^{\bar{\jmath}-1}-1} \frac{1}{2j+1} e^{i\frac{j}{2^{\bar{\jmath}-1}}\pi x}\right].\end{aligned}$$

Finally, we replace these values in formula (3.35) to obtain the pay-off coefficients. Note that the computational complexity of this second strategy is $\mathcal{O}\left(\log\left(2\right)\left(\bar{j}-1\right)2^{\bar{j}-1}\right)$*, while the complexity of a direct computation using formula (3.36) would be* $\mathcal{O}\left(2^{\bar{j}-1}\left(k_2-k_1+1\right)\right)$.

3.4.2 European options pricing

European options were introduced in section 2.2.2. Their pay-off prices in the asset space are given by expressions (2.12) and (2.8) and depend on the value taken by the underlying asset up to the expiration date T. As previously argued, it is more convenient to work in the log-asset space. Consequently, we perform a change of variables to obtain the pay-off function $v\left(y,T\right)$ in log-asset space,

$$v\left(y,T\right) \;=\; \left[\alpha\cdot K\left(e^{y}-1\right)\right]_{+} \quad \text{with} \quad \alpha \;=\; \begin{cases} 1 & \text{for a call,} \\ -1 & \text{for a put.} \end{cases}$$

We again approximate the density function f in terms of the Shannon scaling functions by f_m and truncate the infinite integration range to a finite domain $\mathcal{I}_m := \left[\frac{k_1}{2^m},\frac{k_2}{2^m}\right]$, where k_1 and k_2 are determined in the approximation of f. The valuation formula (3.32) gives

$$v(x,t) \;\approx\; e^{-r(T-t)}\int_{\mathcal{I}_m} v\left(y,T\right)f_m\left(y|x\right)dy \;=\; e^{-r(T-t)}\sum_{k=k_1}^{k_2} c_{m,k}\left(x\right)\cdot V_{m,k}^{\alpha},$$

where the pay-off coefficients are given now by the following integral

$$V_{m,k}^{\alpha} \;:=\; \int_{\mathcal{I}_m} v\left(y,T\right)\phi_{m,k}\left(y\right)dy \;=\; \int_{\mathcal{I}_m}\left[\alpha\cdot K\left(e^{y}-1\right)\right]_{+}\phi_{m,k}\left(y\right)dy. \tag{3.38}$$

Similarly to the cash-or-nothing pay-off coefficients, the integral in (3.38) does not allow a analytical expression and an approximation needs to be made. Next proposition gives an expression to efficiently compute $V_{m,k}^{\alpha}$ together with an error estimate.

Proposition 3.4 (Approximation of European call/put pay-off coefficients and error estimate)**.** *Let us define* $\bar{k}_1 := \max\left(k_1,0\right)$ *and* $\bar{k}_2 := \min\left(k_2,0\right)$*. Then, an approximation of the pay-off coefficients for a European call and put option are computed respectively as*

$$V_{m,k}^{1} \;\approx\; V_{m,k}^{1,*} \;:=\; \begin{cases} \frac{K2^{m/2}}{2^{J-1}}\sum_{j=1}^{2^{J-1}}\left[I_1\left(\frac{\bar{k}_1}{2^m},\frac{k_2}{2^m}\right)-I_2\left(\frac{\bar{k}_1}{2^m},\frac{k_2}{2^m}\right)\right] & \text{if } k_2>0, \\ 0 & \text{if } k_2\leq 0, \end{cases} \tag{3.39}$$

$$V_{m,k}^{-1} \;\approx\; V_{m,k}^{-1,*} \;:=\; \begin{cases} \frac{-K2^{m/2}}{2^{J-1}}\sum_{j=1}^{2^{J-1}}\left[I_1\left(\frac{k_1}{2^m},\frac{\bar{k}_2}{2^m}\right)-I_2\left(\frac{k_1}{2^m},\frac{\bar{k}_2}{2^m}\right)\right] & \text{if } k_1<0, \\ 0 & \text{if } k_1\geq 0, \end{cases} \tag{3.40}$$

where, taking $C_j := (2j-1)/2^J \cdot \pi$ *for each* j, I_1 *and* I_2 *are defined respectively as follows*

$$\begin{aligned} I_1(a,b) &:= \frac{C_j 2^m}{1+(C_j 2^m)^2}\left[e^b \sin\left(C_j\left(2^m b-k\right)\right) - e^a \sin\left(C_j\left(2^m a-k\right)\right)\right. \\ &\quad \left. + \frac{1}{C_j 2^m}\left(e^b \cos\left(C_j\left(2^m b-k\right)\right) - e^a \cos\left(C_j\left(2^m a-k\right)\right)\right)\right], \\ I_2(a,b) &:= \frac{1}{C_j 2^m}\left(\sin\left(C_j\left(2^m b-k\right)\right) - \sin\left(C_j\left(2^m a-k\right)\right)\right). \end{aligned}$$

Additionally, if we consider $J \geq \log_2(\pi N_k)$, *we find the following estimation of the error*

$$\left|V_{m,k}^{\alpha} - V_{m,k}^{\alpha,*}\right| \leq \frac{K}{2^{m/2}} \cdot D \cdot \frac{(\pi N_k)^2}{2^{2(J+1)} - (\pi N_k)^2}, \tag{3.41}$$

$$N_k := \max\left(\left|\bar{k}_1 - k\right|, \left|k_2 - k\right|\right), \quad D := \left|k_2 - \bar{k}_1\right| \cdot \max_{y \in \left[\frac{\bar{k}_1}{2^m}, \frac{k_2}{2^m}\right]} \left|e^y - 1\right| \quad \text{if } \alpha = +1,$$

$$N_k := \max\left(\left|k_1 - k\right|, \left|\bar{k}_2 - k\right|\right), \quad D := \left|\bar{k}_2 - k_1\right| \cdot \max_{y \in \left[\frac{k_1}{2^m}, \frac{\bar{k}_2}{2^m}\right]} \left|e^y - 1\right| \quad \text{if } \alpha = -1.$$

Proof. We start proving expressions (3.39) and (3.40). By definition of the pay-off coefficients (3.38) and bearing in mind the expression of $\phi_{m,k}$, we have

$$V_{m,k}^{\alpha} = \begin{cases} K 2^{m/2} \int_{\mathcal{I}_m \cap [0,+\infty)} (e^y - 1) \operatorname{sinc}\left(2^m y - k\right) dy & \text{if } \alpha = 1, \\ -K 2^{m/2} \int_{\mathcal{I}_m \cap (-\infty,0]} (e^y - 1) \operatorname{sinc}\left(2^m y - k\right) dy & \text{if } \alpha = -1. \end{cases}$$

Let us focus in the case $\alpha = 1$, the other case is analogous. If we replace the approximation of the sinc function (3.21), we obtain the following approximation for $V_{m,k}^1$,

$$\begin{aligned} V_{m,k}^{1,*} &:= K \cdot 2^{m/2} \cdot \frac{1}{2^{J-1}} \sum_{j=1}^{2^{J-1}} \int_{\mathcal{I}_m \cap [0,+\infty)} (e^y - 1) \cos\left(C_j(2^m y - k)\right) dy \\ &= K \cdot 2^{m/2} \cdot \frac{1}{2^{J-1}} \sum_{j=1}^{2^{J-1}} \left(\int_{\frac{\bar{k}_1}{2^m}}^{\frac{k_2}{2^m}} e^y \cos\left(C_j(2^m y - k)\right) dy - \int_{\frac{\bar{k}_1}{2^m}}^{\frac{k_2}{2^m}} \cos\left(C_j(2^m y - k)\right) dy \right) \\ &= K \cdot 2^{m/2} \cdot \frac{1}{2^{J-1}} \sum_{j=1}^{2^{J-1}} \left[I_1\left(\frac{\bar{k}_1}{2^m}, \frac{k_2}{2^m}\right) - I_2\left(\frac{\bar{k}_1}{2^m}, \frac{k_2}{2^m}\right) \right], \end{aligned}$$

where last equality is obtained by a simple computation of the integrals involved in second equality. Notice that we have assumed $k_2 \geq 0$; otherwise, $\mathcal{I}_m \cap [0,+\infty) = \emptyset$ and $V_{m,k}^{1,*} = 0$.

To derive the error estimate, we assume again that $\alpha = 1$, since the case $\alpha = -1$ goes analogously. Taking into account that the approximation $V_{m,k}^{1,*}$ was constructed by replacing

the sinc function by its approximation,

$$\begin{aligned}\left|V_{m,k}^{1}-V_{m,k}^{1,*}\right| &\leq K\cdot 2^{m/2}\cdot\int_{\frac{\bar{k}_1}{2^m}}^{\frac{k_2}{2^m}}\left|e^{y}-1\right|\left|\operatorname{sinc}\left(2^{m}y-k\right)-\operatorname{sinc}^{*}\left(2^{m}y-k\right)\right|dy\\ &\leq \frac{K}{2^{m/2}}\cdot\max_{y\in\left[\frac{k_1}{2^m},\frac{\bar{k}_2}{2^m}\right]}\left|e^{y}-1\right|\cdot\int_{\bar{k}_1-k}^{k_2-k}\left|\operatorname{sinc}\left(t\right)-\operatorname{sinc}^{*}\left(t\right)\right|dy,\end{aligned}$$

where the change of variables $t=2^{m}y-k$ has been performed in last inequality. If we take $J\geq\log_2\left(\pi N_k\right)$, Lemma 3.2 applies and concludes the proof. □

Remark 3.5. *Similarly to the case of cash-or-nothing options, the pay-off coefficients $V_{m,k}^{\alpha,*}$ can be computed beforehand with high accuracy for later use by means of the estimates (3.39) and (3.40) in order to save some CPU time. Another remarkable strategy, which will be used in the numerical examples section, is to fix a constant J for each coefficient defined here by $\bar{\jmath}:=\lceil\log_2\left(\pi N\right)\rceil$, where $N:=\max_{k_1<k<k_2}N_k$, and apply an FFT algorithm. For this purpose, we should rearrange formula (3.39) and (3.40). We start noticing that if we expand the sine and cosine terms in integrals I_1 and I_2, we obtain*

$$\begin{aligned}I_1\left(a,b\right) &= A_j\cdot\Big[e^{b}\cdot\sin\left(C_j2^{m}b\right)\cdot\cos\left(C_jk\right)-e^{b}\cdot\cos\left(C_j2^{m}b\right)\cdot\sin\left(C_jk\right)\\ &\cdot\quad -e^{a}\cdot\sin\left(C_j2^{m}a\right)\cdot\cos\left(C_jk\right)+e^{a}\cdot\cos\left(C_j2^{m}a\right)\cdot\sin\left(C_jk\right)\\ &\quad +B_j\cdot\Big(e^{b}\cdot\cos\left(C_j2^{m}b\right)\cdot\cos\left(C_jk\right)+e^{b}\cdot\sin\left(C_j2^{m}b\right)\cdot\sin\left(C_jk\right)\\ &\quad -e^{a}\cdot\cos\left(C_j2^{m}a\right)\cdot\cos\left(C_jk\right)-e^{a}\cdot\sin\left(C_j2^{m}a\right)\cdot\sin\left(C_jk\right)\Big)\Big]\\ &= A_j\cdot\Big[\Big(e^{b}\cdot\sin\left(C_j2^{m}b\right)-e^{a}\cdot\sin\left(C_j2^{m}a\right)+B_j\cdot e^{b}\cdot\cos\left(C_j2^{m}b\right)\\ &\quad -B_j\cdot e^{a}\cdot\cos\left(C_j2^{m}a\right)\Big)\cdot\cos\left(C_jk\right)\\ &\quad +\Big(-e^{b}\cdot\cos\left(C_j2^{m}b\right)+e^{a}\cdot\cos\left(C_j2^{m}a\right)+B_j\cdot e^{b}\cdot\sin\left(C_j2^{m}b\right)\\ &\quad -B_j\cdot e^{a}\cdot\sin\left(C_j2^{m}a\right)\Big)\cdot\sin\left(C_jk\right)\Big],\end{aligned}$$

$$\begin{aligned}I_2\left(a,b\right) &= B_j\cdot\Big[\Big(\sin\left(C_j2^{m}b\right)-\sin\left(C_j2^{m}a\right)\Big)\cdot\cos\left(C_jk\right)\\ &\quad +\Big(\cos\left(C_j2^{m}a\right)-\cos\left(C_j2^{m}b\right)\Big)\cdot\sin\left(C_jk\right)\Big],\end{aligned}$$

where we have defined $A_j := \frac{C_j 2^m}{1+(C_j 2^m)^2}$ *and* $B_j := \frac{1}{C_j 2^m}$. *Recall as well that* $C_j := \frac{2j-1}{2^{\bar{\jmath}}}\pi$. *Finally, let us introduce the following expressions for each* j *in order to simplify the notation and obtain a more compact expression*

$$
\begin{aligned}
I_{11}^j &= e^b \cdot \sin\left(C_j 2^m b\right) - e^a \cdot \sin\left(C_j 2^m a\right) + B_j \cdot e^b \cdot \cos\left(C_j 2^m b\right) - B_j \cdot e^a \cdot \cos\left(C_j 2^m a\right), \\
I_{21}^j &= \sin\left(C_j 2^m b\right) - \sin\left(C_j 2^m a\right), \\
I_{12}^j &= -e^b \cdot \cos\left(C_j 2^m b\right) + e^a \cdot \cos\left(C_j 2^m a\right) + B_j \cdot e^b \cdot \sin\left(C_j 2^m b\right) - B_j \cdot e^a \cdot \sin\left(C_j 2^m a\right), \\
I_{22}^j &= \cos\left(C_j 2^m a\right) - \cos\left(C_j 2^m b\right).
\end{aligned}
$$

Last step is to efficiently calculate the sum presented in the pay-off coefficients in (3.39) *and* (3.40) *to obtain Formula* (3.42) *(below). This expression allows us to apply an FFT algorithm straightforwardly. In this case, however, we have to apply an FFT algorithm two times, once for the terms with cosines and once for the terms with sines. The computational complexity is reduced from* $\mathcal{O}\left(2^{\bar{\jmath}-1}\left(k_2-k_1+1\right)\right)$, *when the pay-off coefficients are directly computed by formulas* (3.39) *and* (3.40), *to* $\mathcal{O}\left(\log\left(2\right)\left(\bar{\jmath}-1\right)2^{\bar{\jmath}}\right)$ *when we apply an FFT strategy to speed up the computation of* $V_{m,k}^{\alpha,*}$.

$$
\begin{aligned}
&\sum_{j=1}^{2^{\bar{\jmath}-1}} \left[I_1\left(a,b\right) - I_2\left(a,b\right) \right] = \\
&\quad = \sum_{j=1}^{2^{\bar{\jmath}-1}} \left[A_j \cdot \left(I_{11}^j \cos\left(C_j k\right) + I_{12}^j \sin\left(C_j k\right) \right) - B_j \cdot \left(I_{21}^j \cos\left(C_j k\right) + I_{22}^j \sin\left(C_j k\right) \right) \right] \\
&\quad = \sum_{j=1}^{2^{\bar{\jmath}-1}} \left[\left(A_j I_{11}^j - B_j I_{21}^j \right) \cdot \cos\left(C_j k\right) + \left(A_j I_{12}^j - B_j I_{22}^j \right) \cdot \sin\left(C_j k\right) \right] \\
&\quad = \sum_{j=0}^{2^{\bar{\jmath}-1}-1} \left[\left(A_{j+1} I_{11}^{j+1} - B_{j+1} I_{21}^{j+1} \right) \cdot \cos\left(\frac{j+1/2}{2^{\bar{\jmath}-1}} \pi k \right) \right. \\
&\qquad\qquad \left. + \left(A_{j+1} I_{12}^{j+1} - B_{j+1} I_{22}^{j+1} \right) \cdot \sin\left(\frac{j+1/2}{2^{\bar{\jmath}-1}} \pi k \right) \right] \\
&\quad = \Re\left(e^{\frac{i\pi k}{2^{\bar{\jmath}}}} \cdot \sum_{j=0}^{2^{\bar{\jmath}-1}-1} \left[A_{j+1} I_{11}^{j+1} - B_{j+1} I_{21}^{j+1} \right] \cdot e^{\frac{ij\pi k}{2^{\bar{\jmath}-1}}} \right) \\
&\qquad\qquad + \Im\left(e^{\frac{i\pi k}{2^{\bar{\jmath}}}} \cdot \sum_{j=0}^{2^{\bar{\jmath}-1}-1} \left[A_{j+1} I_{11}^{j+1} - B_{j+1} I_{21}^{j+1} \right] \cdot e^{\frac{ij\pi k}{2^{\bar{\jmath}-1}}} \right).
\end{aligned}
\tag{3.42}
$$

3.5 Numerical results

In this section, we carry out several numerical experiments to evaluate the accuracy and robustness of the SWIFT method. Particularly, we put our attention to price a cash-or-nothing option and a European call option under geometric Brownian motion (GBM) dynamics and check the accuracy of the method comparing with the exact price given by the Black-Scholes formulae presented in (2.15). We also consider CGMY and Heston dynamics as the associated process for the underlying asset in order to show the versatility of this pricing technique.

Recall that the first step of the method is to approximate the density function by a linear combination of Shannon scaling functions at a certain level of resolution m and limit values k_1 and k_2 in the summation should be fixed. Although we have seen that the error of the approximation to the density function at scale m depends on the rate of decay of its Fourier transform and the error of the truncation in the interval $[k_1, k_2]$ decrease by enlarging its width, we have not given a criterion to determine them.

3.5.1 Scale of approximation m

We saw in section 3.3 that the error of the approximation at a scale m depends on the Fourier transform of the density function and is given by expression (3.11). As in most cases the characteristic function of the process is available in analytic form, we will choose properly the size of the parameter m by studying its decay properties.

To illustrate the dependency of the parameter m with respect the decay of the characteristic function, we price a cash-or-nothing option considering three dynamics with a different rate of decay and compare it with the scale m. The density functions and the modulus of the characteristic functions of all the dynamics have been numerically computed and represented in Figure 3.2. The results obtained are shown in Table 3.5.1.

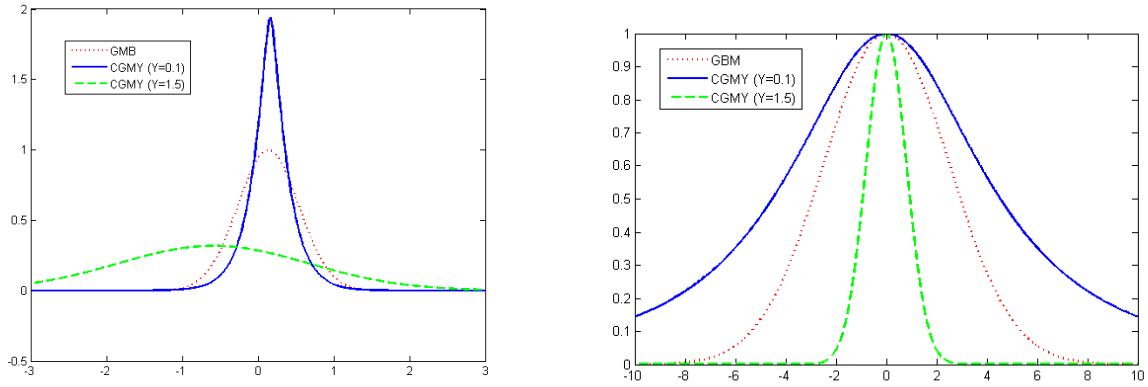

Figure 3.2: Density function (left) and modulus of the characteristic function (right). The dotted red line corresponds to GBM dynamics, the thick blue line to the CGMY dynamics with $Y = 0.1$ and the dashed green line to the CGMY dynamics with $Y = 1.5$.

We first consider GBM dynamics with parameters $S_0 = K = 100$, $r = 0.2$, $\sigma = 0.4$ and $T = 1$, with reference value 0.505903084024195 computed by means of the Black-Scholes formula. We see that the rate of decay of the characteristic function is quite fast and we just need a scale of $m = 4$ to obtain an error of order 10^{-13}. Second, we take CGMY dynamics with parameters $S_0 = K = 100$, $r = 0.2$, $\sigma = 0.4$, $T = 1$, $C = 1$, $G = M = 5$ and $Y = 0.1$, with reference value 0.610849386594073 computed by means of Monte Carlo algorithm with a high number of simulations. Now, the rate of decay of the characteristic function is very slow and consequently we need a big scale ($m = 13$) and CPU time ($0.51s$) to get an error of order 10^{-13}. Finally, we work again with CGMY dynamics with the same parameters as before but taking $Y = 1.5$ instead of $Y = 0.1$. Now, the reference value is 0.260352810962048 computed again by Monte Carlo method and the rate of decay of the characteristic function becomes the fastest of the three dynamics. This translates into needing a really small scale ($m = 1$) and CPU time ($0.007s$) to achieve the same order of the error.

DYNAMICS	DECAY OF THE FT	SCALE	ERROR	CPU TIME (s)
GBM	middle	m=4	$5.2625 \cdot 10^{-14}$	0.013
CGMY (Y=0.1)	slow	m=13	$1.7441 \cdot 10^{-13}$	0.51
CGMY (Y=1.5)	fast	m=1	$1.0180 \cdot 10^{-13}$	0.007

Table 3.1: Scale, error and CPU time of the three dynamics considered to price the cash-or-nothing option.

3.5.2 Limit values k_1 and k_2 in the summation

Once the scale of the approximation m has been fixed, the limit values k_1 and k_2 of the summation should be determined. We present two different approaches to fix them.

The first one has the nice property that does not need to rely on an a priori truncation of the entire real line onto a finite interval. In effect, departing from $k = 0$, we increase and decrease this value obtaining k_1 and k_2. We also compute the area underneath the curve with expression (3.16) on the fly. We stop when the area is close to 1 below some prescribed tolerance. Therefore, this strategy allows us to control the density computation regardless of features like skewness or heavy tails. However, the main drawback of this methodology is that involve extra CPU time since it does not allow the use of an FFT algorithm.

The second approach settles this problem by fixing an initial interval. Although this *a priori truncation* could be arbitrary chosen, a truncation rule based on the cumulants of $\ln(S_t/K)$ (whenever their computation is possible) is more appropriated since they often provide reliable intervals for the approximation. The cumulants, c_n, are defined by the cumulant-generating function, $g(t) = \log\left(E\left(e^{t \cdot X}\right)\right)$, for some random variable X. The nth cumulant is then given by the nth derivative, at zero, of $g(t)$. We propose the following a priori integral of integration $[a, b]$:

$$[a, b] := \left[x_0 + c_1 - L\sqrt{c_2 + \sqrt{c_4}},\ x_0 + c_1 + L\sqrt{c_2 + \sqrt{c_4}}\right], \qquad \text{with } L = 10, \tag{3.43}$$

where $x_t = \ln(S_t/K)$. Expression (3.43) has been confirmed as being accurate for a variety of asset processes and options with different maturities. This interval can be adjusted, if necessary, using the first strategy explained before. The remarkable feature of this methodology is that an unique $\jmath$-value may be fixed and an FFT algorithm can be applied using Remark 3.2. Proceeding this way, the characteristic function is evaluated only once at a fixed grid of points. In order to save even more CPU time, the pay-off coefficients are calculated analogously fixing an unique $\bar{\jmath}$-value and employing an FFT algorithm as detailed in Remark 3.4 for cash-or-nothing options and Remark 3.5 for European options.

3.5.3 Pricing of European options with the SWIFT method.

In this subsection, we carry out some numerical experiments concerning the pricing of European options with the SWIFT method. Specifically, we aim to show the accuracy, efficiency and robustness of the method. Before we proceed to consider the specifics of these experiments, however, we provide a recap of the main steps of algorithm studied in this chapter as well as giving a detailed idea of the numerical implementation. Note that we have implemented the method with the FFT algorithm in order to make it more efficient.

Numerical Implementation of the SWIFT method
Assume we have a European option whose underlying asset price follows a certain dynamics and its characteristic function is analytically available. The following steps provide the price of the option:

1. Fix the scale of approximation m by studying the rate of decay of the characteristic function of the process (provided in the appendix).

2. Fix an integration domain $[a, b]$ using expression (3.43) and the cumulants of the log-asset process (provided in the appendix) and determine the limit values $k_1 := \lceil 2^m \cdot a \rceil$ and $k_2 := \lfloor 2^m \cdot b \rfloor$.

3. Fix a $\jmath$-value with $\jmath := \lceil \log_2(\pi M_m) \rceil$ where $M_m := \max_{k_1<k<k_2} M_{m,k}$ and $M_{m,k} := \max(|2^m a - k|, |2^m a + k|)$ and use Remark 3.2 to apply the FFT algorithm to compute the density coefficients $c^*_{m,k}$ for $k = k_1, \ldots, k_2$.

4. Fix a $\bar{\jmath}$-value and compute the pay-off coefficients $V^*_{m,k}$ for $k = k_1, \ldots, k_2$ using a FFT algorithm with Remark 3.4 for cash-or-nothing options and Remark 3.5 for European options.

5. Determine the price V^*_T of the option using the Feynman-Kac formula, that is, $V^*_T := e^{-r(T-t)} \sum_{k=k_1}^{k_2} c^*_{m,k}(x) \cdot V^*_{m,k}$.

Table 3.2: Numerical Implementation of the SWIFT method for European options.

We start our analysis of the SWIFT method by showing its high efficiency. To this end, we price a European call option with GBM dynamics, assuming that the parameters take the values: $S_0 = 100$, $K = 110$, $r = 0.1$, $\sigma = 0.25$ and $T = 0.1$. The reference value is 0.589616134845691 and has been computed by means of the Black-Scholes formula for European call options given in (2.15). The results are presented in Table 3.5.3. One observes exponential convergence in terms of the scale of the approximation m (see also Figure 3.3). We almost get engineering accuracy with a scale of $m = 4$ and using 25 terms in the approximation of the density and machine accuracy with $m = 5$ and using 50 terms. Note as well that we almost get machine accuracy in 0.011 seconds which gives an idea of the efficiency of the method. It is worth to remark that the CPU time can be further reduced if we precompute beforehand the values of the pay-off coefficients $V^*_{m,k}$.

SCALE	**STRIKE**	k_1	k_2	j	$\bar{j}$	**Error**	**CPU TIME (seconds)**
m=2	110	-3	2	5	4	1.92058	0.006
m=3	110	-7	5	6	6	$4.5142 \cdot 10^{-2}$	0.008
m=4	110	-14	11	7	7	$5.0206 \cdot 10^{-4}$	0.009
m=5	110	-28	22	8	8	$1.4544 \cdot 10^{-14}$	0.011
m=6	110	-56	45	9	9	$6.2172 \cdot 10^{-15}$	0.014

Table 3.3: Absolute errors corresponding to the valuation of a European call option under the GBM dynamics by means of the SWIFT method.

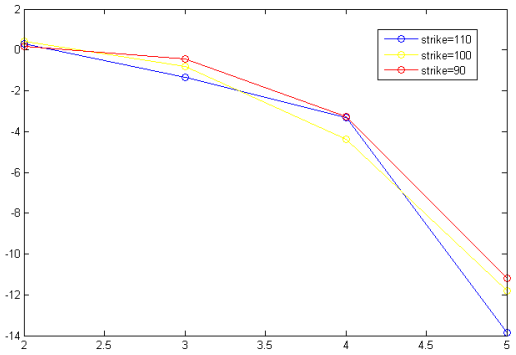

Figure 3.3: Convergence of the valuation of a European call option with strikes 110, 100 and 90.

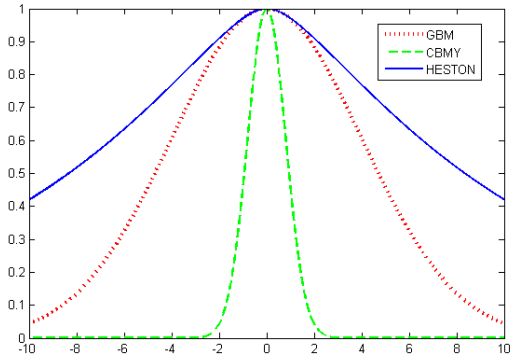

Figure 3.4: Characteristic function for the GBM (red), CGMY (green) and Heston (blue).

In our last example we consider the pricing of a European call and put option with the three dynamics considered: GBM, CGMY and Heston. We have chosen $S_0 = 100$, $K = 110$ and $T = 1$. The parameters for GBM are now $r = 0.1$ and $\sigma = 0.25$, for CGMY are $r = 0.1$, $\sigma = 0.25$, $C = 1$, $G = M = 5$ and $Y = 1.5$, and for Heston are $r = 0.1$, $\lambda = 1.5768$,

$\nu = 0.5751$, $\bar{u} = 0.0398$, $u_0 = 0.0175$ and $\rho = -0.5711$. The results are available in Table 3.5.3. The reference values have been computed by means of the Black-Scholes formulas (2.15) for GBM and with the Monte Carlo method for CGMY and Heston dynamics.

We observe that for the GBM and CGMY we need small scales ($m = 3$ and $m = 1$ respectively) to achieve very accurate results, while for Heston dynamics we need higher scales ($m = 5$ and $m = 7$). This fact is explained by the rate of decay of the characteristic functions as it can be observed in Figure 3.4. Despite this, the SWIFT method shows robustness, being capable of highly accurately pricing European options at very low scales of approximation (at most $m = 7$).

Finally, Table 3.5.3 also shows the versatility of the method. The SWIFT method is easily adaptable to different dynamics. We just need to have the analytic expression of the characteristic function of the process.

MODEL	**SCALE**	**OPTION**	**REFERENCE PRICE**	**ERROR**	**CPU(s)**
GBM	m=3	CALL	10.160052368787559	$1.93778 \cdot 10^{-08}$	0.009
GBM	m=3	PUT	9.692168352744277	$7.27583 \cdot 10^{-10}$	0.009
CGMY	m=1	CALL	47.282869019686792	$2.96796 \cdot 10^{-08}$	0.008
CGMY	m=1	PUT	46.814985002833353	$3.97903 \cdot 10^{-13}$	0.009
HESTON	m=5	CALL	7.238354638623483	$5.42086 \cdot 10^{-05}$	0.015
HESTON	m=7	PUT	6.635136912147874	$3.20111 \cdot 10^{-05}$	0.021

Table 3.4: Absolute errors, scales and CPU times (in seconds) corresponding to the valuation of a European call and put option with initial price $S_0 = 100$ and strike $K = 110$ using GBM, CGMY and Heston dynamics for the underlying asset.

Chapter 4

Discrete Lookback Option Pricing using the SWIFT method

Lookback options are exotic contracts that offer the holder the advantage of being able to exercise at an optimal point. Essentially, at expiration the holder can look back (hence the name) at how the price of the underlying asset has performed and maximize their profits by taking advantage of the biggest price differential between the strike price and the price of the underlying asset. For options traders this is obviously a major benefit, as lookback options can be used to solve one of the biggest problems they face: market timing. This is basically choosing when to enter a position and when to exit it, with the aim obviously being to time entry and exit to make the largest possible returns.

Because of the way lookback options work, the issue of market timing becomes less important as profits are effectively guaranteed to be maximized. Also, the chances of a contract of this type expiring worthless are much lower than other types of options. For these reasons lookbacks are generally more expensive, so the advantages do come at a cost. These attractive features have also made lookback options become increasingly popular in the last few years, specially in insurance contracts or structured notes.

Similarly to European options, lookbacks can be either calls or puts, so it is possible to speculate on either the price of the underlying security going up in value or going down. They are also known as hindsight options, as they actually give the holder the benefit of hindsight when determining when to exercise.

One can also distinguish between two kind of lookback options: continuously and discretely traded. While the theory for pricing continuously monitored lookback options is well developed and a variety of methods exist under popular continuous-time asset price models, the development of the theory of pricing discrete lookback options has been slower and relies largely on numerical methods. The aim of this chapter is precisely to propose a efficient and versatile methodology for pricing discrete lookback options by adapting the SWIFT method presented in Chapter 3 for a wide range of dynamics that have the characteristic function available and allows to evaluate it.

The chapter will be organized as follows. In Section 4.1 we introduce the notation and describe the framework contemplated for pricing lookback options. We also derive the valuation formulas by using the Feynman-Kac pricing theorem. Next sections replicate the steps of the SWIFT method that we saw in Chapter 3 and settle several difficulties which come out. In this way, Section 4.2 provides a recursive formula to compute the characteristic function of the asset log-return maximum together with an efficient recurrence to speed up its computation. We also see that the evaluation of the characteristic function requires the calculation of some coefficients in each step of the recursion. This computation will turn out to be the key point to implement the method efficiently. Then, several approaches are investigated in Section 4.3 using Haar and Shannon wavelets. Finally, in Section 4.4 we derive the expression of the pay-off coefficients and in Section 4.5 we perform several numerical experiments to check the efficiency, robustness and versatility of the methodology.

4.1 Discrete Lookback Options

In this section, we introduce the notation and describe the framework that has been considered for pricing discrete lookback options. First, we define the risk-neutral measure $\mathbb{Q}$ in such a way that the log-return process $L_t := \ln(S_t/S_0)$ at time $t \geq 0$ forms a semimartingale process. As a direct consequence, the risk-neutral dynamics of the asset price turns out to be driven by an exponential semimartingale process given by $S_t = S_0 e^{L_t}$ which, in turn, leads to independent increments of the log-return process. Further details about semimartingale processes can be found in [13]. For brevity, we refer to discretely monitored lookback options simply as lookback options throughout the rest of this thesis.

As has already been explained, lookback options provide a payoff at maturity that depends on the extremum of the stock price over the lifetime of the contract. We assume that the lookback life period is $[T_0, T]$ and the asset price is observed at $q+1$ evenly spaced monitoring times $t_j = T_0 + j(T - T_0)/q$, for $j = 0, \ldots, q$. Since we are interested in pricing the option not only at time T_0 but at any time $t \in [T_0, T]$, we take j^* such that $t_{j^*} \leq t < t_{j^*+1}$. Then, we define the maximum value of the asset price realized from T_0 to t over the discrete monitoring times t_j, $j = 0, \ldots, j^*$, and the observed future maximum log-return process over the monitoring times $t_{j^*+1}, \ldots, t_{j^*+k}$, for $k = 1, \ldots, q - j^*$, respectively by

$$M := \max_{j=0,\ldots,j^*} S_j, \qquad X_k := \max_{j=1,\ldots,k} L_{j^*+j}. \tag{4.1}$$

To simplify the notation, we denote by m the number of future monitoring time points, that is, $m := q - j^*$. There exist several different types of lookback options which will be treated in this thesis. The lookback options with fixed strike and with floating strike.

1) Lookback options with fixed strike: as the name introduces it, these options define its strike at purchase. However, contrary to European options, they are not exercised at the expiration market price. The payoff is the maximum difference between the optimal

underlying asset price and the strike. In the case of a call, the option holder can look back over the life of the option and choose to exercise at the point when the underlying asset was priced at its highest over the life of the option. In the case of a put, the option can be exercised at the asset's lowest price. Their pay-off function is given, respectively, by

$$LC_{fix} := \left(\max_{i=0,\dots,q} S_i - K\right)_+, \qquad LP_{fix} := \left(K - \min_{i=0,\dots,q} S_i\right)_+. \tag{4.2}$$

2) Lookback options with floating strike: these options do not fix the strike price beforehand but is determined by the optimal value of the underlying asset's price during the option life. The payoff is now the maximum difference between the market asset's price at expiration and the floating strike. For a call, the strike price is fixed at the lowest price reached during the life of the option. For a put, it is fixed at the highest price. Their pay-off function is given, respectively, by

$$LC_{float} := \left(S_T - \min_{i=0,\dots,q} S_i\right)_+, \qquad LP_{float} := \left(\max_{i=0,\dots,q} S_i - S_T\right)_+. \tag{4.3}$$

Throughout the rest of the thesis, we focus in fixed-strike lookback call options and floating lookback put options without loss of generality since the pricing theory for fixed-strike lookback put options and floating lookback call options is similar and require minor modification of the results presented in this thesis. Additionally, as has already been mentioned, it is also important to be able to price the derivative at current time $t \in [T_0, T]$. The following proposition gives expressions to value lookback options at any time t.

Proposition 4.1 (Valuation of Lookback Options)**.** *The prices at current time $t \in [T_0, T]$ of a fixed-strike lookback call option, $LC_{fix}(t,T)$, and a floating lookback put option, $LP_{float}(t,T)$, that expire at future time $T > 0$ and were signed at time T_0 in the past are given by*

$$LC_{fix}(t,T) = \begin{cases} S_0 e^{-r(T-t)} E_{\mathbb{Q}}\left[\left(e^{X_m} - \frac{K}{S_0}\right)_+\right] & \text{if } M < K, \\ S_0 e^{-r(T-t)} E_{\mathbb{Q}}\left[\left(e^{X_m} - \frac{M}{S_0}\right)_+\right] + (M-K)\, e^{-r(T-t)} & \text{if } M \geq K, \end{cases} \tag{4.4}$$

$$LP_{float}(t,T) = \begin{cases} S_0 e^{-r(T-t)} E_{\mathbb{Q}}\left[e^{X_m}\right] - S_0 & \text{if } M \leq S_0, \\ S_0 e^{-r(T-t)} \left\{E_{\mathbb{Q}}\left[e^{X_m}\right] + E_{\mathbb{Q}}\left[\left(\frac{M}{S_0} - e^{X_m}\right)_+\right]\right\} - S_0 & \text{if } M > S_0. \end{cases} \tag{4.5}$$

respectively, where M is the maximum value of the asset price realized from T_0 to t defined in (4.1) and r is the risk-free rate of interest.

Proof. We only prove the formula for a fixed-strike lookback call option (4.4), the proof for a floating lookback put option (4.5) goes analogously and is omitted.

The value of a fixed lookback call option at time t is given by the Feynman-Kac formula which says that the option value at time t is computed as a discounted expectation of the pay-off function under the risk-neutral probability measure $\mathbb{Q}$

$$LC_{fix}(t,T) = e^{-r(T-t)}\mathbb{E}_{\mathbb{Q}}\left[\left(\max_{i=0,\dots,q} S_i - K\right)_+ |\mathcal{F}_t\right], \tag{4.6}$$

where $\mathcal{F}_t$ contains all the information up to time t. We distinguish between two cases: first assume that $M < K$, i.e., the observed asset prices do not exceed the strike price. Then,

$$\begin{aligned}\left(\max_{i=0,\dots,q} S_i - K\right)_+ |\mathcal{F}_t &= \left(\max_{i=j^*+1,\dots,q} S_i - K\right)_+ = S_0\left(\max_{i=j^*+1,\dots,q}\left(\frac{S_i}{S_0}\right) - \frac{K}{S_0}\right)_+ \\ &= S_0\left(\max_{i=j^*+1,\dots,q} e^{L_i} - \frac{K}{S_0}\right)_+ = S_0\left(e^{X_m} - \frac{K}{S_0}\right)_+.\end{aligned}$$

Substituting this expression in (4.6), we obtain the first expression in (4.4). In the case that the maximum of the observed asset prices exceeds the strike price, $M \geq K$, one gets

$$\begin{aligned}\left(\max_{i=0,\dots,q} S_i - K\right)_+ |\mathcal{F}_t &= \left(\max_{i=j^*+1,\dots,q}(M, S_i) - K\right)_+ = \max\left(M-K, \max_{i=j^*+1,\dots,q} S_i - K\right) \\ &= (M-K) + \left(\max_{i=j^*+1,\dots,q} S_i - M\right)_+ = (M-K) + S_0\left(e^{X_m} - \frac{M}{S_0}\right)_+.\end{aligned}$$

Introducing this expression in (4.6), one gets the second expression in (4.4). □

Two useful and remarkable simplifications to (4.4) and (4.5) occur in the case $M \geq K$. The first one gives a relation between the price of the fixed lookback call option and the floating lookback put option and allows us to value one of them when we hold the price of the other. The second one provides a simplified formula for the price of a fixed lookback call option. These expressions are given in the following lemma.

Lemma 4.1 (Put-call parity and closed-form price for Fixed Lookback Calls)**.** *It holds:*

1. *If $M \geq K$, then $LC_{fix}(t,T) = LP_{float}(t,T) + S_0 - Ke^{-r(T-t)}$*
2. *If $M \geq K$ and $M \leq S_0$, then $LC_{fix}(t,T) = S_0 e^{-r(T-t)}\left(\phi_{X_m}(-i) - K/S_0\right)$, where we have denoted $\phi_{X_m}(z) = E_{\mathbb{Q}}\left(e^{izX_m}\right)$ as the characteristic function of X_m.*

4.2 The Characteristic Function of the Asset Log-return Maximum X_m

In Chapter 3, we derived the SWIFT method for European options and noticed that it was necessary to have in hands the characteristic function of the log-asset process. We also saw

that its analytic expression was available for all the dynamics treated (GBM, CGMY and Heston) and its evaluation was efficient.

For the lookback option pricing, we need the characteristic function of the asset log-return maximum X_m defined in (4.1). In this case, however, we do not hold an analytic expression. Instead, we will derive a recursive formula which will allow us to evaluate the characteristic function in any point. To this end, we start defining the increments of the log-return process

$$Y_i := L_i - L_{i-1} = \ln\left(\frac{S_i}{S_0}\right) - \ln\left(\frac{S_{i-1}}{S_0}\right) = \ln\left(\frac{S_i}{S_{i-1}}\right), \tag{4.7}$$

for $i = 1 \dots q$. Recall that we are assuming that the dynamics of the asset price are driven by an exponential semimartingale process. As a result, the increments Y_i turn out to be independent and identically distributed. We will exploit this fact to express X_m as the maximal partial sums of a collection of random variables. Then, we will make use of the celebrated Spitzer's Formula, which gives the joint distribution of partial sums and maximal partial sums of a collection of random variables, to finally derive the desired recursion that will allow us to evaluate the characteristic function of X_m.

4.2.1 A recursive formula for the characteristic function of X_m

Theorem 4.1 (Spitzer's Formula)**.** *Let Y_1, Y_2,... be independent and identically distributed random variables. Define the partial sums $G_n := Y_1 + Y_2 + \ldots + Y_n$ and the maximal partial sums $R_n := \max(0, G_1, \ldots, G_n)$ for $n \in \mathbb{Z}^+$. Then,*

$$\sum_{n=0}^{\infty} \psi_n(\alpha, \beta)\, t^n = \exp\left[\sum_{n=1}^{\infty} \frac{t^n}{n} \left(a_n(\alpha) + b_n(\beta) - 1\right)\right], \tag{4.8}$$

where we have introduced the following auxiliar functions

$$\begin{aligned} \psi_n(\alpha, \beta) &= \mathbb{E}\left(\exp\left[i(\alpha R_n + \beta(R_n - G_n)\right]\right), \\ a_n(\alpha) &= \mathbb{E}\left(\exp\left[i\alpha G_n^+\right]\right), \\ b_n(\beta) &= \mathbb{E}\left(\exp\left[i\beta G_n^-\right]\right), \end{aligned} \tag{4.9}$$

being $G_n^+ = \max(0, G_n)$ the positive part and $G_n^- = \max(0, -G_n)$ the negative part of G_n.

Proof. The original proof can be found in [29] and is based on a combinatorial argument. □

Spitzer's Formula is a remarkable result since it embraces a wide range of important applications in many fields. In particular, we make use of this theorem to compute the characteristic function of maximal partial sums of random variables which will serve us in turn to derive a recursive formula for the characteristic function of the asset log-return maximum X_m. We provide the results obtained in the following two propositions.

Proposition 4.2 (Characteristic function of maximal partial sums)**.** *Consider the random variables* $\{Y_i\}_{i\in\mathbb{Z}^+}$*,* G_n *and* R_n *defined in Theorem 4.1. Then, the characteristic function of the maximal partial sums* R_n *is given by the following recursive formula:*

$$\Phi_{R_0}(z) = 1, \quad \Phi_{R_m}(z) = \frac{1}{m}\sum_{k=0}^{m-1}\Phi_{R_k}(z)\, a_{m-k}(-z), \quad \text{for } m = 1, 2, \ldots. \tag{4.10}$$

Proof. If we take $\alpha = -z$ and $\beta = 0$ in Theorem 4.1, one gets that $\psi_n(-z, 0) = \Phi_{R_n}(z)$ and formula (4.8) becomes for this particular case

$$\sum_{n=0}^{\infty}\Phi_{R_n}(z)\, t^n = \exp\left[\sum_{n=1}^{\infty} a_n(-z)\frac{t^n}{n}\right]. \tag{4.11}$$

Writing $f(t) := \sum_{n=0}^{\infty}\Phi_{R_n}(z)\, t^n$ and $g(t) := \exp\left[\sum_{n=1}^{\infty} a_n(-z)\frac{t^n}{n}\right]$, it follows from (4.11) that $f'(s) = f(s)g'(s)$. Leibniz's formula now yields

$$f^{(n+1)}(s) = \sum_{j=0}^{n}\binom{n}{j} f^{(j)}(s)\, g^{(n+1-j)}(s), \quad n \in \mathbb{N}.$$

If we take $s = 0$ and expand the combinatorial number, we obtain

$$\frac{f^{(n+1)}(0)}{(n+1)!} = \frac{1}{n+1}\sum_{j=0}^{n}\frac{f^{(j)}(0)}{j!}\frac{g^{(n+1-j)}(0)}{(k-j)!}, \quad n \in \mathbb{N}. \tag{4.12}$$

Finally, noticing that from the definitions of $f(t)$ and $g(t)$ we have the following equalities

$$\Phi_{R_n}(z) = \frac{f^{(n)}(0)}{n!},\ n \in \mathbb{N}, \quad \text{and} \quad a_n(-z) = \frac{g^{(n)}(0)}{(n-1)!},\ n \in \mathbb{Z}^+,$$

we deduce from (4.12) that the characteristic function of the maximal partial sums Φ_{R_n} is given by expression (4.10). □

Proposition 4.3 (Characteristic function of the asset log-return maximum)**.** *Consider the maximum asset log-return* X_m *and the increments of the log-returns* Y_i *introduced in (4.1) and (4.7) respectively. Define* $G_n := Y_{j^*+2} + \ldots + Y_{j^*+n+1}$ *and* $R_n = \max(0, G_1, \ldots, G_n)$ *for* $n = 1 \ldots m-1$*. Then, the characteristic function of* X_m *is given by*

$$\Phi_{X_m}(z) = \Phi_{L_{j^*+1}}(z) \cdot \Phi_{R_{m-1}}(z), \tag{4.13}$$

where $\Phi_{L_{j^*+1}}(z)$ *is the characteristic function of the log-return* L_{j^*+1} *and* $\Phi_{R_{m-1}}(z)$ *is computed by means of the recursive formula (4.10) with*

$$a_n(-z) = \mathbb{E}\left(e^{-izL_n^+}\right), \quad \text{for } n = 1, \ldots, m.$$

Proof. We start rewriting the log-returns L_{j^*+n} in terms of the sum G_n

$$\begin{aligned} L_{j^*+n} &= \ln\left(\frac{S_{j^*+n}}{S_0}\right) = \ln\left(\frac{S_{j^*+n}}{S_{j^*+n-1}}\right) + \ln\left(\frac{S_{j^*+n-1}}{S_{j^*+n-2}}\right) + \ldots + \ln\left(\frac{S_{j^*+1}}{S_0}\right) \\ &= Y_{j^*+n} + Y_{j^*+n-1} + \ldots + Y_{j^*+2} + L_{j^*+1} = G_{n-1} + L_{j^*+1}, \end{aligned}$$

for $n = 1 \ldots m$. Then, if we take into account the definition of X_m in (4.1), we get

$$\begin{aligned} X_m &= \max\left(L_{j^*+1}, L_{j^*+2}, \ldots, L_{j^*+m}\right) \\ &= L_{j^*+1} + \max\left(0, G_1, \ldots, G_{m-1}\right) = L_{j^*+1} + R_{m-1}. \end{aligned} \tag{4.14}$$

Finally, substituting (4.14) in the definition of the characteristic function of X_m leads to

$$\begin{aligned} \Phi_{X_m}(z) &= \mathbb{E}\left(e^{-izX_m}\right) = \mathbb{E}\left(e^{-izL_{j^*+1}} e^{-izR_{m-1}}\right) \\ &= \mathbb{E}\left(e^{-izL_{j^*+1}}\right) \mathbb{E}\left(e^{-izR_{m-1}}\right) = \Phi_{L_{j^*+1}}(z) \cdot \Phi_{R_{m-1}}(z). \end{aligned}$$

Since the increments Y_i are independent and identically distributed, Proposition (4.2) applies and $\Phi_{R_{m-1}}(z)$ can be computed by means of the recursive formula (4.10). Additionally,

$$\begin{aligned} a_n(-z) &= \mathbb{E}\left(e^{-izG_n^+}\right) = \mathbb{E}\left(e^{-iz\max\left(Y_{j^*+2}+\ldots+Y_{j^*+n+1}, 0\right)}\right) \\ &= \mathbb{E}\left(e^{-iz\max(L_n, 0)}\right) = \mathbb{E}\left(e^{-izL_n^+}\right). \end{aligned}$$

where we have used that Y_i are identically distributed random variables to L_1 and consequently L_n follows the same distribution than $Y_{j^*+2} + \ldots + Y_{j^*+n+1}$. □

4.2.2 Spitzer-recurrence Expansion Formula

The main drawback with the recursive formula provided in Proposition 4.3 is that is not computationally efficient since, as it can be proven, it exhibits sub-exponential complexity. Particularly, the most involved part in (4.13) is the computation of ϕ_{R_m}. To settle this problem, we derive in next theorem an expansion formula for ϕ_{R_m} which is significantly more effective for large monitoring times m.

Theorem 4.2 (Spitzer-recurrence Expansion Formula)**.** *Let $Coeff_{t^m}(\cdot)$ denote the coefficient in front of t^m. The characteristic function of the maximal sums R_m can be expressed as*

$$\phi_{R_m}(z) = Coeff_{t^m}\left(\sum_{j=0}^{m} \frac{1}{j!} \cdot \left(\sum_{k=1}^{m} \frac{a_k(-z)}{k} t^k\right)^j\right), \qquad for\ m = 1, 2 \ldots. \tag{4.15}$$

Proof. We start with the recursive formula of $\phi_{Rm}(z)$ provided in (4.10). For brevity, we omit the dependence of $\phi_{R_m}(z)$ and $a_k(-z)$ on the argument z and write ϕ_m and a_k. Taking into account that $a_0 = 1$, we can rewrite (4.10) as

$$(m+1) \cdot \phi_m = \sum_{k=0}^{m} \phi_k \cdot a_{m-k}. \tag{4.16}$$

Let us introduce the function $U(u) = \sum_{m=0}^{\infty} u^m \cdot \phi_m$. Additionally, we take as initial condition $U(0) = 1$. Noting that its derivative is $U'(u) = \sum_{m=0}^{\infty} m \cdot u^{m-1} \cdot \phi_m$, we get that U satisfies the following differential equation

$$U \; + \; u \cdot U' \; = \; \sum_{m=0}^{\infty} (m+1) \cdot u^{m-1} \cdot \phi_m. \tag{4.17}$$

Now multiplying both sides of (4.16) by u^m and summing over m from 0 to ∞, we deduce

$$\begin{aligned} \sum_{m=0}^{\infty} (m+1)\, u^m \phi_m \; &= \; \sum_{m=0}^{\infty} u^m \sum_{k=0}^{m} \phi_k \cdot a_{m-k} \\ &= \sum_{m=0}^{\infty} \sum_{k=0}^{m} \phi_k u^k \cdot a_{m-k} u^{m-k} \; = \; U \cdot A, \end{aligned} \tag{4.18}$$

where $A := \sum_{j=0}^{\infty} a_j u^j$. Then, it follows from (4.17) and (4.18) that $U + u \cdot U' = U \cdot A$. This is a separable ordinary differential equation whose solution is

$$U(t) = \exp\left(\int_0^t \frac{A(t) - 1}{u} du \right). \tag{4.19}$$

Now, consider the integral

$$\begin{aligned} \int_0^t \frac{A(t) - 1}{u} du \; &= \; \int_0^t \frac{\sum_{k=0}^{\infty} a_k u^k - 1}{u} du \; = \; \int_0^t \sum_{k=1}^{\infty} a_k u^{k-1} du \\ &= \sum_{k=1}^{\infty} a_k \int_0^t u^{k-1} du \; = \; \sum_{k=1}^{\infty} a_k \frac{t^k}{k}. \end{aligned} \tag{4.20}$$

where in the last equality we have assumed that a_k are bounded, that is, $|a_k| < B$. Now, from the definition of U, (4.19) and (4.20), we deduce (4.15) which completes the proof of the theorem. □

Formula (4.15) derived in Theorem 4.2 is in fact a special case of the Spitzer formula (4.8) provided in Theorem 4.1. Here, we have given a significantly simpler proof based on the recursive formula deduced in Proposition 4.3.

Remark 4.1. *Theorem 4.2 is an important result that enables the evaluation of ϕ_{X_m} with much greater efficiency that is with (4.13). It can be seen that the complexity of formula (4.2) is $\mathcal{O}(m^3)$, while the recursion (4.13) has a sub-exponential complexity. Additionally, it easy to check that (4.15) can be obtained by convoluting the vector $(a_1(-z)/1, \ldots, a_m(-z)/m)$ with itself j times for $j = 0, 1, \ldots, m$ and summing across the anti-diagonal.*

$$Coeff_{t^m}\left(\sum_{j=0}^{m} \frac{1}{j!} \cdot \left(\sum_{k=1}^{m} \frac{a_k(z)}{k} t^k \right)^j \right) \; = \; \sum_{j=0}^{m} \left(\left(a_1(-z)/1, \ldots, a_m(-z)/m^{*j} \right) \right)_{m-j}.$$

4.3 Computation of the coefficient $a_k(z)$

The calculation of the coefficients $a_k(z)$ turns out to be the central point in the evaluation of the characteristic function Φ_{X_m} of the future maximum of the log-returns as one may notice in the recursive formula (4.10). As has already been shown, these coefficients are calculated by the expression $a_k(-z) = E_{\mathbb{Q}}\left(e^{-izL^+_{j^*+k}}\right)$, for $k = 1, \ldots, m$, that is, the coefficients coincide with the characteristic function of the greater of the log-return process at time t_{j^*+k} and zero. For simple models, such as the Black-Scholes model, a closed formula can be found by integrating the probability distribution. However, for more complex and relevant models, the computation becomes tedious and cumbersome. Actually, it is impossible to derive a closed formula in most cases and some approximations need to be made. In this section, we present several approaches to compute these coefficients. The first technique provides a general methodology for calculating a_k, $k = 1, \ldots, m$, based on inverting the characteristic function of the log-return process L_{j^*+k} using Haar Wavelets. The second one uses the same idea using the Shannon Wavelet family and will allow us to compute the coefficients in a more efficient way. We start introducing the Haar Wavelet family and deriving what have been called the WA$^{[a,b]}$ method.

4.3.1 Haar Wavelets

In section 3.2, we introduced the Shannon Wavelet family in order to approximate the probability density function. Particularly, we saw that it formed a multiresolution analysis and we could applied the theory developed in section 3.1. In this section, we define a new family of wavelets, the so-called *Haar Wavelet family*, which will be used in our future analysis to find a simpler and more flexible way to compute the coefficients $a_k(-z)$.

As we did with the Shannon wavelets, the starting point for the definition of the Haar Wavelet family is to define its scaling function or father wavelet. In this case, it is given by the unit step function defined as

$$\phi(x) := \mathcal{X}_{[0,1]}(x) = \begin{cases} 1 & \text{if } 0 \leq x \leq 1, \\ 0 & \text{otherwise.} \end{cases} \tag{4.21}$$

Its dilated and translated instances $\phi_{m,k}(x) := 2^{m/2}\phi(2^m x - k)$ forms an orthonormal basis and gives rise to a multiresolution analysis. Thus, the theory introduced in Section 3.1 applies and a probability density function can be approximated by Haar wavelets functions.

For our purposes, it turns out also convenient to work in the frequency domain. Consequently, we should also consider the Fourier transform of the scaling functions, given by

$$\hat{\phi}_{m,k}(w) := 2^{-m/2} e^{-\frac{iwk}{2^m}} \left(\frac{1 - e^{-iw/2^m}}{iw/2^m}\right). \tag{4.22}$$

Next section uses the Haar Wavelets to introduce a general methodology called $\text{WA}^{[a,b]}$ that will be applied to approximate the coefficients $a_k(-z)$. The underlying idea of this strategy is similar to the fundamentals of the SWIFT method.

4.3.2 Approximation of $f(x)$: the $\text{WA}^{[a,b]}$ method.

In this section, we present a method to recover a probability density function f from its characteristic function using the Haar Wavelet family. This method consists on fixing a priori interval for the approximation and then using Haar wavelets on this bounded interval.

We start considering a probability density function $f(x)$ with Fourier transform $\hat{f}(x)$ of a given random variable X. One can expect that f decays to zero at infinity, so it can be approximated in a finite interval $[a, b]$. Particularly, as it has been recommended by various authors and argued in the previous chapter, we consider the following approximation

$$[a,b] := \left[c_1 - L\sqrt{c_2 + \sqrt{c_4}}, c_1 + L\sqrt{c_2 + \sqrt{c_4}}\right], \tag{4.23}$$

where c_n denotes the nth cumulant of X. Then, following the multiresolution analysis theory as we did with the Shannon wavelets, we can approximate the density f in this bounded interval at a given level of resolution m by:

$$f(x) \approx f_m^c(x) := \sum_{k=0}^{2^m-1} c_{m,k} \cdot \phi_{m,k}\left(\frac{x-a}{b-a}\right) \tag{4.24}$$

Our next objective is to find a methodology to compute the density coefficients $c_{m,k}$. For this, we will approximate $\hat{f}$ by $\hat{f}_m^c$ and then compute $c_{m,k}$ by inverting the Fourier transform. Proceeding this way, we have:

$$\begin{aligned}
\hat{f}(w) &= \int_{-\infty}^{+\infty} e^{-iwx} f(x)dx \approx \int_{-\infty}^{+\infty} e^{-iwx} f_m^c(x)\,dx \\
&= \sum_{k=0}^{2^m-1} c_{m,k} \int_{-\infty}^{+\infty} e^{-iwx} \phi_{m,k}\left(\frac{x-a}{b-a}\right) dx \\
&= (b-a)\cdot e^{-iaw} \cdot \sum_{k=0}^{2^m-1} c_{m,k} \hat{\phi}_{m,k}\left((b-a)\,w\right),
\end{aligned} \tag{4.25}$$

where we have performed the change of variables $y = (x-a)/(b-a)$ and identified the Fourier transform of $\phi_{m,k}$. This expression leads to the following result:

Lemma 4.2. *Define the following functions:*

$$P_m(z) := \sum_{k=0}^{2^m-1} c_{m,k} z^k, \qquad Q_m(z) := \frac{2^{\frac{m}{2}} z^{-\frac{2^m a}{b-a}} \hat{f}\left(\frac{2^m}{b-a} i \cdot \log(z)\right)}{(b-a)\cdot \hat{\phi}(i\cdot\log(z))}. \tag{4.26}$$

Then, the function $P_m(z)$ can be approximated by $Q_m(z)$, that is, $P_m(z) \approx Q_m(z)$.

Proof. Notice first that from (4.22) one deduces that $\hat{\phi}_{m,k}(w) = 2^{-\frac{m}{2}}\hat{\phi}\left(\frac{w}{2^m}\right)e^{-i\frac{k}{2^m}w}$. If we use this identity in the approximation made in (4.25) and take $y = \frac{2^m}{b-a}i\cdot\log(z)$, we get

$$\begin{aligned}\hat{f}\left(\frac{2^m}{b-a}i\cdot\log(z)\right) &\approx 2^{-\frac{m}{2}}(b-a)\cdot z^{\frac{2^m a}{b-a}}\cdot\hat{\phi}_{m,k}(i\cdot\log(z))\cdot\sum_{k=0}^{2^m-1}c_{m,k}z^k \\ &= 2^{-\frac{m}{2}}(b-a)\cdot z^{\frac{2^m a}{b-a}}\cdot\hat{\phi}_{m,k}(i\cdot\log(z))\cdot P_m(z).\end{aligned}$$

From this expressions it is immediate to conclude that $P_m(z) \approx Q_m(z)$ which finish the proof of the lemma. □

Observe that the function $P_m(z)$ defined in (4.26) is a polynomial and particularly it is analytic inside a disc of the complex plane $\{z\in\mathbb{C}: |z|<R\}$ for $R>0$. Then, Cauchy's integral formula can be applied and gives rise to the following closed expression for the density coefficients

$$c_{m,k} = \frac{1}{2\pi i}\int_{C_R}\frac{P_m(z)}{z^{k+1}}dz, \qquad \text{for } k = 0,\ldots,2^m-1, \tag{4.27}$$

where C_R denotes the circle of radius $R>0$ about the origin. Next theorem uses expression (4.27) together with Lemma 4.2 to derive an approximation for the numerical computation of the density coefficients $c_{m,k}$.

Theorem 4.3 (Approximation of the density coefficients $c_{m,k}$)**.** *Consider the function Q_m defined in Lemma 4.2. Then, the density coefficents can be approximated by*

$$\begin{aligned}c_{m,0} \approx c^*_{m,0} &= \frac{1}{\pi}\int_0^\pi \Re\left(Q_m\left(Re^{iu}\right)\right)du, \\ c_{m,k} \approx c^*_{m,k} &= \frac{2}{\pi R^k}\int_0^\pi \Re\left(Q_m\left(Re^{iu}\right)\right)\cos(ku)\,du,\end{aligned} \tag{4.28}$$

for $k = 1,\ldots,2^m-1$ and where R is a positive real number different from 1.

Proof. Bearing in mind the definition of $P_m(z)$ given by (4.26) in Lemma 4.2, if we make the change of variables $z = R\cdot e^{iu}$ with $R\neq 1$ positive, take the real part of $P_m(Re^{iu})$ and multiply it by $\cos(ku)$, we obtain

$$\begin{aligned}\Re\left(P_m\left(Re^{iu}\right)\right)\cos(ku) &= \sum_{l=0}^{2^m-1}c_{m,l}R^l\cos(lu)\cos(ku) \\ &= \frac{1}{2}\sum_{l=0}^{2^m-1}c_{m,l}R^l\left(\cos((l+k)u)+\cos((l-k)u)\right).\end{aligned} \tag{4.29}$$

Next, we integrate last expression between 0 and π and distinguish the case $k = 0$ and the case $k \neq 0$. We get respectively:

$$\circ \int_0^\pi \Re\left(P_m\left(Re^{iu}\right)\right) du = \sum_{l=0}^{2^m-1} c_{m,l} R^l \int_0^\pi \cos(lu)\, du = \pi \cdot c_{m,0},$$

$$\circ \int_0^\pi \Re\left(P_m\left(Re^{iu}\right)\right) \cos(ku)\, du$$

$$= \frac{1}{2} \sum_{l=0}^{2^m-1} c_{m,l} R^l \int_0^\pi \left(\cos\left((l+k)u\right) + \cos\left((l-k)u\right)\right) du = \frac{\pi}{2} c_{m,k} R^k.$$

By Lemma 4.2, we can replace the function P_m by its approximation Q_m to obtain (4.28). □

Remark 4.2. *In practice, both integrals in (4.28) are computed by means of a numerical integration method. In order to speed up the computation, we have adapted a trapezoidal rule in such a way that a FFT algorithm can be applied. For brevity, we show this technique for the second integral in (4.28) since the computation for first integral is analogous. Thus, applying the trapezoidal rule in the second integral using as grid points $h_s = s \cdot \pi/2^m$, $s = 0, \ldots, 2^m$,*

$$c_{m,k} \approx \frac{2}{\pi R^k} \int_0^\pi \Re\left(Q_m\left(re^{iu}\right)\right) cos(ku)\, du$$

$$\approx \frac{1}{2^m \cdot R^k} \cdot \left[Q_m(R) + (-1)^k Q_m(-R) + 2 \cdot \sum_{s=1}^{2^m-1} \Re\left(Q_m\left(Re^{ih_s}\right)\right) \Re\left(e^{\frac{ik\pi s}{2^m}}\right)\right],$$

for $k = 1, \ldots, 2^m - 1$. This expression allows to apply a FFT algorithm. The computational complexity associated to a direct computation of the density coefficients by the trapezoidal rule is $\mathcal{O}(2^{2m})$, while the complexity during the application of the FFT algorithm explained above reduces to $\mathcal{O}(\log(2) \cdot m \cdot 2^m)$.

4.3.3 Approximation of $a_k(z)$ using the WA$^{[a,b]}$ method.

In this section, we provide a general methodology to compute the coefficients $a_k(z)$ which relies on the WA$^{[a,b]}$ method. This technique will be independent of the dynamics of the log-asset price and will just need the characteristic function of the log-returns of the process L_{j^*+k}, $k = 1, \ldots, m$, which is known in most cases. This fact will make the method really versatile and flexible since it could be applicable even in the situations where an expression for the coefficients $a_k(z)$ cannot be found analytically.

The underlying idea of this strategy is to approximate the density function using the WA$^{[a,b]}$ method as we did in (4.24) and compute the analogous of the pay-off coefficients. We derive two feasible expressions for these pay-off coefficients. The first one comes directly from replacing the approximation of the density function in the definition of $a_k(z)$ as a characteristic function. The second one involves the Cauchy Residue theorem and provides a more desirable formula.

Theorem 4.4 (Approximation of coefficients $a_k(-z)$)**.** *Let $z \in \mathbb{R}^+$. Let $c_{m,j}$ be the coefficients resulting from the approximation of the density of L_{j^*+k} in (4.24). Define $J := \lfloor -a2^m/(b-a) \rfloor$. Then, the coefficients $a_k(-z)$ can be approximated by*

$$\begin{aligned} a_k(-z) \approx\ & (b-a)\,2^{-\frac{m}{2}} \sum_{j=0}^{J-1} c_{m,j} \ + \ (b-a) \sum_{j=J+1}^{2^m-1} c_{m,j} \cdot e^{-iza} \cdot \hat{\phi}_{m,j}\left((b-a)\,z\right) \\ & + 2^{\frac{m}{2}} \left(-a - \frac{(b-a)\,J}{2^m} - \frac{1}{iz} \cdot \left[e^{-iz\left(a+(b-a)\frac{J+1}{2^m}\right)} + 1 \right] \right) c_{m,J}. \end{aligned} \tag{4.30}$$

Proof. Let $f_{L_{j^*+k}}$ denote the density function of L_{j^*+k}. By definition, the coefficient $a_k(z)$ can be written as follows

$$a_k(-z) \ = \ \mathbb{E}\left(e^{-izL^+_{j^*+k}}\right) \ = \ \int_{-\infty}^{0} f_{L_{j^*+k}}(y)\,dy \ + \ \int_{0}^{+\infty} e^{-izy} f_{L_{j^*+k}}(y)\,dy. \tag{4.31}$$

We take the approximation of the density function (4.24) and treat each one of the integrals in (4.31) separately. We start studying the first integral in (4.31). If we make the change of variables $x = (y-a)/(b-a)$ and bear in mind the definition of $\phi_{m,j}(x)$, we get

$$\begin{aligned} \int_{-\infty}^{0} f_{L_{j^*+k}}(y)\,dy \ &\approx \ \sum_{j=0}^{2^m-1} c_{m,j}\,(b-a) \int_{-\infty}^{\frac{-a}{b-a}} \phi_{m,j}(x)\,dx \\ &= \ \sum_{j=0}^{2^m-1} c_{m,j}\,(b-a)\,2^{m/2} \int_{\left(-\infty,\frac{-a}{b-a}\right)\cap\left[\frac{k}{2^m},\frac{k+1}{2^m}\right]} dx \\ &= \ (b-a)\,2^{-\frac{m}{2}} \sum_{j=0}^{J-1} c_{m,j} \ - \ 2^{\frac{m}{2}} \left(a + \frac{(b-a)\,J}{2^m}\right) c_{m,J}. \end{aligned} \tag{4.32}$$

In the same way, if we make the same change of variables for the second integral in (4.31)

$$\begin{aligned} \int_{0}^{+\infty} e^{-izy} f_{L_{j^*+k}}(y)\,dy \ &\approx \ \sum_{j=0}^{2^m-1} c_{m,j}\,(b-a)\,e^{-iza} \int_{\frac{-a}{b-a}}^{+\infty} \phi_{m,j}(x)\,e^{-(b-a)izx} dx \\ &= \ \sum_{j=0}^{2^m-1} c_{m,j}\,(b-a)\,e^{-iza} \cdot 2^{m/2} \int_{\left(\frac{-a}{b-a},+\infty\right)\cap\left[\frac{k}{2^m},\frac{k+1}{2^m}\right]} e^{-(b-a)izx} dx \\ &= \ (b-a) \sum_{j=J+1}^{2^m-1} c_{m,j} \cdot e^{-iza} \cdot \hat{\phi}_{m,j}\left((b-a)\,z\right) \\ &\qquad - \ \frac{2^{m/2}}{iz} \left[e^{-iz\left(a+(b-a)\frac{J+1}{2^m}\right)} + 1 \right] c_{m,J}. \end{aligned} \tag{4.33}$$

Finally, introducing the expressions (4.32) and (4.33) in (4.31), and rearranging the terms gives the approximation (4.30) and concludes the proof. □

Theorem 4.4 provides a closed formula for the numerical computation of the coefficient $a_k(z)$. Notice that this expression (4.30) involves all the density coefficients in the calculation. An alternative approximation which needs to compute a lower number of density coefficients can be found applying the Cauchy Residue Theorem. For this purpose, we proceed to formulate the following theorem which gives an expression that connects the coefficient $a_k(-z)$ and the characteristic function $\Phi_{L_{j^*+k}}$ by means of a complex integral.

Proposition 4.4 (Fourier representation of $a_k(z)$)**.** *Assume $M_{L_{j^*+k}}(v) = E_{\mathbb{Q}}\left(e^{vL_{j^*+k}}\right)$, the moment generating function of L_{j^*+k}, exists for all $v \in (a,b)$, where $a<0$ and $b > Im(z) > -1/2$. Take $\alpha \geq Im(z) > -1/2$, then the coefficient $a_k(-z)$ can be computed by:*

$$a_k(z) = 1 - \frac{i}{2\pi}\int_{i\alpha-\infty}^{i\alpha+\infty} \Phi_{L_{j^*+k}}(-\xi)\,\frac{z}{\xi\,(\xi+z)}d\xi, \quad k=1,\ldots,m. \tag{4.34}$$

Proof. The proof is based on applying the Cauchy residue theorem and the technical details are therefore omitted. □

Next, we apply the $\mathrm{WA}^{[a,b]}$ method to approximate the characteristic function $\Phi_{L_{j^*+k}}$. Proceeding as in last section, we first truncate the integration domain by (4.23) using the cumulants and later we approximate the probability density function of L_{j^*+k} by means of the Haar wavelet family as in (4.24). Finally, if we apply the same computation as in (4.25), we get that the characteristic function $\Phi_{L_{j^*+k}}$ can be approximated by

$$\Phi_{L_{j^*+k}}(\xi) \approx (b-a)\cdot e^{-ia\xi}\cdot \sum_{k=0}^{2^m-1} c_{m,k}\cdot \hat{\phi}_{m,k}\left((b-a)\,\xi\right), \tag{4.35}$$

where the density coefficients $c_{m,j}$ are calculated using the expressions provided in Theorem 4.3. Notice that this approximation can be analytically extended to the complex plane. This fact allows us to apply the Cauchy Residue theorem and gives rise to a closed expression for the computation of $a_k(-z)$ given in next theorem.

Theorem 4.5 (Approximation of coefficients $a_k(z)$)**.** *Let $z \in \mathbb{R}^+$. Let $c_{m,j}$ be the coefficients resulting from the approximation of the density of L_{j^*+k} in (4.24). Define Then, the coefficients $a_k(z)$ can be approximated by the following expression*

$$a_k(z) \approx 1 - (b-a)\cdot \sum_{j=J}^{2^m-1} c_{m,j} V_{m,j}, \tag{4.36}$$

where we have defined $J := \lfloor -a2^m/(b-a)\rfloor$ and the coefficients $V_{m,j}$ as

$$V_{m,j} := 2^{-m/2}\cdot\left(1 - e^{-iz\left(\frac{j}{2^m}(b-a)+a\right)}\left(\frac{1-e^{-i\frac{b-a}{2^m}z}}{i\frac{b-a}{2^m}z}\right)\right). \tag{4.37}$$

Proof. Note that $z \in \mathbb{R}^+$ and particularly $Im(z) = 0$. Then, Proposition 4.4 applies with $\alpha = 1$ and the coefficients $a_k(z)$ are

$$\begin{aligned} a_k(z) &= 1 - \frac{i}{2\pi}\int_{i-\infty}^{i+\infty} \Phi_{L_{j^*+k}}(\xi)\,\frac{z}{\xi(\xi+z)}d\xi \\ &= 1 - \frac{i}{2\pi}\int_{-\infty}^{+\infty} \Phi_{L_{j^*+k}}(i+t)\,\frac{z}{(i+t)(i+t+z)}dt \\ &\approx 1 - \frac{i(b-a)}{2\pi}\sum_{k=0}^{2^m-1} c_{m,j}\int_{-\infty}^{+\infty} e^{-ia(i+t)}\cdot\hat{\phi}_{m,j}((b-a)(i+t))\,\frac{z}{(i+t)(i+t+z)}dt, \end{aligned}$$

where we have taken the parameterization $\xi(t) = i + t$ for $t \in (-\infty, \infty)$ in the second equality and we have introduced expression (4.35) in the approximation. Define

$$\begin{aligned} V_{m,j} &:= \int_{-\infty}^{+\infty} \frac{i}{2\pi}\cdot e^{-ia(i+t)}\cdot\hat{\phi}_{m,j}((b-a)(i+t))\,\frac{z}{(i+t)(i+t+z)}dt \\ &= \int_{-\infty}^{+\infty} \frac{i2^{-m/2}}{2\pi}\cdot e^{-i(i+t)\left(a+\frac{j(b-a)}{2^m}\right)}\cdot\hat{\phi}\left(\frac{(b-a)}{2^m}(i+t)\right)\frac{z}{(i+t)(i+t+z)}dt. \end{aligned} \tag{4.38}$$

It remains to show that $V_{m,j}$ equals zero for $j \le J$ and (4.37) for $j > J$. We will use the Cauchy's residue theorem to evaluate the integral in (4.38). Let us first define by $g(t)$ the function inside the integral in (4.38) and study the case $j \le J$. We consider the contour shown in Figure 4.1 on the left. As g has not poles inside, the Cauchy's residue theorem leads to

$$\int_{\Upsilon_R} g(w)dw = -\int_{\Gamma_R} g(w)dw. \tag{4.39}$$

Let us show that the integral on Γ_R goes to 0 as $R \to \infty$. If we consider $w(\theta) = R\cos(\theta) + iR\sin(\theta)$, $\theta \in [0,\pi]$, a parameterization of Γ_R, we obtain

$$\begin{aligned} \left|\int_{\Gamma_R} g(w)dw\right| &= \left|\int_0^\pi \frac{i\cdot\frac{2^{-m/2}}{2\pi}\cdot z\cdot e^{-i(i+w(\theta))\left(a+\frac{j(b-a)}{2^m}\right)}\cdot\hat{\phi}\left(\left(\frac{b-a}{2^m}\right)(i+w(\theta))\right)}{[R\cos(\theta)+i(1+R\sin(\theta))]\cdot[(R\cos(\theta)+z)+i(1+R\sin(\theta))]}d\theta\right| \\ &\le \frac{z}{2\pi}2^{-m/2}e^{a+\frac{j(b-a)}{2^m}}\left(1+e^{(b-a)/2^m}\right)\frac{1}{R^3}\pi \overset{R\to+\infty}{\longrightarrow} 0, \end{aligned}$$

where we have used that $\left|e^{-i(i+w(\theta))\left(a+\frac{j(b-a)}{2^m}\right)}\right| = e^{(1+R\sin(\theta))\left(a+\frac{j(b-a)}{2^m}\right)}$. Then, as $\theta \in [0,\pi]$ and $j \le J \le -a2^m/(b-a)$, this expression is bounded by $e^{a+j(b-a)/2^m}$. We have also used that

$$\begin{aligned} &\frac{1}{|R\cos(\theta)+i(1+R\sin(\theta))|\cdot|(R\cos(\theta)+z)+i(1+R\sin(\theta))|} \\ &\qquad\le \frac{1}{|R\cos(\theta)+iR\sin(\theta)|\cdot|R\cos(\theta)+iR\sin(\theta)|} = \frac{1}{R^2} \end{aligned}$$

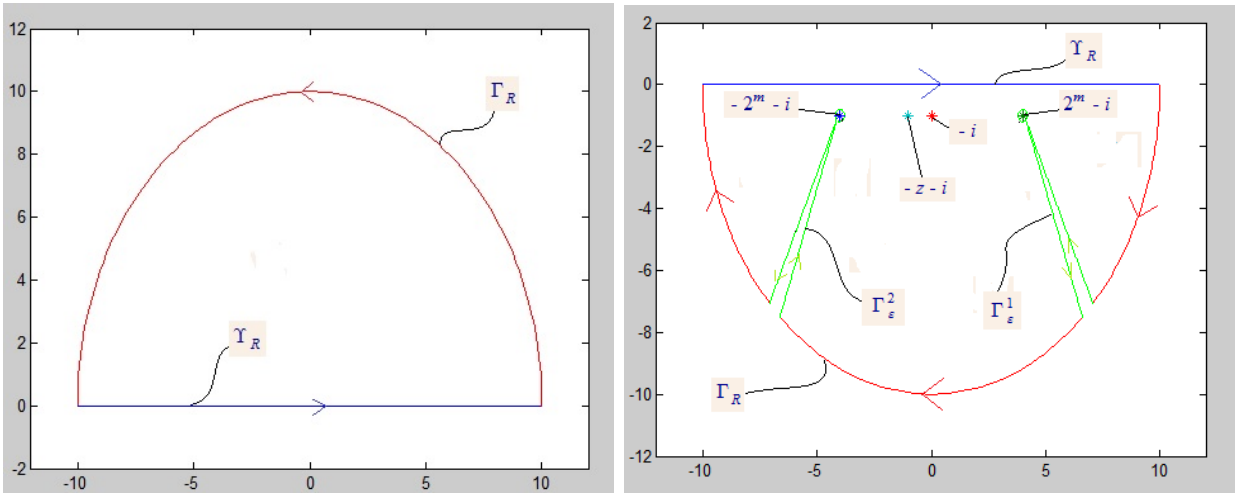

Figure 4.1: The figure on the left shows the contour used to evaluate the integral when $j \leq J$. The figure on the right shows the contour to evaluate the integral when $j > J$.

and $\hat{\phi}\left(\frac{(b-a)}{2^m}(i+t)\right)$ can be bounded by $\left(1+e^{(b-a)/2^m}\right)/R$. Finally, taking limits as $R \to \infty$ in (4.39) and noticing that the term on the left coincides with $V_{m,j}$, we conclude that the approximation coefficient $V_{m,j} = 0$ when $j \leq -a2^m/(b-a)$.

The case $j > J$ requires to evaluate $g(w)$ over the contour on the right in Figure 4.1. Again, as the function $g(w)$ is holomorphic inside the contour, we can apply the Cauchy's residue theorem. Notice, however, that in this case the function has two poles at $w = -i$ and $w = -z - i$. Thus, the Cauchy's residue theorem gives us now:

$$\int_{\Upsilon_R} g(w)dw + \int_{\Gamma_R} g(w)dw = 2\pi i \left(\text{Res}\left(g, -i\right) + \text{Res}\left(g, -z-i\right)\right), \tag{4.40}$$

As the poles are simple, their residues can be computed respectively as follows:

$$\begin{aligned}
\bullet \lim_{w \longrightarrow -i} (w+i)\, g(w) &= \lim_{w \longrightarrow -i} \frac{i}{2\pi} \cdot e^{-ia(i+t)} \cdot \hat{\phi}_{m,j}\left((b-a)(i+t)\right) \frac{z}{(i+w+z)} \\
&= \frac{i}{2\pi} \cdot 2^{-m/2}, \\
\bullet \lim_{w \longrightarrow -i-z} (w+i+z) g(w) &= \lim_{w \longrightarrow -i-z} \frac{i}{2\pi} \cdot e^{-ia(i+t)} \cdot \hat{\phi}_{m,j}\left((b-a)(i+t)\right) \frac{z}{(i+w)} \\
&= \frac{i}{2\pi} \cdot 2^{-m/2} e^{-iz\left(\frac{j}{2^m}(b-a)+a\right)} \left(\frac{1-e^{-i\frac{b-a}{2^m}z}}{i\frac{b-a}{2^m}z}\right).
\end{aligned} \tag{4.41}$$

In the same way as we did in the case $j \leq J$, one shows that the integral of $g(w)$ over Γ_R goes to 0 as $R \to \infty$. Then, taking limits as $R \to \infty$ in (4.40), noticing that the first integral on the left-hand side coincides with $V_{m,j}$ and using the expressions of the residues (4.41), one obtains (4.35). □

4.3.4 Approximation of $a_k(z)$ using Shannon wavelets.

Recall that our aim is to apply the SWIFT method for pricing discrete lookback options. The first step is to approximate the density function of the asset log-return maximum f_{X_m} in terms of the Shannon scaling functions as stated in Proposition 3.2, that is,

$$f_{X_m}(y|x) \approx f^*_{X_m}(y|x) = \sum_{k=k_1}^{k_2} d_{m,k}(x)\,\phi_{m,k}(y), \tag{4.42}$$

where $d_{m,k}$ are now the density coefficients. These coefficients will be computed by means of (3.29) fixing first a J-value, denoted here by $\jmath$, and using a FFT algorithm as in Remark 3.2. Notice also that, using this strategy, we should evaluate the characteristic function $\phi_{X_m}(z)$ at points $z_s = (2s+1)\,\pi 2^m/2^\jmath$ for $s = 0, \ldots, 2^{\jmath-1}-1$.

The main drawback of using Haar wavelets to approximate the coefficients $a_k(z_s)$ is that a high level of resolution m is needed as it will be seen in the section of numerical experiments. In addition, this methodology does not allow to apply a FFT algorithm and the coefficients $a_k(z_s)$ need to be calculated one by one. Then, motivated by the good approximation properties of the Shannon wavelets, we derive in Theorem 4.6 an approximation which relies on this wavelet family. This formula has the noteworthy feature of allowing the application of a FFT algorithm which considerably reduces the CPU time.

Theorem 4.6 (Approximation of coefficients $a_k(-z)$ by means of Shannon wavelets)**.** *Let $c_{\widetilde{m},j}$ be the coefficients resulting from approximating the density function of L_{j^*+k} by Shannon wavelets at a level of resolution $\widetilde{m}$ and j_1 and j_2 the limits values in the summation. Let $\delta_{i,j}$ denote the Dirac's delta. Define $\bar{j}_2 := \max(0, j_2)$ and $\bar{j}_1 := \min(0, j_1)$. Then, the coefficients $a_k(-z)$ can be approximated by*

$$\begin{aligned} a_k(-z) \approx\ & \frac{1}{2^{\widetilde{m}/2}} \cdot \left(\frac{1}{2} \cdot c_{\widetilde{m},j_1} + \sum_{j=j_1+1}^{-1} c_{\widetilde{m},j} + \frac{1}{2} \cdot c_{\widetilde{m},0} \right) \cdot \delta_{\bar{j}_1,j_1} \\ & + \frac{1}{2^{\widetilde{m}/2}} \cdot \left(\frac{1}{2} \cdot c_{\widetilde{m},0} + \sum_{j=1}^{j_2-1} e^{-iz\frac{j}{2^{\widetilde{m}}}} \cdot c_{\widetilde{m},j} + \frac{1}{2} \cdot c_{\widetilde{m},j_2} \right) \cdot \delta_{\bar{j}_2,j_2}. \end{aligned} \tag{4.43}$$

Proof. We start estimating the density function of L_{j^*+k} by means of the Shannon scaling functions (3.4) and truncating the infinite integration domain to a finite domain $\mathcal{I}_{\widetilde{m}} = [j_1/2^{\widetilde{m}}, j_2/2^{\widetilde{m}}]$. Then, if we introduce these approximations in the expression of the coefficient $a_k(-z)$ in (4.31), we get

$$a_k(-z) \approx \sum_{j=j_1}^{j_2} c_{\widetilde{m},j} \cdot \left(\int_0^{\bar{j}_2/2^{\widetilde{m}}} e^{-izy} \cdot \phi_{\widetilde{m},j}(y)dy + \int_{\bar{j}_1/2^{\widetilde{m}}}^{0} \phi_{\widetilde{m},j}(y)dy \right). \tag{4.44}$$

We treat each one of the integrals in (4.44) separately. We start analyzing the first integral. If we apply a trapezoidal rule with grid points $\left\{0, 1/2^{\widetilde{m}}, \ldots, \bar{j}_2/2^{\widetilde{m}}\right\}$ and we take into account

that $\phi_{\widetilde{m},j}(h/2^{\widetilde{m}}) = 2^{\widetilde{m}/2}\delta_{j,h}$ as we saw Lemma 3.1, we obtain:

$$\begin{aligned}\int_0^{\bar{j}_2/2^{\widetilde{m}}} e^{-izy}\phi_{\widetilde{m},j}(y)dy &\approx \frac{1}{2^{\widetilde{m}}}\cdot\left(\frac{1}{2}\phi_{\widetilde{m},j}(0) + \sum_{s=1}^{\bar{j}_2-1} e^{-iz\frac{s}{2^{\widetilde{m}}}}\phi_{\widetilde{m},j}\left(\frac{s}{2^{\widetilde{m}}}\right) + \frac{1}{2}e^{-iz\frac{\bar{j}_2}{2^{\widetilde{m}}}}\phi_{\widetilde{m},j}\left(\frac{\bar{j}_2}{2^{\widetilde{m}}}\right)\right)\\ &= \frac{1}{2^{\widetilde{m}/2}}\cdot\left(\frac{1}{2}\delta_{j,0} + \sum_{s=1}^{\bar{j}_2-1} e^{-iz\frac{s}{2^{\widetilde{m}}}}\cdot\delta_{j,s} + \frac{1}{2}\cdot\delta_{j,\bar{j}_2}\right).\end{aligned}$$

In the same way, if we apply a trapezoidal rule to the second integral in (4.31) with grid points $\left\{\bar{j}_1/2^{\widetilde{m}}, (\bar{j}_1+1)/2^{\widetilde{m}}, \ldots, -1/2^{\widetilde{m}}, 0\right\}$, one gets a similar expression:

$$\begin{aligned}\int_{\bar{j}_1/2^{\widetilde{m}}}^0 \phi_{\widetilde{m},j}(y)dy &\approx \frac{1}{2^{\widetilde{m}}}\cdot\left(\frac{1}{2}\cdot\phi_{\widetilde{m},j}\left(\frac{\bar{j}_1}{2^{\widetilde{m}}}\right) + \sum_{s=\bar{j}_1+1}^{-1}\phi_{\widetilde{m},j}\left(\frac{s}{2^{\widetilde{m}}}\right) + \frac{1}{2}\cdot\phi_{\widetilde{m},j}(0)\right)\\ &= \frac{1}{2^{\widetilde{m}/2}}\cdot\left(\frac{1}{2}\cdot\delta_{j,\bar{j}_1} + \sum_{s=\bar{j}_1+1}^{-1}\delta_{j,s} + \frac{1}{2}\cdot\delta_{j,0}\right).\end{aligned}$$

If we replace both integrals in (4.44) by their approximations, we obtain expression (4.43). □

The main advantage of approximating coefficients $a_k(-z)$ using Theorem 4.6 is that we work with Shannon wavelets which exhibit better approximation properties of the probability density function L_{j^*+k} than Haar wavelets. Another noteworthy feature of this strategy is that it allows the application of a FFT algorithm in order to speed up the computation. Next remark provides the basis to do that.

Remark 4.3. *The reason why we are evaluating the coefficients a_k is to compute the characteristic function of the asset log-return maximum $\phi_{X_m}(z)$ at points $z_s = (2s+1)\pi 2^m/2^\jmath$ for $s = 0, \ldots, 2^{\jmath-1}-1$. In consequence, we particularly need to evaluate $a_k(-z)$ at these points. This can be done efficiently by rewriting (4.43) at z_s as:*

$$\begin{aligned}a_k(-z_s) \approx{}& \frac{1}{2^{\widetilde{m}/2}}\cdot\left(\frac{1}{2}\cdot c_{\widetilde{m},j_1} + \sum_{j=j_1+1}^{-1} c_{\widetilde{m},j} + \frac{1}{2}\cdot c_{\widetilde{m},0}\right)\cdot\delta_{\bar{j}_1,j_1}\\ &+ \frac{1}{2^{\widetilde{m}/2}}\cdot\left(-\frac{1}{2}\cdot c_{\widetilde{m},0} + \sum_{j=0}^{j_2-1}\left(c_{\widetilde{m},j}\cdot e^{-\frac{ij\pi}{2^{\jmath+\widetilde{m}-m}}}\right)e^{-\frac{2\pi isj}{2^{\jmath+\widetilde{m}-m}}} + \frac{1}{2}\cdot c_{\widetilde{m},j_2}\right)\cdot\delta_{\bar{j}_2,j_2}.\end{aligned} \tag{4.45}$$

This expression (4.45) allows to apply the FFT algorithm in the second term of the sum to compute the coefficients $a_k(-z_s)$. We just need to extend the summation from j_2-1 to $2^{\jmath+\widetilde{m}-m}-1$ by assuming that the terms $c_{\widetilde{m},j}\cdot e^{-\frac{ij\pi}{2^{\jmath+\widetilde{m}-m}}}$ are zero in this range. The computational complexity is reduced from $\mathcal{O}\left(2^{\jmath+\widetilde{m}-m}\cdot j_2\right)$ when we use directly expression (4.45) to $\mathcal{O}\left(\log(2)\cdot(\jmath+\widetilde{m}-m)\cdot 2^{\jmath+\widetilde{m}-m}\right)$ by using the FFT algorithm.

4.4 The pay-off coefficients for Discrete Lookback Options

As we saw in Chapter 3 for the pricing of European options, the last step of the SWIFT method is to determine the pay-off coefficients $V_{m,k}$. To this end, the strategy to follow is to approximate, first of all, the density function of the asset log-return maximum f_{X_m} in terms of the Shannon scaling functions as in (4.42).

Next, we should introduce this approximation in the valuation formula of the corresponding derivative. As has already been mentioned, we mainly focus in *fixed lookback call options* and *floating lookback put options*. Since using Lemma 4.1 the price of the floating lookback put option can be directly determined if we hold the price of the fixed lookback call options in the case $M \geq K$, we concentrate in this last one. Its valuation formula is given by (4.4) in Proposition 4.1. Then, if we introduce the approximation (4.42), we obtain:

$$\begin{aligned} LC_{fix}(t,T) &= S_0 e^{-r(T-t)} \cdot E_{\mathbb{Q}}\left[\left(e^{X_m} - R\right)_+\right] + (M-K)\, e^{-r(T-t)} \mathbb{1}_{[K,+\infty]}(M) \\ &= S_0 e^{-r(T-t)} \cdot \int_{\mathbb{R}\cap\mathcal{I}_m} (e^x - R)_+ \cdot f_{X_m}(x)\, dx + (M-K)\, e^{-r(T-t)} \mathbb{1}_{[K,+\infty]}(M) \\ &= S_0 e^{-r(T-t)} \cdot \sum_{k=k_1}^{k_2} d_{m,k} \cdot V_{m,k} + (M-K)\, e^{-r(T-t)} \mathbb{1}_{[K,+\infty]}(M), \end{aligned}$$

where $R := K/S_0$ and $\mathbb{1}_{[K,+\infty]}(M)$ is the indicator function. Note also that we have truncated the infinite integration domain to a finite domain $\mathcal{I}_m = [k_1/2^m, k_2/2^m]$ and we have defined the pay-off coefficients in the following way:

$$V_{m,k} := \int_{\mathbb{R}\cap\mathcal{I}_m} (e^x - R)_+ \cdot \phi_{m,k}(x)\, dx = \int_{[\ln(R),\infty]\cap\mathcal{I}_m} (e^x - R) \cdot \phi_{m,k}(x)\, dx.$$

Notice, however, that this integral cannot be computed analytically. Next proposition provides an expression to efficiently compute $V_{m,k}$ together with an error estimate.

Proposition 4.5 (Approximation of Fixed Lookback call option pay-off coefficients and error estimate)**.** *Let us define* $\bar{k}_1 := \max(k_1, \ln(R)\cdot 2^m)$. *Then, an approximation of the pay-off coefficients for a Fixed Lookback call option is computed as*

$$V_{m,k} \approx V^*_{m,k} := \begin{cases} \frac{2^{m/2}}{2^{J-1}} \sum_{j=1}^{2^{J-1}} \left[I_1\left(\frac{\bar{k}_1}{2^m}, \frac{k_2}{2^m}\right) - R \cdot I_2\left(\frac{\bar{k}_1}{2^m}, \frac{k_2}{2^m}\right)\right] & \text{if } k_2 > \ln(R), \\ 0 & \text{if } k_2 \leq \ln(R), \end{cases} \tag{4.46}$$

where the integrals I_1 *and* I_2 *are defined as in Proposition 3.4. Additionally, if we consider* $J \geq \log_2(\pi N_k)$, *we find the following estimation of the error*

$$\left|V_{m,k} - V^*_{m,k}\right| \leq \frac{1}{2^{m/2}} \cdot D \cdot \frac{(\pi N_k)^2}{2^{2(J+1)} - (\pi N_k)^2}, \tag{4.47}$$

$$N_k := \max\left(\left|\bar{k}_1 - k\right|, \left|k_2 - k\right|\right), \quad D := \left|k_2 - \bar{k}_1\right| \cdot \max_{y \in \left[\frac{\bar{k}_1}{2^m}, \frac{k_2}{2^m}\right]} \left|e^y - R\right|.$$

Proof. The proof is completely analogous to the one made in Proposition 3.4 to approximate the European option pay-off coefficients. □

Remark 4.4. *Similar formulas to those provided in Remark 3.5 for the computation of integrals I_1 and I_2 can be derived in this case for lookback options. As a consequence, the pay-off coefficients $V^*_{m,k}$ may be computed using a FFT algorithm by fixing a constant J value defined here by $\bar{\jmath} := \lceil \log_2(\pi N) \rceil$, where $N := \max_{k_1<k<k_2} N_k$. Another feasible strategy is to calculate the pay-off coefficients beforehand with high accuracy for later use by means of the estimate (4.47) in order to save some CPU time.*

4.5 Numerical experiments

In this section, we carry out several numerical experiments to evaluate the accuracy, efficiency and robustness of the SWITF method for pricing Discrete Lookback options. We take into account three dynamics for the asset log-return L_t in order to show the versatility of this pricing technique: the first one is the geometric Brownian motion (GBM) for which an analytic expression for the coefficients $a_k(z)$ will be derived. The other two are the Variance Gamma process (VG) and the Heston model. These last dynamics do not hold an analytic expression for a_k and they will be computed with the approximations described in Theorem 4.4 (using Haar Wavelets) and Theorem 4.5 (using Shannon Wavelets).

We also implement the evaluation of the characteristic function of the asset log-return maximum X_m by means of the recursive formula (4.13) and recursion (4.15). We show that although recursion (4.15) provides a lower theoretical computational complexity, the restrictions of programming with MATLAB make more efficient the recursive formula (4.13). Finally, we demonstrate the efficiency and accuracy of the method by comparing our results with those obtained with the FTBS method in [9]. Before starting to show the results obtained, however, we should still fix a criterion to determine the scale of approximation m of the probability density function and the limit value k_1 and k_2 in the summation.

4.5.1 Scale of approximation m

Recall that the error of approximation at a scale m depends on the decay of the Fourier transform of the probability density function and is given by expression (3.11). In the case of European option pricing analyzed in Chapter 3, we studied the decay properties of the analytic expression of the Fourier transform of the underlying process in order to determine a proper scale m. For lookback options, however, we do not hold an analytic formula of the characteristic function of X_m. Instead, we have in hands a recursive formula that allows its evaluation and the decays properties may be studied numerically.

To illustrate the dependency of the parameter m with respect to the decay of the characteristic function, we price a *lookback put option with fixed strike* considering three dynamics with a different rate of decay and compare it with the scale m. The probability density function and the modulus of the characteristic functions of all the dynamics have been numerically computed and represented in Figure 4.2 on the left and right respectively. The results of the experiments obtained are shown in Table 4.5.1.

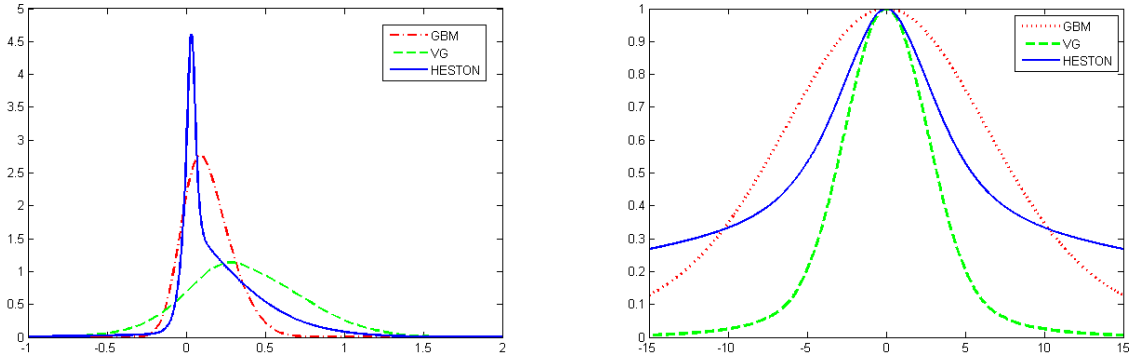

Figure 4.2: Density function (left) and modulus of the characteristic function (right). The dotted red line corresponds to GBM dynamics, the thick blue line to Heston dynamics and the dashed green line to VG dynamics.

We first consider Variance Gamma (VG) dynamics with parameters $S_0 = 100$, $K = 110$, $r = 0.0548$, $\sigma = 0.1927$, $\mu = -0.2859$, $\nu = 0.25$ and six monitoring points evenly spaced in $T = [0, 5]$. The reference value is 19.746659329720089 computed using a high scale m with the SWIFT method [1]. We see in Table 4.5.1 that we achieve the smaller error with the lower scale ($m = 4$). The explanation of this fact is that the Variance Gamma process shows the fastest rate of decay of the characteristic function as it can be observed in Figure 4.2. Second, we consider GBM dynamics with parameters $S_0 = 100$, $K = 110$, $r = 0.1$, $\sigma = 0.3$ and six monitoring points evenly spaced in $T = [0, 0.5]$. The reference value is 13.300135659395124. Now, we also use an scale of $m = 4$, but the error is higher since the rate of decay of ϕ_{X_m} is slower in this case. Finally, we work with Heston dynamics with parameters $S_0 = 100$, $K = 110$, $r = 0.1$, $\lambda = 1.5768$, $\nu = 0.5751$, $\bar{u} = 0.0398$, $u_0 = 0.0175$, $\rho = -0.5711$ and six monitoring points evenly spaced in the lifetime of the option $T = [0, 0.5]$. Now, the reference value is 27.020436365846209 and the rate of decay of the characteristic function becomes the slowest of the three dynamics. This translates into needing a big scale ($m = 10$) to achieve a smaller error.

[1] All the reference values in this section are computed by means of the SWIFT method using a high scale m. Particularly, we take $m = 20$ and we assume that the value obtained is the exact price.

PROCESS	DECAY OF FT	SCALE	NUMERICAL VALUE	ERROR
VG	fast	m=3	19.74666301974	$8.235 \cdot 10^{-08}$
GBM	middle-fast	m=4	13.30013522239	$4.3699 \cdot 10^{-07}$
HESTON	slow	m=10	27.02036351942	$4.0129 \cdot 10^{-04}$

Table 4.1: Scale and error of the three dynamics considered in the pricing of the lookback put option with fixed strike $K = 110$.

Another remarkable fact which is worth noting is that the rate of decay of the characteristic function of the asset log-return maximum X_m decreases as we add more monitoring points in the lifetime of the option. This implies that we may need to take larger scales of approximation m when we consider lookback options with a high frequency of monitoring points to keep the accuracy of the approximation. This feature is exemplified in Figure 4.3, where we consider GBM and VG dynamics for the log-asset process L_t with the same parameters as before and a lifetime of $T = [0, 0.5]$ and $T = [0, 5]$ respectively. We represent the modulus of the characteristic function for 3, 6, 11, 16 and 21 monitoring points.

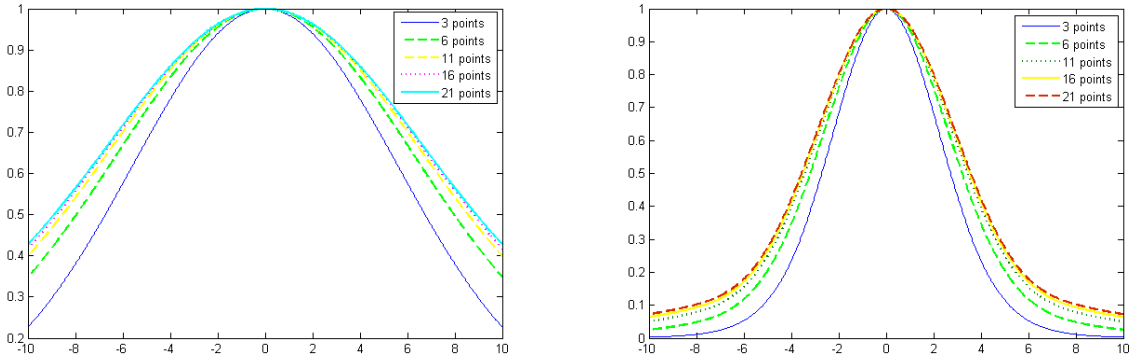

Figure 4.3: Modulus of the characteristic function ϕ_{X_m} compared with the number of monitoring points for GBM (left) and VG (right) dynamics.

4.5.2 Limit values k_1 and k_2 in the summation

Once the scale of the approximation m has been fixed, the limit values k_1 and k_2 of the summation should be determined. For the European option case, we used a formula involving the cumulants. In this case, we do not hold an expression for the cumulants of the asset log-return maximum X_m and this strategy cannot be practiced.

A possible alternative to overcome this problem is the following: departing from $k = 0$, we increase and decrease this value obtaining k_1 and k_2. We also compute the area underneath the curve with expression (3.16) on the fly. We stop when the area is close to 1 below some prescribed tolerance. Notice, however, that although we do not need a priori truncation of

the domain, this strategy involve extra CPU time since it does not allow the use of an FFT algorithm for computing the density coefficients.

Thus, the strategy that we finally adopt is to take an a priori truncation of the integration domain based on the analysis of the numerical density function. In other words, we plot the probability density function beforehand by computing the density coefficients with large k_1 and k_2 values. Then, we take a integration domain truncation by choosing two proper values that enclose most of the area underneath the curve. Finally, we make sure that the approximation is good enough by checking numerically that the area is close to 1.

Table 4.2 shows the truncations of the integration domain for the dynamics considered in the previous subsection 4.5.1. Initial values of a and b has been taken by observing the probability density functions of X_m represented in Figure 4.2. Then, we have refined these values until we have obtained the errors displayed in the table. The same technique is used in the subsequent experiments.

MODEL	**STRIKE**	**a**	**b**	$f\left(k_1/2^m\right)$	$f\left(k_2/2^m\right)$	**ERROR**
GMB	110	-0.6	1.3	$1.9769 \cdot 10^{-09}$	$4.5546 \cdot 10^{-10}$	$2.4281 \cdot 10^{-09}$
VG	110	-3	3.3	$2.8294 \cdot 10^{-11}$	$6.8447 \cdot 10^{-14}$	$8.7101 \cdot 10^{-11}$
HESTON	110	-0.2	0.9	$1.7228 \cdot 10^{-09}$	$4.4206 \cdot 10^{-12}$	$4.9116 \cdot 10^{-10}$

Table 4.2: Absolute error of the computed area under the recovered density by the SWIFT method at a scale $m = 12$ corresponding to GMB, VG and Heston dynamics.

4.5.3 Computation of the characteristic function ϕ_{X_m}

The computation of the characteristic function of the asset log-return maximum X_m is the most involved part in the valuation of Discrete Lookback options. In Section 4.2, we saw that it may be calculated using the recursive formula (4.13). Additionally, we derived a recursion in Theorem 4.2 which enabled the evaluation of ϕ_{X_m} and significantly reduced the complexity of its computation for a large number of monitoring points.

In table 4.3, we provide a comparison of the numerical complexity between the recursive formula (4.13) and recursion (4.15) by showing the number of terms involved in the evaluation of ϕ_{X_m}. It clearly shows that recursion (4.15) dominates for $m \geq 30$ and therefore provides a greater efficiency in pricing discrete lookback options with a high number of monitoring points. For example, at $m = 200$, the recursive formula (4.13) requires approximately $9.25 \cdot 10^{15}$ terms to calculate ϕ_{X_m} compared to $1.33 \cdot 10^6$ using the recursion (4.15).

In order to analyze its computational performance, we have implemented both techniques in our method for the valuation of Discrete Lookback options. This has been done using the software MATLAB. It is worth mentioning that MATLAB loses efficiency with loops and consequently we have vectorized our implementation. Table 4.4 provides a comparison of the CPU times between this two techniques when pricing a lookback put option with fixed strike under GBM dynamics with parameters $S_0 = 100$, $K = 110$, $r = 0.1$, $\sigma = 0.3$ and lifetime $T = [0, 0.5]$. Contrary to our expectations, one observes that the CPU times required when

we use the recursive formula (4.13) are lower than those obtained with recursion (4.15), and this difference becomes larger with the number of monitoring times. The reason for this apparent contradiction with the results showed in Table 4.3 is that the implementation of the method requires the computation of many loops, and recursive formula (4.13) allows to be efficiently vectorized contrary to recursion (4.15). It is highly likely that the efficiency of our method improves by implementing it in a software such that C++ with recursion (4.15).

MONITORING P.	RECURSIVE F. (4.13)	RECURSION (4.15)	RATIO
30	4525	5604	$8.1 \cdot 10^{-1}$
50	20875	204226	$1.0 \cdot 10^{-1}$
100	166750	190569292	$8.8 \cdot 10^{-4}$
150	562625	40853235313	$1.4 \cdot 10^{-5}$
200	1333500	$3.973 \cdot 10^{12}$	$3.4 \cdot 10^{-7}$
300	4500250	$9.253 \cdot 10^{15}$	$4.9 \cdot 10^{-10}$
500	20833750	$2.300 \cdot 10^{21}$	$9.1 \cdot 10^{-15}$

Table 4.3: Comparison of the number of terms in evaluating the characteristic function ϕ_{X_m} using the recursive formula (4.13) and recursion (4.15).

MONIT. P.	CPU (s) RECURSIVE F.	CPU (s) RECURSION	RATIO
6	0.011	0.013	1.1818
21	0.032	0.067	2.0938
41	0.067	0.214	3.2084
101	0.181	1.364	7.5357
301	1.212	14.745	12.1652
501	3.681	45.998	13.4093

Table 4.4: Comparison of the CPU time (in seconds) to price a lookback put option with fixed strike under GBM dynamics using the recursive formula (4.13) and recursion (4.15).

4.5.4 Pricing of Discrete Lookback options with the SWIFT method.

In this subsection, we carry out some numerical experiments concerning the pricing of Discrete Lookback options with the SWIFT method. Specifically, we aim to show the accuracy, efficiency and robustness of the method. Before we proceed to consider the specifics of these experiments, however, we provide in Table 4.5.4 a recap of the main steps of algorithm studied in this chapter as well as giving a detailed idea of the numerical implementation. Note that we have implemented the method with the FFT algorithm in order to make it more efficient. Additionally, we have selected the version of the algorithm which uses the recursive formula (4.13) and the Shannon wavelet family since it turns out to be the fastest choice.

Numerical Implementation of the SWIFT method
Assume we have a Discrete Lookback option whose underlying asset log-returns L_j follows a certain dynamics and its characteristic function is analytically available. The following steps provide the price of the option:
1. Fix the scale of approximation m by studying the rate of decay of the asset log-return maximum X_m as detailed in 4.5.1.
2. Fix an integration domain truncation $[a, b]$ by studying the area underneath the curve of the density function of X_m as detailed in Section 4.5.2 and determine the limit values $k_1 := \lceil 2^m \cdot a \rceil$ and $k_2 := \lfloor 2^m \cdot b \rfloor$.
3. Evaluate the characteristic function using the recursive formula (4.13) or the recursion (4.15). Evaluate each of the coefficients $a_k(z)$ using Theorem 4.5 (Haar Wavelets) or a FFT algorithm with Remark 4.3 (Shannon Wavelets).
4. Fix a $\jmath$-value with $\jmath := \lceil \log_2(\pi M_m) \rceil$ where $M_m := \max_{k_1<k<k_2} M_{m,k}$ and $M_{m,k} := \max(\lvert 2^m a - k \rvert, \lvert 2^m a + k \rvert)$ and use Remark 3.2 to apply the FFT algorithm to compute the density coefficients $c^*_{m,k}$ for $k = k_1, \ldots, k_2$.
5. Fix a $\bar{\jmath}$-value and compute the pay-off coefficients $V^*_{m,k}$ for $k = k_1, \ldots, k_2$ using a FFT algorithm with Remark 4.4.
6. Determine the price V^*_T of the Discrete Lookback option using the Feynman-Kac formula, that is, $V^*_T := e^{-r(T-t)} \sum_{k=k_1}^{k_2} c^*_{m,k}(x) \cdot V^*_{m,k}$.

Table 4.5: Numerical Implementation of the SWIFT method for Discrete Lookback options.

We check the accuracy and efficiency of the SWIFT method by pricing a lookback put option with fixed strike under GBM dynamics and a lookback call with floating strike under a VG process. We take as reference values the results given in the valuation of the same options in [9] and compare the CPU times reported. We should notice that *the Fourier transform B-spline method (FTBS)* is used in [9]. Additionally, the authors of this method perform the experiments using an Intel Core I7-3610QM processor and carry out the implementation in C++. It is worth noting that the comparison is a bit unfair since we perform our experiments in a worse computer. We also carry out our implementation in MATLAB which precludes us to use recursion (4.15) that would make our method much more efficient. Then, we just include the comparison to give an idea of the high efficiency of our algorithm.

We start our numerical analysis by pricing a lookback put option with fixed strike under GBM dynamics with parameters $S_0 = 100$, $r = 0.1$, $\sigma = 0.3$ and lifetime $T = [0, 0.5]$. We consider different strikes ($K = 110$ and $K = 120$) and monitoring times ranging from 5 to 160. We also note that under GBM dynamics, an analytic expression for the coefficients a_k can be derived by the simple integration of (4.31) against to the probability density function

of a Normal Distribution with probability cumulative function Φ. This computation leads to the following expression:

$$a_k(z) = \Phi\left(-\frac{\mu\cdot\sqrt{t_{j^*+k}}}{\sigma}\right) + e^{z\cdot t_{j^*+k}\cdot\left(-\frac{1}{2}z\sigma^2+i\mu\right)} - \frac{1}{2}\cdot e^{\frac{\mu^2\cdot t_{j^*+k}}{2\sigma^2}}\cdot\text{fadd}\left(-\sqrt{\frac{t_{j^*+k}}{2}}\cdot(-z\cdot\sigma+i\cdot\mu/\sigma)\right).$$

where fadd(w) denotes the complex Faddeeva function which has been implemented using an algorithm by [26] which ensures an accuracy of 13 digits in almost the entire complex plane.

The results are described in Table 4.6. We first observe that the implementation with the exact analytic expression of $a_k(z)$ makes the method much more efficient than if we use Haar wavelets. We also see that the scale of the approximation m increases as we add more monitoring points in the same way that we predicted in Section 4.5.1 where we saw that the rate of decay of the characteristic function decreases with the number of monitoring points. Finally, if we compare the CPU times of the SWIFT using Shannon wavelets with the FTBS method [2], we can see that our method approaches the efficiency of the FTBS method in spite of the limitations that we previously mentioned. Actually, there is a case (80 monitoring times) in which the SWIFT method performs faster than the FTBS method.

K	m	SCALE	PRICE	FTBS	SWIFT (exact)	SWIFT (haar)
110	5	3	13.300	0.002	0.011	0.799
120	5	3	18.837	0.002	0.011	0.799
110	10	4	14.123	0.004	0.019	1.621
120	10	4	19.323	0.004	0.019	1.621
110	20	4	14.806	0.012	0.036	3.271
120	20	4	19.743	0.012	0.036	3.271
110	40	5	15.345	0.040	0.089	6.046
120	40	5	20.083	0.040	0.089	6.046
110	80	5	15.745	0.145	0.142	14.728
120	80	5	20.346	0.145	0.142	14.728
110	160	6	16.059	0.663	0.866	28.901
120	160	6	20.544	0.663	0.866	28.901

Table 4.6: CPU times (in seconds) of the valuation of a lookback put option with fixed strike under GBM dynamics using the FTBS method and SWIFT method with the exact expression of $a_k(z)$ and Haar Wavelets. Here, m denotes the number of monitoring points.

[2]The FTBS method also uses the analytic expression of the coefficients $a_k(x)$. Additionally, it also implements the evaluation of the characteristic functions by means of recursion (4.15).

We conclude our numerical experiments by pricing a discrete lookback call option with floating strike under a VG process with parameters $S_0 = 100$, $r = 0.0548$, $\sigma = 0.1927$, $\mu = -0.2859$ and $\nu = 0.25$. We consider strike prices $K = 105$, $K = 110$ and $K = 115$ for contracts with annual monitoring points and contract duration T, ranging from 5 to 75 years. The results obtained are shown in Table 4.7. Again, the implementation of the SWIFT method with Shannon wavelets clearly dominates the Haar Wavelet's alternative. The scale of the approximation m keeps constant for the different numbers of monitoring points while the width of the integration domain truncation increases. Finally, comparing the CPU times of the SWITF method with Shannon basis and the FTBS method [3], we observe that for a small number of monitoring points ($m = 5$) the FTBS method is more efficient. However, when we consider a larger number of monitoring points ($m = 10$ and $m = 20$), the SWIFT method becomes increasingly faster. We note again that this greater efficiency of the SWIFT method could well become much more noticeable if it were implemented in C++ with recursion (4.15).

K	**T, m**	**scale**	**price**	**FTBS**	**a**	**b**	**SWIFT (shannon)**	**SWIFT (haar)**
105	5	4	39.080	0.03	-3	3.3	0.071	1.191
110	5	4	36.110	0.03	-3	3.3	0.071	1.191
115	5	4	33.303	0.03	-3	3.3	0.071	1.191
105	10	4	64.126	0.20	-3	3.8	0.181	2.335
110	10	4	61.626	0.20	-3	3.8	0.181	2.335
115	10	4	59.205	0.20	-3	3.8	0.181	2.335
105	20	4	94.639	1.16	-3	5.8	0.507	17.846
110	20	4	93.096	1.16	-3	5.8	0.507	17.846
115	20	4	91.580	1.16	-3	5.8	0.507	17.846

Table 4.7: CPU times (in seconds) of the valuation of a discrete lookback call option with floating strike using the FTBS method and SWIFT method with Shannon and Haar Wavelets. Parameters a and b are the values of the integration domain truncation.

[3] In this case, coefficients $a_k(z)$ do not allow a closed expression. The FTBS derives a numerical approximation using the Cauchy Residue Theorem to compute them.

Chapter 5

Conclusions

During this thesis, we have explored a recently proposed method for pricing European options, the so-called *SWIFT method*, introduced by Luis Ortiz-Gracia and Cornelis W. Oosterlee in 2016 (see [19]). This method explodes the outstanding approximation properties of Shannon wavelets within the European option pricing framework. More precisely, we use the Shannon father wavelet, which is the sinus cardinal function, and carry out an approximation of the density function of the log-asset price in a multiresolution analysis environment where the desired scale of approximation is fixed. Both the density and pay-off coefficients are computed using Vieta's formula to derive an expression which allows the application of a FFT algorithm in order to speed up their computation. This research is accompanied with the subsequent error analysis of each of the approximations.

The presented numerical results show that this methodology is highly robust and accurate. Very low scales of approximation are generally needed to converge accurately to the solution. This feature together with the fact that this method allows the usage of a FFT algorithm make this strategy extremely efficient, showing exponential convergence and being able to price options in milliseconds. The SWIFT method also turns out to be very versatile since it is easily adaptable to different log-asset price dynamics if the analytic expression of the characteristic function of the process is available.

Finally, another remarkable property of this method is that it does not rely on an a priori truncation of the entire real line, since it can do it adaptively in order to meet a predefined tolerance error regarding the mass underneath the density function. The accuracy is then not affected by the width of the interval for the approximation and it automatically computes the number of coefficients needed for the new interval.

Encouraged by the extraordinary results obtained for European options, we have researched the adaptation of the SWIFT method for one of the preferred exotic options among investors nowadays, the Discrete Lookback options. Although the underlying idea of the methodology is essentially analogous (first we approximate the density function by Shannon Wavelets and then we compute the density and pay-off coefficients), the complexity of the pay-off function leads to emerging challenges concerning the characteristic function com-

putation, termed here as the *characteristic function of the asset log-return maximum* X_m. It turns out impossible to derive an analytic expression for this function and it should be calculated by a recursive formula which, in turn, involves the computation of a large number of new coefficients a_k. The efficient calculation of a_k becomes the central point to make the SWIFT method for Discrete Lookback option highly efficient. Additionally, for the most relevant dynamics, we do not hold a closed expression for a_k and numerical approximations need to be done. Next, we provide a list of the key **contributions** of our own research carried out in the second part of this thesis:

- We derive a recursive formula for the evaluation of the *characteristic function of the asset log-return maximum* X_m based on the application of the Spitzer's Formula and using similar ideas to those in [18]. Further, we compare it with an alternative recursion introduced in [9]. Although the theoretical computational complexity is clearly lower for this recursion, our derivation turns out to be considerably more efficient as we implement it with the software MATLAB. It is also worth mentioning that our recursive formula allows to price the option at any monitoring time.

- We develop a general methodology to approximate numerically the coefficients a_k. We explore several approaches: first we use Haar wavelets and rule out this technique since it results excessively inefficient. Second, we derive a strategy using Shannon wavelets which allows a fast computation of a_k by the application of a FFT algorithm. Furthermore, this methodology turns out to be remarkably versatile and flexible since it does not depend on the dynamics and only requires the availability of the characteristic function of the log-return process L_t.

- We provide an efficient implementation of the SWIFT method for Discrete Lookback options in MATLAB and analyze our results by comparing them with those reported in [9]. Again, the method shows to be robust, efficient and accurate. Additionally, although the comparison of CPU times is a bit unfair due to the fact that our method has been implemented in a worse computer and with a different programming software, the SWIFT method seems to be more efficient than the highly efficient FTBS method introduced in [9] as the number of monitoring points increases (case of interest), specially for the Variance Gamma Process.

The lack of time has left several aspects open both to complete the method and to verify that it is actually more efficient than the FTBS method. **Further research** needs then to be done to improve the methodology derived in this thesis. This includes the derivation of an expression for the cumulants of the characteristic function of X_m in order to avoid the dependence on an a priori truncation of the integration domain, the performance of an error analysis for each of the approximations and the implementation of the method in C++ to include the recurrence of the characteristic function developed in [9] which exhibits a lower computational complexity. It would also be convenient to implement the FTBS method in the same computer and programming language to a fair comparison of CPU times.

Appendix A

Processes and Characteristic functions

In this chapter, we provide the definition of the models considered in the numerical experiments sections together with their characteristic functions which have been used in the implementation of the SWIFT method. Our definition of the characteristic function coincides with the following definition of the Fourier transform of the density function f of the process:

$$\hat{f}\left(\xi\right) \,=\, \int_{\mathbb{R}} f(x) \cdot e^{-i \cdot x \cdot \xi} dx.$$

For further details on these processes, we refer to the reader to [30] for the Geometric Brownian Motion, [22] for the CGMY model, [15] for the Heston model and [6] for Variance Gamma.

1) The Geometric Brownian Motion (GBM). The GBM is a continuous-time stochastic process used in mathematical finance to describe stock prices dynamics in one of the most important and notorious models in modern financial theory, the Black-Scholes model. This model was developed in 1973 by Fisher Black, Robert Merton and Myron Scholes and is still widely used in 2017 since computations become relatively easy. The model assumes that the price of heavily traded assets S_t follows a geometric Brownian motion with constant drift μ and volatility σ depicted by the following SDE:

$$dX_t \,=\, \left(r - \sigma^2/2\right) \cdot dt \,+\, \sigma \cdot W_t,$$

where $X_t = \log(S_t/K)$ is the log-asset price and r is the risk-less interest rate. We have also assumed risk-neutral probability measure. It is easy to see from this expression that the log-asset price X_t follows a normal distribution. Hence, one may derive the characteristic function of the GBM straightforwardly by computing the Fourier transform of a normal probability distribution. One obtains then:

$$\hat{f}_{GBM}\left(\xi\right) \,=\, \exp\left(-i\xi \cdot \left(r - q - \frac{1}{2}\sigma^2 \right) \cdot (T-t) - \frac{1}{2}\sigma^2 \xi^2 \cdot (T-t) \right),$$

where parameter q represents a dividend yield, which is often set to zero in our experiments.

2) The CGMY model. One problem with the GBM model is that it is not able to reproduce the volatility skew or smile present in most financial markets. Over the past few years it has been shown that several exponential Lévy models are, at least to some extent, able to reproduce the skew or the smile. One particular model is the CGMY model introduced by Carr and explained with detail in [22]. The main feature of this model is the incorporation of a jump component which intuitively models the abrupt news arrival. Now, the dynamics of the log-asset price X_t are driven by the following SDE:

$$dX_t \,=\, (r - v) \cdot dt \,+\, dL_t,$$

where again r is the risk-less interest rate, v is a convexity adjustment so that $E_{\mathbb{Q}}\left(S_T\right) = e^{r(T-t)S_t}$ and dL_t is the increment of a Lévy process. In this case, the probability density function does not allow an analytic expression and the characteristic function of the log-asset price should be found employing other techniques. It reads:

$$\begin{aligned}\hat{f}_{CGMY}\left(\xi\right) \,=\, &\exp\Big(-i\xi\cdot(r-q+s)\cdot(T-t)\Big)\\ &\cdot\exp\Big(C\cdot\Gamma\left(-Y\right)\cdot\Big(\left(M+i\xi\right)^{Y}-M^{Y}+\left(G-i\xi\right)^{Y}-G^{Y}\Big)\cdot(T-t)\Big),\end{aligned}$$

with C, G, M and Y parameters governing the density and $\Gamma(\cdot)$ represents the Gamma function. Additionally,

$$s \,=\, -C\cdot\Gamma\left(-Y\right)\cdot\Big(\left(M-1\right)^{Y}-M^{Y}+\left(G+1\right)^{Y}-G^{Y}\Big).$$

The parameter C controls the overall kurtosis of the distribution. The parameters G and M control the overall rate of exponential decay on the right and left of the Lévy density, respectively. When they are equal to each other, the distribution of the CGMY model becomes symmetric. The case $G \neq M$ leads to a skewed distribution. Finally, the parameter Y is used to characterize the fine structure of the stochastic process.

3) The Heston Model. The main drawback of the CGMY model (also present in the Black-Scholes model) is the assumption that volatility remains constant over the option's life and unaffected by the changes in the price level of the underlying security, which is not the case because volatility fluctuates with the level of supply and demand. To settle this shortcoming, *stochastic volatility models* were introduced. These models adopt the approach that the volatility of the underlying price is a stochastic process rather than a constant or a deterministic function. We particularly focus on the Heston Model developed in 1993 by Steven Heston. This model integrates now a new SDE for the volatility, denoted here by $\sqrt{u_t}$ in addition to the one of the underlying asset:

$$\begin{cases} dX_t \,=\, \left(\mu - \frac{1}{2}u_t\right)\cdot X_t\cdot dt \,+\, \sqrt{u_t}\cdot X_t\cdot dW_{1t}, \\ du_t \,=\, \lambda\cdot(\bar{u}-u_t)\cdot dt \,+\, \eta\cdot\sqrt{u_t}\cdot dW_{2t}, \end{cases}$$

where X_t denotes the log-asset price and u_t the variance of the asset price process. Parameters $\lambda \geq 0$, $\bar{u} \geq 0$ and $\nu \geq 0$ are called the speed of mean reversion, the mean level of variance, and the volatility of the volatility, respectively. Furthermore, the Brownian motions W_{1t} and W_{2t} are assumed to be correlated with correlation coefficient ρ. Thus, ρ is another parameter of the model. As in the case of the CGMY model, it is not possible to find a closed expression for the probability density function and the characteristic function should be found using more sophisticated methodologies. It is given now by:

$$\hat{f}_{Heston}(\xi; u_0) = \exp\left(-i\xi\mu \cdot (T-t) + \frac{u_0}{\eta^2} \cdot \left(\frac{1 - e^{-D\cdot(T-t)}}{1 - G \cdot e^{-D\cdot(T-t)}} \right) \cdot (\lambda + i\rho\eta\xi - D) \right)$$
$$\cdot \exp\left(\frac{\lambda\bar{u}}{\eta^2} \cdot \left((\lambda + i\rho\eta\xi - D) \cdot (T-t) - 2 \cdot \ln\left(\frac{1 - G \cdot e^{-D\cdot(T-t)}}{1-G} \right) \right) \right),$$

where we have introduced the following variables depending on ξ,

$$D = \sqrt{(\lambda + i\rho\eta\xi)^2 + (\xi^2 - i\xi)\,\eta^2} \quad \text{and} \quad G = \frac{\lambda + i\rho\eta\xi - D}{\lambda + i\rho\eta\xi + D}.$$

4) The Variance Gamma (VG) process. This process is another three parameter generalization of Brownian motion as a model for the dynamics of the logarithm of the stock price. Again, it allows for a wider modeling of skewness and kurtosis than the Brownian motion does. This new process is obtained by evaluating a Brownian motion $W(t)$, with constant drift and volatility, at a random time change $\Gamma(t; 1, \nu)$ which has a gamma density and is often viewed as "business time", reflecting the random speedups and slowdowns in real-time economic and business activity. The dynamics of the log-asset price X_t are given by:

$$X_t = \mu \cdot \Gamma(t; 1, \nu) + W(\Gamma(t; 1, \nu)),$$

where μ and $\sigma > 0$ are the drift and the volatility of the Brownian motion respectively, and $\nu > 0$ is the variance rate of the gamma time change. This model allows us to control the skew via the parameter μ and the kurtosis by means of parameter ν. We are interested, however, in the risk-netural dynamics since we aim to apply the Feynman-Kac formula. In this case, the dynamics equation reads:

$$X_t = r \cdot t + \mu \cdot \gamma_t + \sigma W(\gamma_t) - \omega \cdot t,$$

where again $W(t)$ is the standard Brownian Motion and we have introduced $\gamma_t \sim \Gamma(t/\nu, \nu)$ and the compensator $\omega = -(1/\nu) \cdot \ln\left(1 - \mu \cdot \nu - \frac{1}{2}\sigma^2\nu\right.$. The probability density function does not allow a closed expression and the characteristic function should be found using more sophisticated methodologies. It reads:

$$\hat{f}_{VG}(\xi) = e^{-i\cdot\xi\cdot(r-\omega)\cdot(T-t)} \cdot \left(\frac{1}{1 + i \cdot \mu\nu\xi + \frac{1}{2} \cdot \sigma^2\nu\xi^2} \right)^{\frac{T-t}{\nu}}.$$

Appendix B

Cumulants of the processes

The cumulants c_n of a probability distribution are a set of quantities that provide an alternative to the moments of the distribution. The moments determine the cumulants in the sense that any two probability distributions whose moments are identical will have identical cumulants as well, and similarly the cumulants determine the moments. We provide in next statement the exact definition of the nth cumulant c_n by means of the introduction of the *cumulant generating function* $g(\omega)$ of a random variable:

Definition B.1 (Cumulant generating function)**.** *Let ϕ_X be the characteristic function corresponding to a random variable X. We define the cumulant generating function of this random variable by the following expression,*

$$g(\omega) := \log \mathbb{E}\left(e^{\omega X}\right) = \log \phi_X\left(-i\omega\right), \tag{B.1}$$

and the nth cumulant of X, denoted here by c_n, is given by the nth derivative at zero of the cumulant genrating function $g(\omega)$, that is, $c_n := g^{(n)}(0)$.

The first cumulant c_1 is the mean, the second cumulant c_2 is the variance, and the third cumulant c_3 is the same as the third central moment. But fourth and higher-order cumulants are not equal to central moments. As have been mentioned in the section of numerical experiments, we use the cumulants to determine the size of the integration interval since they often provide reliable intervals for the approximation. We particularly use the following formula to determine the integration interval:

$$[a,b] := \left[x_0 + c_1 - L\sqrt{c_2 + \sqrt{c_4}},\, x_0 + c_1 + L\sqrt{c_2 + \sqrt{c_4}}\right], \qquad \text{with } L = 10.$$

Next table summarizes the values of the cumulants for the different processes considered in this thesis: the geometric Brownian motion (GBM), the CGMY model, the Heston model and the Variance Gamma process (VG).

GBM	$c_1 = \mu \cdot T$ $c_2 = \sigma^2 \cdot T$ $c_4 = 0$ $w = 0$
CGMY	$c_1 = \mu T + C \cdot T \cdot \Gamma(1-Y) \cdot \left(M^{Y-1} - G^{Y-1}\right)$ $c_2 = \sigma^2 T + C \cdot T \cdot \Gamma(2-Y) \cdot \left(M^{Y-2} + G^{Y-2}\right)$ $c_4 = C \cdot T \cdot \Gamma(4-Y) \cdot \left(M^{Y-4} + G^{Y-4}\right)$ $w = -C \cdot \Gamma(-Y) \cdot \left[(M-1)^Y - M^Y + (G+1)^Y - G^Y\right]$
HESTON	$c_1 = \mu \cdot T + \left(1 - e^{-\lambda T}\right) \cdot \frac{\bar{u} - u_0}{2\lambda} - \frac{1}{2}\bar{u} \cdot T$ $c_2 = \frac{1}{8 \cdot \lambda^2} \cdot \Big[\eta T \lambda e^{-\lambda T} \cdot (u_0 - \bar{u}) \cdot (8\lambda\rho - 4\eta)$ $+ \lambda\rho\eta \cdot \left(1 - e^{-\lambda T}\right) \cdot (16\bar{u} - 8u_0)$ $+ 2\bar{u}\lambda T \cdot \left(-4\lambda\rho\eta + \eta^2 + 4\lambda^2\right)$ $+ \eta^2 \cdot \left((\bar{u} - 2u_0) \cdot e^{-2\lambda T} + \bar{u} \cdot \left(6e^{-\lambda T} - 7\right) + 2u_0\right)$ $+ 8\lambda^2 \cdot (u_0 - \bar{u}) \cdot \left(1 - e^{-\lambda T}\right)\Big]$ $c_4 = 0$ $w = 0$
VG	$c_1 = (r + \mu) \cdot T$ $c_2 = \left(\sigma^2 + \nu\mu^2\right) \cdot T$ $c_4 = 3 \cdot \left(\sigma^4\nu + 2\mu^4\nu^3 + 4\sigma^2\mu^2\nu^2\right) \cdot T$ $w = \frac{1}{\nu} \cdot \ln\left(1 - \mu\nu - \sigma^2\nu/2\right)$

Table B.1: Cumulants for the GBM, CGMY and Heston dynamics.

Bibliography

[1] F. AitSahlia and T.L. Lai. "Valuation of discrete barrier and hindsight options". In: *Journal Financ. Eng.* 6 (1997), pp. 169–177.

[2] S. Babbs. "Binomial valuation of lookback options". In: *Unpublished Working Paper* (1992).

[3] Fischer Black and Myron Scholes. "The Pricing of Options and Corporate Liabilities". In: *Journal of Political Economy* 81 (1973), pp. 637–654.

[4] K. Borovkov and A. Novikov. "On a new approach to calculating expectations for option pricing". In: *Journal of Applied Probability* 39 (2002), pp. 889–895.

[5] Seungmook Choi and Mark E. Wohar. "S&P 500 index options prices and the Black-Scholes option pricing model". In: *Journal of Applied Financial Economics* 26 (1994), pp. 249–264.

[6] Peter Carr Dilip Madan and Eric Chang. "The Variance Gamma Process and Option Pricing". In: *Review of Finance* 2 (1998), pp. 79–105.

[7] F. Fang and C.W. Oosterlee. "A novel pricing method for European Options based on Fourier-cosine series expansions". In: *SIAM Journal Sci. Comput.* 31 (2008), pp. 826–848.

[8] William B. Gearhart and Harris S. Shultz. "The function sin(x)/x". In: *The College Mathematics Journal* 21.2 (1990), pp. 90–99.

[9] Gareth G. Haslip and Vladimir K. Kaishev. "Lookback option pricing using the Fourier transform B-spline method". In: *Journal of Quantitative Finance* 14 (2014), pp. 789–803.

[10] J. Holst. "Sequential calibration of options". In: *Computational Statistic Data Analysis* 52 (2008), pp. 2877–2891.

[11] J.C. Hull and A.D. White. "Efficient procedures for valueing European and American path-dependent options". In: *J. Deriv.* 1 (1993), pp. 21–31.

[12] John C. Hull. *Options, futures and other derivatives.* Prentice Hall, 2002.

[13] Jean Jacod and Albert N. Shiryaev. *Limit Theorems for Stochastic Processes.* Vol. 288. Springer-Verlag Berlin Heidelberg, 2003.

[14] George Papanicolaou Jean-Pierre Fouque and K. Ronnie Sircar. *Derivatives in financial markets with stochastic volatility*. Cambridge University Press, 2000.

[15] Nassim Nicholas Taleb Jim Gatheral. *The Volatility Surface: A Practitioner's Guide (Wiley Finance)*. Wiley Finance. Wiley, 2006.

[16] R.W. Lee. "Option pricing by transform methods: Extensions, unification, and error control". In: *Journal of Computational Finance* 7 (2004), pp. 51–86.

[17] Dilip Madan and Peter Carr. "Option valuation using the fast Fourier transform". In: *Journal of Computational Finance* 2 (1999), pp. 61–73.

[18] A. Ohgren. "A remark on the pricing of discrete lookback options". In: *Journal of Computational Finance* 4 (2001), pp. 141–147.

[19] Luis Ortiz-Gracia and Cornelis W. Oosterlee. "A highly efficient Shannon Wavelet Inverse Fourier Technique for pricing European Options". In: *SIAM Journal Sci. Comput.* 38 (2016), B118–B143.

[20] Luis Ortiz-Gracia and Cornelis W. Oosterlee. "Efficient VaR and expected shortfall computations for nonlinear portfolios within the delta-gamma approach". In: *Appl. Math. Comput.* 244 (2014), pp. 16–31.

[21] Luis Ortiz-Gracia and Cornelis W. Oosterlee. "Robust pricing of European otions with wavelets and the characteristic function". In: *SIAM Journal Sci. Comput.* 35 (2013), B1055–B1084.

[22] D. B. Madan P. Carr H. Geman and Marc YorSource. "The fine structure of asset returns: An empirical investigation". In: *The Journal of Business* 75 (2002), pp. 305–333.

[23] J. Dewynne P. Wilmott and S. Howison. *Option Pricing: Mathematical Models and Computation*. Oxford Financial Press, 1993.

[24] K.R. Vetzal P.A Forsyth and R. Zvan. "A finite element approach to the pricing of discrete lookbacks with stochastic volatility". In: *Appl. Math. Finance* 6 (1999), pp. 87–106.

[25] Giovanni Petrella and Steven Kou. "Numerical pricing of discrete barrier and lookback options via Laplace transforms". In: *Journal of Computational Finance* 8 (2004), pp. 1–38.

[26] G.P.M. Poppe and C.M.J. Wijers. "More efficient computation of the complex error function". In: *ACM Trans. Math. Softw. (TOMS)* 16 (1990), pp. 38–46.

[27] B.M. Quine and S.M. Abrarov. "Application of the spectrally integrated Voigt function to line-by-line radiative transfer modelling". In: *J. Quantitative Spectroscopy Radiative Transfer* 127 (2013), pp. 37–48.

[28] M. Ruijter and C.W. Oosterlee. "Two-dimensional Fourier cosines series expansion method for pricing financial options". In: *SIAM J. Sci. Comput.* 34 (2012), pp. 642–671.

[29] Frank Spitzer. "A combinatorial lemma and its application to probability theory". In: *Transactions of the American Mathematical Society* 82 (1956), pp. 323–339.

[30] Peter Tankov. *Financial Modelling with Jump Processes*. Chapman & Hall/CRC Financial Mathematics Series. CRC, 2003.

[31] L.K. Li W.M. Tse and K.W. Ng. "Pricing discrete barrier and hindsight options with the tridiagonal probability algorithm". In: *Manage. Sci.* 47 (2001), pp. 383–393.